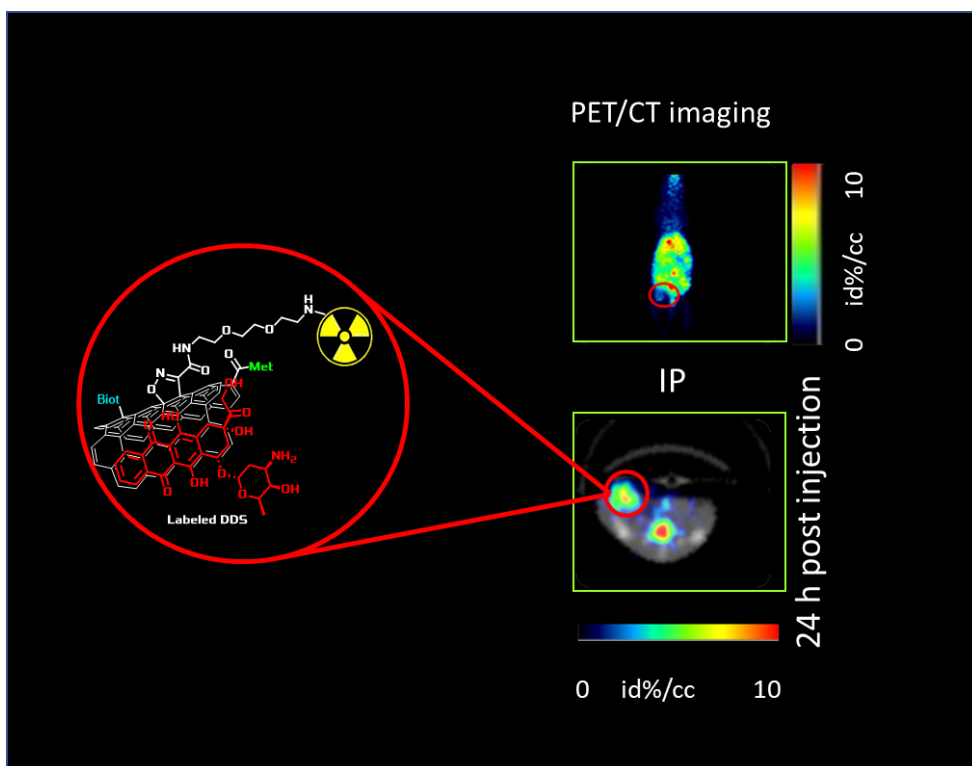# DOTTORATO DI RICERCA IN SCIENZE CHIMICHE

CICLO XXXI

COORDINATORE Prof. PIERO BAGLIONI

Discovery of a Drug Delivery System Based on Carbon Nanotubes: Synthesis and Biological Studies

Dottorando
Dott. Giacomo Biagiotti

Tutore
Prof. Alberto Brandi

DOTTORATO DI RICERCA IN

SCIENZE CHIMICHE

CICLO XXXI

COORDINATORE PROF. PIERO BAGLIONI

Discovery of a Drug Delivery System Based on Carbon Nanotubes: Synthesis and Biological Studies

Settore Scientifico Disciplinare CHIM/06

Dottorando	**Tutore**
Dott. Biagiotti Giacomo	Prof. Alberto Brandi
_____	_____
(firma)	*(firma)*

Coordinatore

Prof. Piero Baglioni

_____

(firma)

Anni 2015/2018

INDEX

— Chapter 1 —

1.1 Preface and objectives

Nanomedicine is a recently developed field of nanotechnology which uses nanosized tools and molecular knowledge of human body to diagnose, treat, and prevent diseases and traumatic injuries. Five main disciplines of nanomedicine have been defined by the European Science Foundation: analytical tools, nanoimaging, nanomaterials and nanodevices, clinical and toxicological issues, and drug delivery systems.[1] The main subject of this PhD thesis belongs to the last discipline of nanomedicine. In this work, the design, synthesis characterization and biological study of a Multimodal Drug Delivery System (DDS) will be described. As it will be shown in the introduction chapter, even if limited to carbon nanotubes, nanomedical devices are able to increase the efficacy of drugs, improving their bioavailability, pharmacokinetics and delivery. Furthermore, the use of devices with active targeting moieties avoids the insurgence of side effects when using drugs with a general cytotoxicity. A properly designed nanocarrier can circulate in the blood stream for a longer period, compared to small molecules, and deliver the active compound directly in the site of interest. A fine tuning of the functionalization chemistry can provide the required stability during the biodistribution process, while a rapid release can take place once the system reaches the target.

The project of this PhD thesis mainly concerns the design and synthesis of a DDS, based on short oxidized multiwalled carbon nanotubes, as a device suitable for cancer treatment. A multimodal approach was chosen, targeting both metabolism and proliferation of tumor cells with two different drugs, in such a way to address cells of different sub-populations of the tumor: proliferative and staminal cancer cells (stem cells).

The synthetic approach, exploiting the chemical flexibility of carbon nanotubes, was planned in a way to decorate the delivery system with the highest quantities of two

different drugs, and a targeting component, a small molecule reported to increase tumor uptake. Then, with minor changes to the synthetic protocol, the system was modified to study the pharmacokinetic in tumor bearing mice models (**Figure 1**).
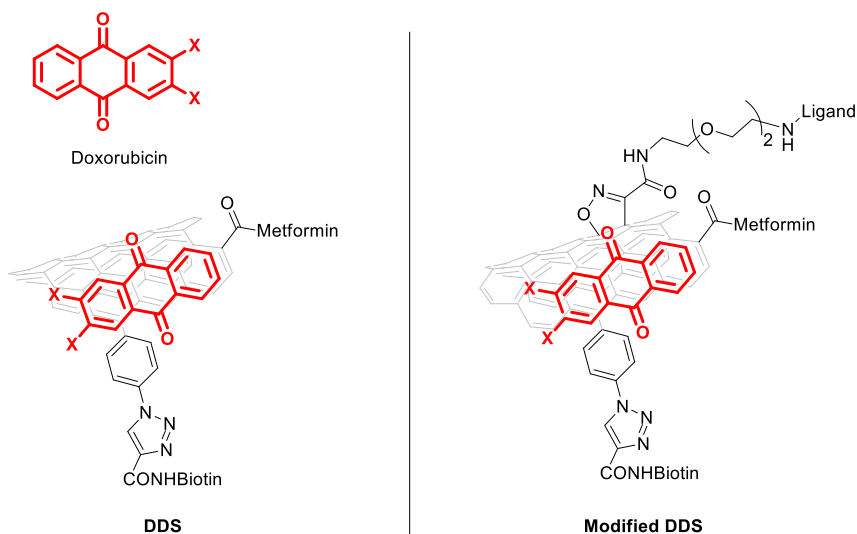
Figure 1. Structure of the designed DDS for the biologycal studies.

The biological properties of these systems were studied thanks to the collaborations with the Department of Clinical and Experimental Biomedical Sciences, which carried out *in vitro* studies, and with the University of Texas MD Anderson Cancer Centre which hosted me for the radio-labeling of the DDS and their *in vivo* studies.

The main goals of this project are listed below:

- Development of a synthetic strategy for the decoration of ox-MWCNTs exploiting both covalent and supramolecular approaches.

- Development of a protocol for the characterization of the synthesized adducts.

- Investigation of the biological properties of the prepared materials *in vitro*.

- Development of a protocol for the radiolabeling of CNTs using radiometals.

- Evaluation of the pharmacokinetics, the efficacy, and the target engagement of the DDS *in vivo*.

To complete this main project, it was necessary to test the feasibility of different synthetic approaches, to prepare different classes of intermediates, to synthesize different fluorescent probes and to optimize new functionalization procedures. For this reason, three minor satellite projects were also developed (described briefly at the end of the main project): 1) preparation of new BODIPY fluorescent probes and their assembly into flexible and rigid dyads, and study of their physicochemical properties; 2) decoration of carbon nanotubes using nitroacetamide derivatives of sugars; 3) functionalization of CNT with phosphorus-containing moieties for the preparation of heterogeneous organic catalysts.

The first project, developed in collaboration with Prof. Paolo Foggi (UniPg and LENS), concerned the synthesis of different BODIPY fluorescent probes that were linked to flexible or rigid scaffolds. The energy transfer processes between the two fluorescent probes are modulated by the nature of the scaffold as was demonstrated by time-resolved spectroscopic techniques. (**Figure 2**, **A**)

The second project, developed in collaboration with Prof. Cristina Nativi, concerned the preparation of CNT derivatives characterized by the presence of sugar moieties that could act as mimetic of a tumor associated carbohydrate antigens (TACAS). The critical decoration of CNT was performed using the Machetti-De Sarlo reaction, involving the copper catalyzed nitroacetamide cycloaddition reaction to CNT. This was an excellent tool for tuning the reaction conditions that were also used for the decoration of the DDS with a radioactive label in the main project (**Figure 2**, **B**)

The third project was developed in collaboration with prof. Michal Pietrusiewicz (University of Lublin, Poland) and concerned the decoration of CNT using different phosphinoxide derivatives characterized by the presence of an amino or azido group. The derivatives were used in different organocatalyzed reactions (**Figure 2**, **C**).
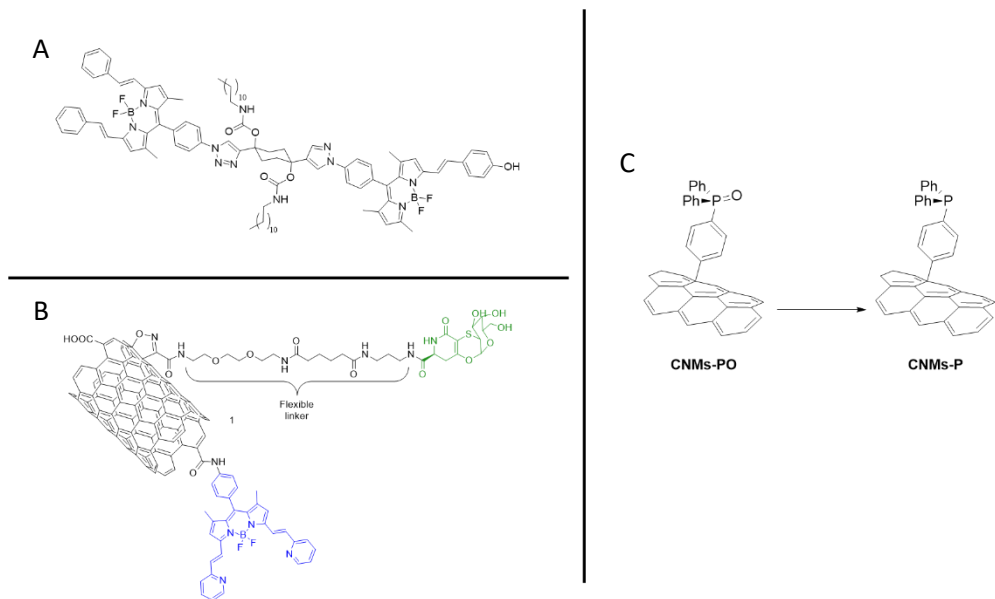
Figure 2. Structure of the products synthesized for side projects.

— Chapter 1 —

1.2 Introduction

1.2.1 Carbon nanotubes (CNTs)

Carbon Nanotubes (CNTs) since their discovery, in 1991 by Ijima,[2] have attracted the interest of the scientific community thanks to their chemical and physical properties.[3,4] CNTs are one of the allotropic forms of carbon, like graphite, diamond and other form of nanostructured carbon as fullerenes and nanoonions (**Figure 3**). CNTs are composed by only sp^2 hybridized carbons forming a network of fused benzene ring in a rolled "chicken wire" shape. Depending on the number of graphene layers that form their walls, they can be called single-walled (SWCNT), double-walled (DWCNT) and multi-walled carbon nanotubes (MWCNT). All of them have a high aspect ratio (generally higher than 1000) and their structure makes them suitable for a wide variety of applications ranging from electronics to biomedical.[3,5]
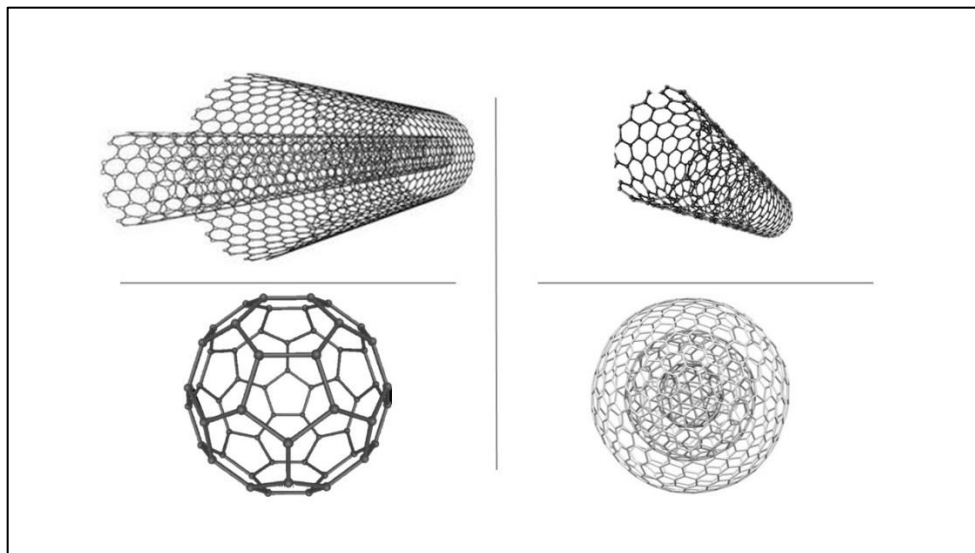
Figure 3. Different allotropic forms of carbon: top on the left MWCNTs, top on the right SWCNTs, bottom on the left fullerene C_{60} and on the right carbon nanoonion.

The main unique properties of this class of nanoparticles are listed below.

I.   The high surface area and the hollow structure make CNT suitable for drug loading, but also as nano-adsorbents for the scavenging of metallic ions and organic compounds from aqueous solutions.

II.   The ease functionalization of CNT allows their modification and tailoring for several different applications.[6–9]

III. The excellent conductive profile offers a unique platform for the development of sensors and biosensors[10] as well as a large number of applications in electronic devices.

IV.   Their mechanical strength has promoted them as reinforcement additives in polymeric matrix, or in biology as surface for cell adhesion, proliferation and differentiation.[11,12]

The high appeal of these materials had boosted the efforts of the industries to develop mass production techniques. Up to date, the most promising and investigated procedure is the chemical vapor deposition (CVD): this technique involves the pyrolysis of hydrocarbons, or other carbon feedstock, carried out in a stream of inert gas into a chamber with a metal catalyst (Ni, Fe and Co). The basic structure of CNT (e.g., diameter, length, and alignment) can be controlled effectively by controlling the several different parameters that influence this transformation: temperature, gas pressure, presence of inert gases. MWCNTs with diameters of 40–60 nm were prepared by the catalytic decomposition of methane at 680 °C for 120 min, using nickel oxide–silica binary aerogels as catalyst. The diameter of synthesized CNTs was found to be dependent on the temperature; as the temperature increased, the diameter also increased. The synthesis of SWCNTs was generally optimized under high temperature conditions around 900 °C, while that of MWNTs was optimized under low temperature conditions at around 650 °C. [13]

Care should be taken for the removal of metal catalyst impurities for any method employed to synthesize CNTs, because metals may affect the electro-catalytic properties of the CNTs.

Pristine materials present a high hydrophobicity and a poor dispersibility in water and other common organic solvent,[5] and these characteristics limit their application. Therefore, functionalization plays an important role in providing materials suitable for widespread applications, and also helps in removing any residue of metallic catalyst.

1.2.2 Functionalization of carbon nanotubes: covalent and supramolecular approach

The importance of functionalization initially arises from the need to improve CNT solubility in water and common organic solvents. From the discovery of this class of carbon nanostructured materials (CNM) a huge effort has been taken by chemists to provide different tools for surface modification. The decoration of CNT is based on two different approaches: a) the covalent approach in which new C-C bonds are formed between the sidewall and other molecules; b) the non-covalent approach, based on the formation of supramolecular complexes exploiting weak interactions. The covalent approach is based on the reactivity of sp^2 carbons. Such reactivity is quite impressive if we consider the stability of the benzene ring itself. Even if CNT seems to be composed by fused benzene rings, there are several factors which contribute to increase their reactivity: 1) the closed curved surface cause the misalignment of p_z orbitals, reducing the stabilization of the delocalized π system; 2) the curved surface causes a pyramidalization of the sp^2 carbon atoms and induces an internal strain which partially destabilizes the system. The influence of these contributes depends on the diameter of the tubes. As a result, thin nanotubes are more reactive than large tubes. Analogously to olefins, CNT undergo addition and cycloaddition reactions, and both these classes of reactions have been exploited to introduce new functionalities on the materials.[3,14] Other possibilities for the functionalization are offered from the oxidation of CNT. By

treating the material with a mixture of sulfuric and nitric acid (4:1 or 3:1), under heating or sonication, a deep modification of the material is obtained. The treatment not only introduces oxygenated functionalities, like hydroxy and carboxy groups, but also causes the opening, the curtail of the tubes, moreover removing all the residues of metal catalysts and amorphous carbon. The obtained material is highly dispersible in water and polar solvents, the length and the diameter are shorter than the pristine nanotubes. The introduction of carboxylic groups opens the access for further functionalization exploiting classical chemistry techniques.[14] However, a covalent modification of the CNT, altering the π-system, alters the electronic properties of the material and must be taken in consideration in the case the foreseen application depends onto these characteristics.

On the other hand, the supramolecular decoration does not compromise the electronic properties of the material. This approach uses the hydrophobic or π-π stacking interaction with the sidewall of the tubes. Pyrene derivatives carrying charged groups (usually ammonium, but also sulfate) have been used to disperse pristine CNT in water. Pyrene derivatives were also used to disperse CNT in organic solvents using proper substituents.[14] The most interesting application of a non-covalent interaction was developed by the Tromp group.[15] They reported the diameter-selective separation of CNTs using a pentacene Diels-Alder alkylated adduct able to suspend CNTs in solvents in which they would otherwise be insoluble. Examples of decoration of CNTs, using hydrophobic interactions with molecules that act as surfactant to disperse pristine CNT in water, are also abundant in the literature.[14]

1.2.3 Characterization of CNT-based materials

Characterization of any new substance is fundamental to understand the experimentally observed properties. In organic chemistry all new synthesized substances must be supported by a robust characterization before being accepted by

the scientific community. The role of characterization is to prove the effective structure and composition of the new substances and different techniques are useful to obtain this goal: proton and carbon (eventually also heteroatom) NMR spectroscopy, mass spectrometry, FT-IR spectroscopy, elemental analysis. Cross-checking these data allows to claim a supposed structure for an organic compound. Unfortunately, most of these techniques cannot be applied to CNTs - nor to other nanomaterials – with the exception of FT-IR and elemental analysis. Only techniques which work on solid state can be successfully used, mainly because of the difficulty to obtain a homogenous solution.

Looking at new materials, the characteristics which are required to be determined are morphology, chemical composition and structure. Morphology can be determined using microscopy, atomic force microscopy (AFM), transmission electron (TEM) and scanning electron microscopy (SEM), commonly used to measure dimensions and to assess the macroscopic structure (like aggregates) of the material. The structural characterization is more complicated, because, as mentioned before, none of the classical techniques used for structural analysis can be used. In particular, it is hard to discern between adsorbed and covalently bound molecules, and for this reason it is important, after any reaction on CNTs, to remove carefully all the unreacted reagents by thorough and repeated washing of the materials, followed by drying them under vacuum and at high temperature. The structural determination is a stepwise process, changes are evidenced by comparing the results of an analysis before and after the functionalization reaction. The parameter which are considered are: variation in the thermogravimetric profile (TGA), variation in the functional groups (FT-IR), variation in the elemental composition (elemental analysis CHN, or Ion coupled plasma atom emission spectroscopy), variation in UV-Vis absorption or fluorescence emission. Information on the chemical state of atoms on the material surface can be obtained by XPS analysis. In case of covalent functionalization of SWCNTs, Raman spectroscopy can provide an estimation of the number of new defects, by measuring the ration between the G and D bands.[16,17] This technique can discern the electronic structure of atoms

giving different signals, and allowing to disclose modifications on the atomic scale. As for organic molecule, it is necessary to cross-check different analyses to confirm the effective functionalization of the material.

1.2.4 Toxicity and asbestos fiber paradigm

The growth of interest of scientists for these fascinating materials goes aside with the growth for concerns about their toxicity due to their similarity with the asbestos fibers. Many studies have been published evaluating the *in vitro* and *in vivo* toxicity of CNTs. However, only the *in vivo* studies can provide information about the biological interaction with living organisms. This evaluation is furthermore complicated by the heterogeneity of the samples, which resulted in conflicting evidence for carcinogenicity of CNT in rodents.[18] At the moment only one commercially available type of CNTs, namely *"MWCNT-7"*, were classified as possible carcinogenic to humans by the International Agency for Research on Cancer (IARC).[19] This classification was based on rodent carcinogenicity studies using MWCNT-7 samples, which are long (5.7 ±0.49 µm), large-diameter (40-90 nm), rigid multiwall tubes delivered by intraperitoneal or intrascrotal injection.[20,21] Other studies, carried out on rats tested with different samples of MWCNT (average diameter and length 11 nm and 0.7 µm respectively) with different levels of structural defect, showed opposite results, with no evidence of induced mesotheliomas over two year.[22] After the IARC evaluation, Rittinghausen *et al*. published a more extensive rat peritoneal assay using different type of CNTs with similar results: long, rigid multiwall carbon nanotubes were more potent than thinner, flexible or curved carbon nanotubes in inducing mesothelioma.[23] The hypothesis on the mechanism of carcinogenicity are multiple, but according to the fiber pathogenicity paradigm, long, rigid nanoparticles are likely to induce frustrated phagocytosis, impaired clearance from lungs and pleura which leads to a persistent inflammation and subsequently carcinogenicity.[24] The effect of functionalization on the biocompatibility

of CNT was also investigated for both SWCNT and MWCNT. Kagan et al. demonstrated that short oxidized SWCNT can be degraded by human myeloperoxidase (hMPO). The results were supported by blocking experiments using inhibitors of the enzyme.[25] Similar results were also reported by Bianco and coworkers: using OxMWCNT and functionalized OxMWCNT, it was observed a reduction of length in the order of 10 to 27% depending on the decoration of the functionalized materials.[26] The degradation was also observed on macroscale by Mata et al. They reported the biocompatibility and biodegradation of functionalized MWCNT-membrane *in vitro* and *in vivo*.[27] Similar results were reported by Bianco and coworkers which observed degradation of f-MWCNTs internalized in microglial cells (**Figure 4**).[28]
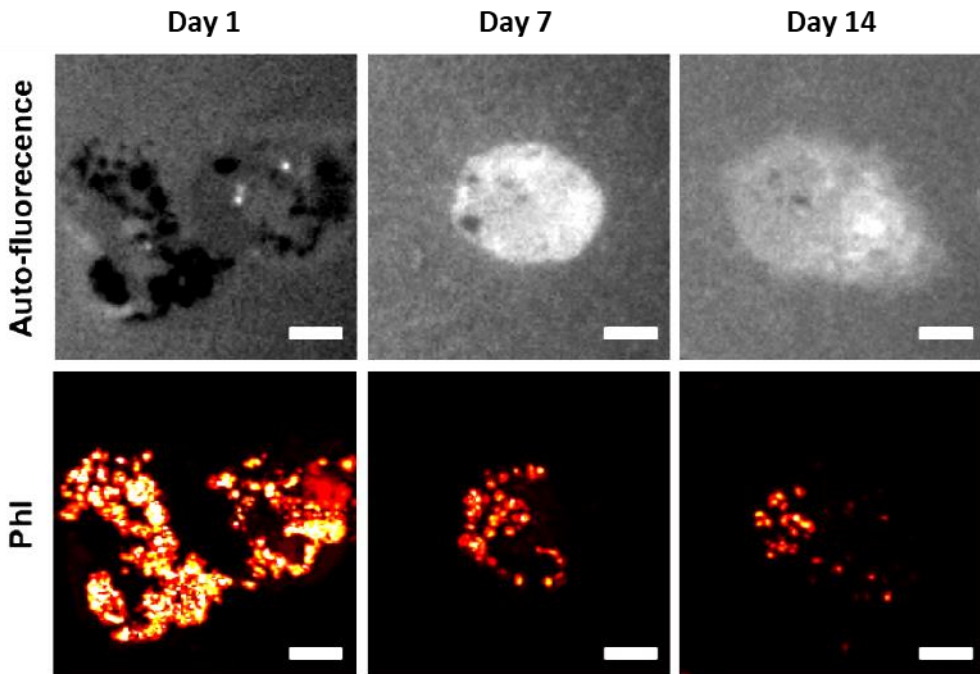
Figure 4. Direct visualization of *in vitro* degradation of *f*-MWCNTs internalized in microglial cells, reported by Bianco et al. on *Nanoscale*.[28]

Based on all these studies we can conclude that the toxicity of the CNT is strongly related to their nature and morphological properties. Indeed, it is possible to obtain a biocompatible material by chemical modification of the pristine material by removing any residue of catalyst and increasing its hydrophilicity with an oxidative treatment. Furthermore, the selection of proper dimensions (reduced length and diameter) helps in increasing the biocompatibility.

1.2.5 Cellular internalization of CNTs

Concerns of toxicity not only arise from the structural similarity with asbestos fibers, but also from the early discovery by Prato et al. that CNTs are able to translocate across cell membranes.[29] Different mechanisms for the interaction with cells' membrane have been proposed (**Figure 5**). A possible mechanism is pinocytosis and includes: micropinocytosis (particle > 1 μm), clathrin-mediated endocytosis (120 nm), caveolin-mediated endocytosis (60 nm) and receptor independent endocytosis (90 nm).[30] This pathway seems to be independent from any functionalization, since both covalently modified or non-covalently coated SWCNT are internalized via endocytosis.[31,32] Macrophages, and other immune cells like monocytes and neutrophils, are able to internalize significant quantities of CNT via active phagocytosis without any sign of toxycity.[33] Moreover specifically functionalized CNT are able to directly penetrate the plasma membrane as well as the nuclear membrane.[30] Probably, because of the heterogeneity of CNT samples, all these mechanisms commonly occur simultaneously and the nature of the main uptake process depends on the characteristics of the CNT used.
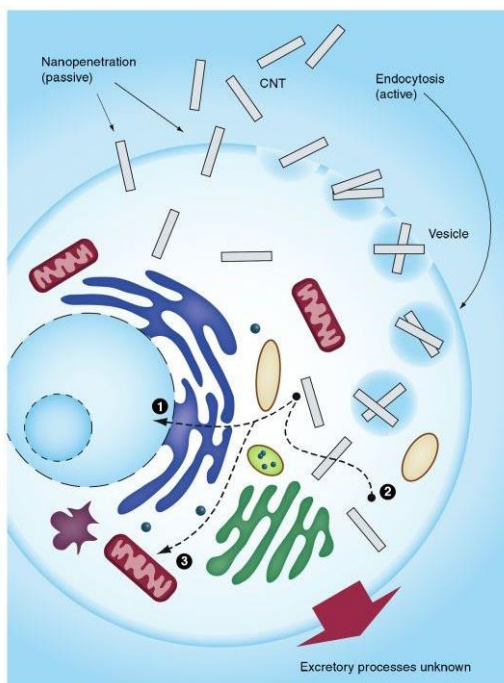
Figure 5. CNTs internalization pathways into cells (Tan, A.; Yildirimer, L.; Rajadas, J.; De La Peña, H.; Pastorin, G.; Seifalian, A. Nanomedicine **2011**, 6 (6), 1101–1114).

1.2.6 Carbon nanotubes as nanocarriers

The ability of CNT to translocate cell membrane together with the versatility of functionalization chemistry paved the way to the design and synthesis of numerous devices in the field of nanomedicine, especially in the field of drug delivery. DDS are usually composed by, at least, three different modules with specific functions: the carrier (the CNT), i.e. the platform on which to build up all the system that guarantees a longer circulation time; the drug, which is the biologically active molecule; and a selector, a molecule recognized by receptors which are overexpressed on the membrane of the target cells. These characteristics are useful to improve the delivery and the efficacy of already known drugs whose application is partially limited by a poor pharmacokinetic profile. Therefore, this class of nanodevices have met the interest of chemists and biologists working in the field of cancer research, and as a result, a lot of

DDS bearing different active compounds were synthesized.[34–36] However, reaching the tumor compartment is only the first step towards a good nanocarrier. While designing the molecular structure of these devices it is important to bear in mind that, once the carrier has reached its target cells, the drug may require to be released in form of free molecule to carry out its biological activity. So it is necessary to consider how the drug payload could be released: this can occur in response to certain stimuli or after an elapsed time. Internal stimuli can be found in changes in temperature or pH, enzyme activity, and redox potential. For example, CNTs non-covalently loaded with doxorubicin (DOX) give a complex which is stable at physiological pH (pH 7.4 with phosphate buffer), but the DOX is rapidly released in mild acidic condition (pH 5.4).[37] Alternatively, artificial stimuli can be provided from external sources, like change in magnetic or electric field or light irradiation.[13] The vast majority of these drug-loaded DDS have been investigated in oncology where their efficacy is even increased by the fact that in the tumor mass, the endothelial tissue is more permeable than in normal tissues. This condition allows increased permeability of the drug carrier into the tumor. This, together with the prolonged blood circulation time provided by the CNT, leads to enhanced permeability and retention (EPR).

Despite the encouraging *in vitro* and *in vivo* results obtained by the first generation of DDS, the research requires an upgrade to keep up with continuous follow-up in the cancer biology. Given the heterogeneity of a tumor mass, cancer researchers and clinicians agree that combination therapy is one of the possible ways to win the fight against cancer. Combination therapy faces several challenges, one of which being that different drugs have different PK pharmacokinetics profiles that not always translate into a synergistic effect. A DDS tries to address this issue. Therefore, producing DDS able to accommodate more than one active compound at same time is highly desirable. In this way, it is possible to translate into nanomedicine a well-known clinical practice: combination therapies (or multimodal treatments), based on the simultaneous use of different therapeutic agents or even therapeutic approaches. Such combinations can

comprise drugs with different molecular targets as well as with the same kind of action. Their synergy could avoid drug resistance and the incidence of relapses. For this reason, many nanotechnological devices have been modified to host such combinations of drugs.[38] The use of a DDS for the delivery of combinations of drugs has the potential advantage, with respect to the classical administration methods, to allow a better control onto the site and time of action, overcoming issues related to the different drugs' pharmacokinetics profile.[38] Examples of multimodal approach are: 1) co-delivery of chemotherapeutics, 2) combined gene and chemo-therapy, 3) co-delivery of immunotherapy, 4) co-delivery of genes, 5) combined chemo- and photothermal therapy.

1.2.7 The fate of CNT-based materials in vivo: an introduction to Biodistribution and Metabolism

The growth of interest for this class of nanocarriers goes aside with the concern about their safety. As mentioned before, some pristine nanotubes have shown to be able to induce mesothelioma after inhalation and in some case even after injection. So, it is obvious that their fate after administration must be considered, in particular their biodistribution and pharmacokinetic after injection (which is the most common type of administration). People working in this field must pay attention on how their devices distribute once they are injected and if the *in vitro* properties are transferred *in vivo*, or if the system is subjected to any modification.

Pharmacokinetic describes how a compound interacts with tissues after administration; pharmacokinetic studies provide information on bioaccumulation in the organs and blood circulation lifetime. Once a foreign object reaches the blood stream, different mechanisms are activated for its elimination. Depending on the nature of the object, different excretion pathways are possible: small charged molecules are reported to be rapidly excreted in the urine through renal filtration,

while large hydrophobic molecules are blocked by the liver and slowly excreted via hepatobiliary pathway. In the case of CNTs, the argument is complicated by the heterogeneity of the sample and, even if only pristine materials are considered, the pool is still wide. CNTs, which are simply dispersed with surfactant, are easily cleared from blood circulation and accumulate in reticuloendothelial system (RES) organs. Tween 80 and Pluronic F108 dispersed ^{13}C-labeled SWCNTs injected in mice showed to accumulate mainly in lung, liver and spleen and only small changes in quantities were found after 28 days.[39] Pluronic F108 dispersed ^{13}C-SWCNT, centrifuged to remove aggregates, are retained into the liver while lung uptake is nearly undetectable using NIR fluorescence.[40] PEG decoration has demonstrated to be a good strategy to increase blood circulation time by shielding from opsonin recognition,[41] however does not prevent the accumulation in the RES organs.[42,43] Changes in the biodistribution profile were obtained using amino functionalized CNT by cycloaddition; in these materials functional groups were directly attached to CNT sidewall.[44] Amino-CNTs were, firstly, reported to be cleared very quickly via urinary excretion, and only small amounts were trapped in kidney, bladder, skin and muscles. However, such results were hardly reproduced, even in the same authors' hands.[36,44–46] The renal filtration was studied by McDevitt and coworkers. They proposed a mechanism by which CNTs would be filtrated by the kidneys. According to these authors the blood flow is sufficiently strong to steer the CNT into the pores, which provides a physical explanation for their rapid clearance into urine.[34,47] It is undoubtable that the pharmacokinetics of CNTs is very important for biomedical applications. There are many parameters regulating the pharmacokinetics of CNT, such as size, charge and surface chemistry. In the case of CNTs, when the length is smaller than 2 µm, they can escape the pulmonary capillary vessels and their pharmacokinetics is mainly determined by the surface chemistry.[48]

Similarly to pharmacokinetics, the metabolism is strongly connected to the nature of the CNT derivatives: dispersed or functionalized. Metabolism can lead to the formation of toxic products, hampering their application as biomedical devices. Unfortunately,

the metabolism of carbon nanomaterials is very difficult to study, because limited analytical techniques able to discern between original material and metabolites are available. The detachment of decorating molecules from both covalently and non-covalently decorated CNT is highly reasonable, and reported results support this hypothesis. In case of non-covalent functionalization, the metabolism is related to the desorption of loaded molecules and the replacement with some plasma proteins, although high protein concentrations are required in case of stable surfactant absorption.[48] In the case of covalently modified CNTs, their metabolism is strictly related to their pharmacokinetic and different stability was reported for PEG-SWCNT in liver and spleen. Liver enzymes were able to slowly defunctionalize the material; on the contrary in the spleen, which is the biggest immunological organ, the material was stable for over 8 weeks.[48]

Metabolism is not limited to the CNT functionalization. Recently the fate of the carbon skeleton has been also investigated. As mentioned before, both oxidized SW- and MWCNT can be degraded by peroxidase: catechol conjugated MWCNT proved to be good substrates for myeloperoxidase (MPO) and other leukocyte peroxidase.[26] Other enzymes were reported to biodegrade CNT: horseradish peroxidase (HRP) and lactoperoxidase (LPO). However all these data were provided by *in vitro* experiment and have to be confirmed also *in vivo*.[49]

To summarize, pharmacokinetics and metabolism are influenced by functionalization and the liver is the prominent organ for their blood clearance. Amine functionalized CNT seems to be the only exception undergoing renal excretion. Metabolism mainly affects the surface functionalization and it is dependent on the type of decoration and on the organ of accumulation. Not surprisingly, covalent functionalization provides higher stability compared to supramolecular loading, the latter undergoing desorption and replacement mediated by plasma protein.

1.2.8 Design of the DDS

When planning the synthesis of a DDS, the first step is the choice of the desired biological activity. As mentioned in the preface, the first goal of this thesis work was the preparation of a nanocarrier able to target both proliferative and stem cancer cells. Hence, two different drugs were selected to achieve this goal. On one hand, targeting the proliferative cells in the tumor mass is quite easy and all the classical chemotherapy drugs are designed for this. Among them, Doxorubicin (DOX) has been elected as gold standard to test the efficacy of our CNT based DDS, because, despite its side effects, it is currently used for treatment of several different types of cancer. DOX belongs to the anthracycline family, its structure is reported in **Figure 6** . Despite the aminosugar moiety, the molecule is highly hydrophobic (logP 0.567).[50] The cytotoxic activity is strictly related to its molecular structure, and in its activity two different pathways are involved: I) the planar structure of the anthracycline intercalates the DNA strain causing the disruption of topoisomerase-II-mediated DNA repair; II) DOX can be oxidized to semiquinone, such unstable metabolite is then converted back to DOX in a process that releases reactive oxygen species (ROS). ROS are known to lead to oxidative stress which triggers the apoptosis pathways of cell death.[51]

Whereas the hydrophobicity-related poor pharmacokinetic can be solved by its formulation as liposome encapsulated drug,[52] its off-target toxicity and the multi drug resistance, that is often observed, are still unsolved problems. The use of CNTs as nanocarriers with proper selectors can help in dealing with both these problems. DOX can be loaded simply by supramolecular interaction with high yields,[53–55] and its release is triggered by acidic pH. These properties allow a good stability during blood circulation and a fast detachment of the drug during the internalization in the lysosome (internal pH ≈ 5.4).[53,55]

Doxorubicin   Metformin
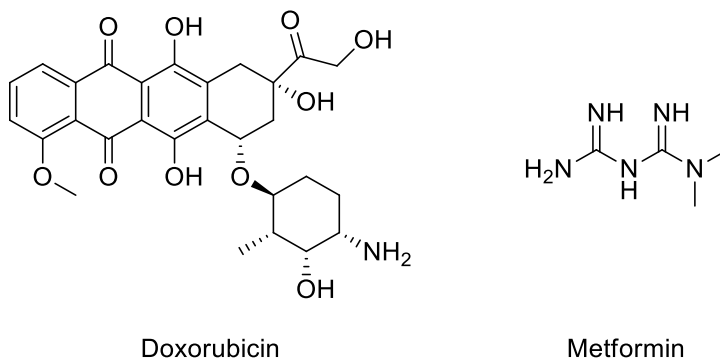
Figure 6. Molecular structures of Doxorubicin (DOX) and metformin (MET)

As the second synergetic drug, we opted for metformin (MET), an already approved drug in type B diabetes' therapy which recently was reported to have antimetabolic properties.[56–58] The mechanism of action of MET as antimetabolic drug is still debated. However, there is a good agreement in the literature on the fact that it is able to inhibit the oxidative phosphorylation (OxPhos) process.[56,59] The biological effect on cancer cells is actuated at mitochondrial level where it seems to inhibit the complex 1 of the electron transfer chain. This action is responsible of the shut-down of the production of energy *via* OxPhos. Interestingly, a sort of synergetic effect was observed when employed in combination with DOX: different authors confirmed the ability of the combined therapy to reduce the tumor mass and to prevent the cancer relapse up to 60 days with different tumor model (MCF-7, MCF-10A, ER-Src, BT-474 and MDA-MB-231).[58,60,61] However, the direct applicability of these therapies is limited by the amount of MET necessary to achieve steady antitumor effect. The millimolar amount of MET required for the inhibition of OxPhos can cause a degree of energy stress (resulting in AMPK activation) in normal cells, and these extremely high doses are not well tolerated in vivo.[57] Despite combination therapy of MET and different chemotherapy drugs have been largely studied, there are only few of MET loaded on CNTs as anticancer DDS. Yoo et al. reported the synthesis and the biological properties of a MET-loaded multimodal DDS based on pegylated OxMWCNTs.[62] Yoo in its seminal work documented the

synergistic effect between MET and light irradiation in killing HepG2 cells and started to address the problem of aggressive doses necessary to observe any cytotoxic effect. Drugs' efficacy can be maximized if the DDS is designed to preferentially accumulate on the tumor mass. To achieve this, a selector is often incorporated into the DDS design. In our DDS, we decided to use biotin as selector to increase the DDS uptake in tumor cells overexpressing biotin receptors.[53,63,64]
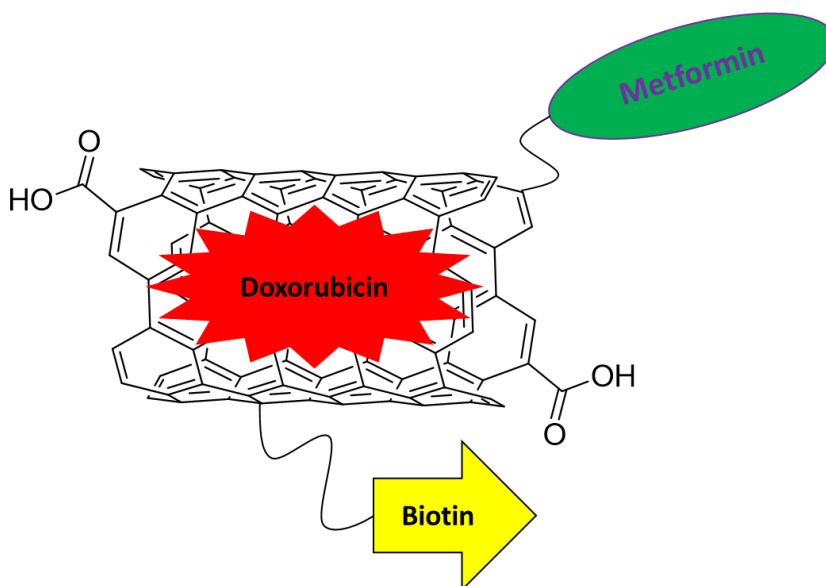
Figure 7. Schematic representation of the multimodal Drug Delivery System

The second part of the design was focused on the planning of a proper synthetic strategy. The introduction of three different modules on CNT required the choice of orthogonal approaches that could maximize the loading of each component. While the decoration with DOX is straightforward, profiting of the π-π interactions with CNT sidewalls, the small dimensions and the polar nature of MET hampered a similar approach and forced us to use the carboxylic groups, present on the oxidized walls of the CNT, to form covalent bonds with MET. Analogously, biotin was covalently linked to the CNT sidewalls with an orthogonal approach developed in our research group.[65,66]

1.3 Discussion

1.3.1 Decoration of the nanostructured platform

The synthetic work started with the preparation of the carrier: pristine MWCNT needed to be treated to increase the water dispersibility of the material and to remove all impurities, like residues of the metallic catalysts and amorphous carbon. Such feature can be obtained through an oxidation process where CNTs are chopped at defect sites and oxygenated functionalities are created on their sidewall and edges. This process requires harsh conditions: concentrated oxidant acids, high energy sonication for prolonged time or heating at high temperatures.[67] To guarantee the highest purity and water dispersibility, MWCNT (diameter 6-9 nm and 5 µm length) were treated with a refluxing 3:1 mixture of concentrated sulfuric acid and nitric acid for 30 minutes. Accordingly to a previous procedure, oxidized material was recovered after quenching with demineralized water, two centrifugation cycles (replacing the supernatant with fresh water) and filtration followed by washing with water until the filtrated solvent was neutral.[65] The OxMWCNTs obtained have an average length ranging from 50 to 1000 nm and are dispersible in water. Considering that, as mentioned above, shorter OxCNTs are more biocompatible than longer ones, and are believed to be more easily internalized by tumor cells, we harvested the shortest fraction using a series of centrifugation cycles (**Figure 8**), (see experimental part for details).[68]
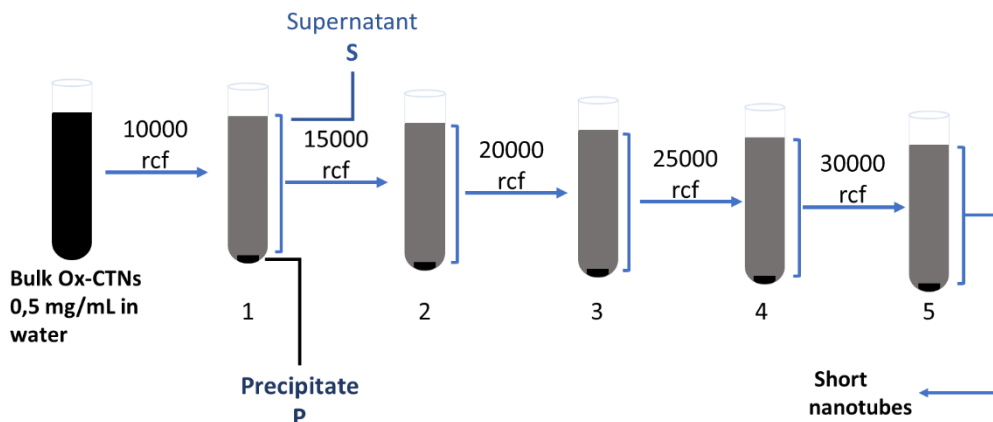
Figure 8. Schematic representation of the separation process.

The procedure allows to collect a fraction with highly oxidized short multi-walled CNTs (from now on called CNTs). The length measured by TEM (**Figure 9**) ranges from 50 to 200 nm with a mean value of 130.
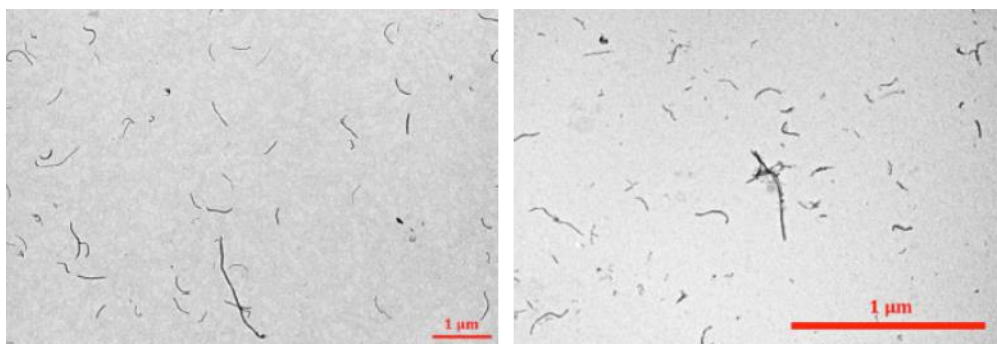
Figure 9.TEM images of CNTs bulk material on the left, collected short fraction on the right.

The synthetic strategy for the decoration of CNT was planned considering the stability of each derivative and the required reaction conditions for each subsequent step. Due to the harsh conditions required for the activation of the carboxylic groups on CNTs, the first component to be loaded was MET. There are many different ways to activate

carboxylic groups: *N*-hydroxysuccinimide or other modern coupling reagents can be used. However, they lack reproducibility when used on CNTs. From our experience, simple chemistry generally performs better with CNTs, and in this case the best and reproducible results have been achieved using oxalyl chloride to convert the carboxylic groups into the corresponding acyl chlorides (CNTs-COCl). The resulting material was directly used in the coupling with MET after removal of the oxalyl chloride excess under vacuum. It is important to keep the CNT-COCl always under inert atmosphere to assure good loading of MET; the reaction (**Figure 10**), repeated three times, showed high reproducibility, with a loading of 1.99 ± 0.01 mmol of MET/g of material **3**, based on elemental analysis. Comparable results were reported by Yoo et al. that covalently decorated CNTs with a similar approach.[62]
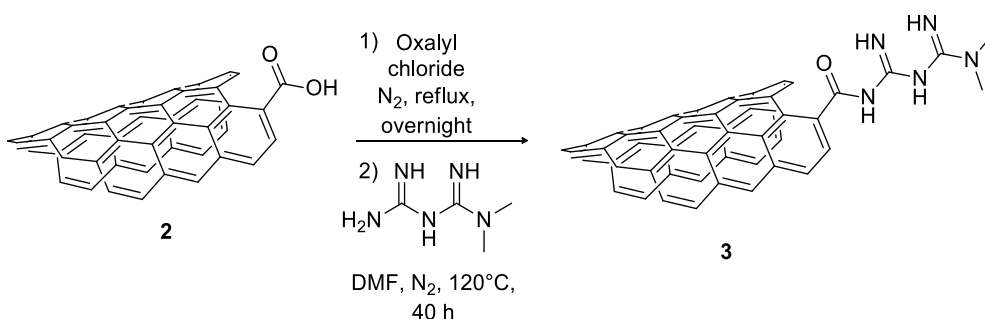
Figure 10. Covalent decoration of CNT with MET to afford **3** (MET-CNT).

Material 3 was the starting point for the addition, to the carrier, of the targeting module. A "click approach" developed in our group, demonstrated versatile, requiring relatively mild conditions and affording reproducible yields.[53] This approach required pre-decoration of CNTs' sidewall with aryl azide groups followed by the real click step (a CuAAC reaction between azides and alkynes).

A simple and highly reliable protocol to insert azide groups on CNT is the Tour reaction.[69,70] The reaction is a radical addition between aromatic diazonium ion and the

sp^2 carbon on the CNTs. The mechanism was elucidated by Schmidt et al. and confirms the radical nature of the process (**Figure 11**). The initiation step follows two possible pathways: the diazonium anhydride, formed by *in situ* Gomberg-Bachmann reaction, can decompose in homolytic cleavage into aryl radical in case of neutral pH (**Figure 11**, a); alternatively, the diazonium ion can be reduced to aryl radical by a single electron transfer from the CNTs (**Figure 11**,b). Then, in the propagation step, the aryl radical can react with CNTs to form the aryl-CNT˙ (**Figure 11**, c), the new radical can regenerate aryl radical through a single electron transfer to diazonium ions (**Figure 11**, d). The chain is terminated when two radicals coupled each other (**Figure 11**, e).[71] The reaction gives access to the *in situ* formation of diazonium ion starting from a *para*-substituted aniline via Sandmeyer reactions.[69,71–73] Moreover different substituted anilines can be synthesized with standard methods, enabling production of a library of functionalities.
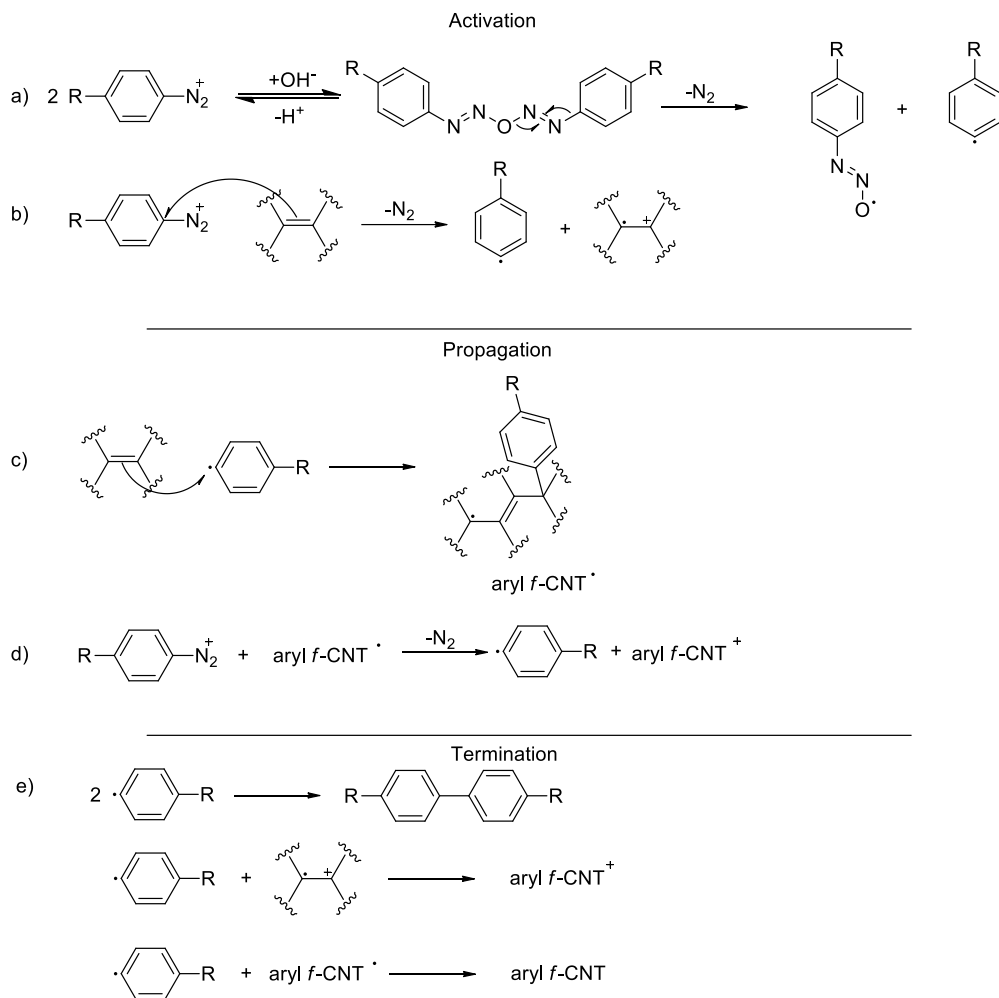
Figure 11. Mechanism of Tour reaction.

We performed the Tour reaction starting from *p*-azido aniline, as showed in **Figure 12**, the Sandmeyerreaction was performed *in situ* using isoamyl nitrite solving all the problems of handling the resulting highly instable diazonium compound. The radical addition can also occur on the benzene ring of the aniline, leading to polymerization products.[74] To remove all the undesired products, material **5** have been washed thoroughly with DMF and methanol and dried accurately under vacuum. The functionalization was confirmed by FT-IR analysis showing a new peak at ~2100 cm^{-1}

diagnostic for the azide group. Elemental analysis confirmed the presence of nitrogen and allowed quantification of the substitution degree (1.7 mmol/g). Material **5** was the substrate for the Copper Catalyzed Azide Alkyne Cycloaddition, a metal catalyzed version of the Huisgen reaction. Thanks to the high reliability and mild conditions required, and easily accessible reagents - azides and alkynes -, this reaction arose at symbol of the "Click chemistry" approach. In our group this reaction demonstrated to be a useful tool for the decoration of nanotubes with different moieties with good yields.[37,66,75] The reaction between MET-CNTs **5** and the propargylamide **6** proceeded smoothly at 60 °C using the organic solvent soluble complex of $CuI \bullet P(OEt)_3$. The binding ability of metformin for copper was considered, and to assure a minimum quantity of Copper available for the catalysis a slight excess of catalyst, respect to the amount of Met on the CNTs, has been employed. The copper salt was accurately removed washing with a solution of 5% ammonium hydroxide in methanol (for all details see experimental section). The loading was evaluated using ICP-AES, the biotin content was found to be 0.28 mmol/g of material **7**.
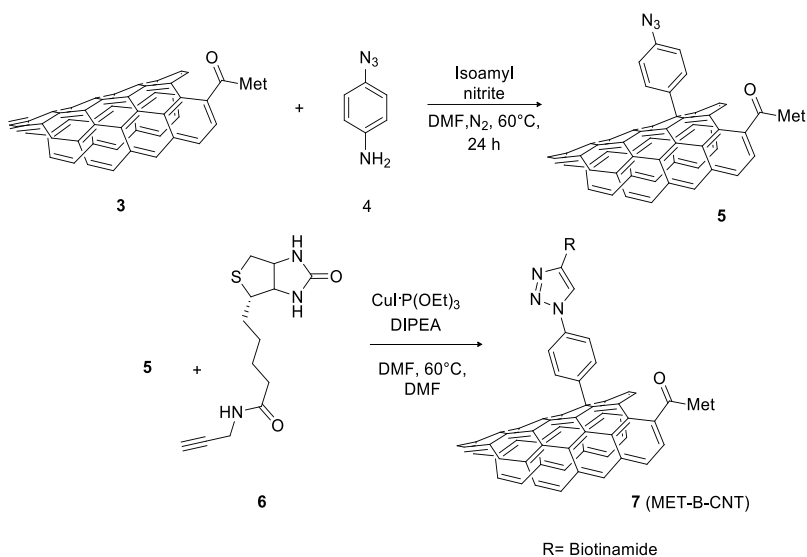
Figure 12. "Click-approach" for the decoration of MET-CNTs to afford MET-B-CNTs

The DDS was then completed with the cytotoxic drug, DOX, exploiting the supramolecular chemistry of CNTs. The supramolecular adhesion is due to the formation of π-π stacking interaction between the anthracycline moiety of DOX and the π-system on the CNTs. The decoration, described in literature,[53] is carried out in very mild conditions: CNTs **7** are dispersed in phosphate buffer at pH 7.4 to leave the amine group on the glycosylic moiety unprotonated. (**Figure 13**). To preserve the integrity of the drug, exposure to sunlight must be minimized and for this reason all vessels were wrapped in aluminum foil during the whole process. The decorated material was recovered by filtration over a polycarbonate membrane and dried under vacuum; the unbound DOX was washed away with fresh phosphate buffer solution. The filtrates were collected and diluted to 100 mL in a volumetric flask, the UV-Vis absorbance of such solution was measured to quantify the leftover of DOX, and, by difference, the amount of loaded DOX (see experimental section for details).
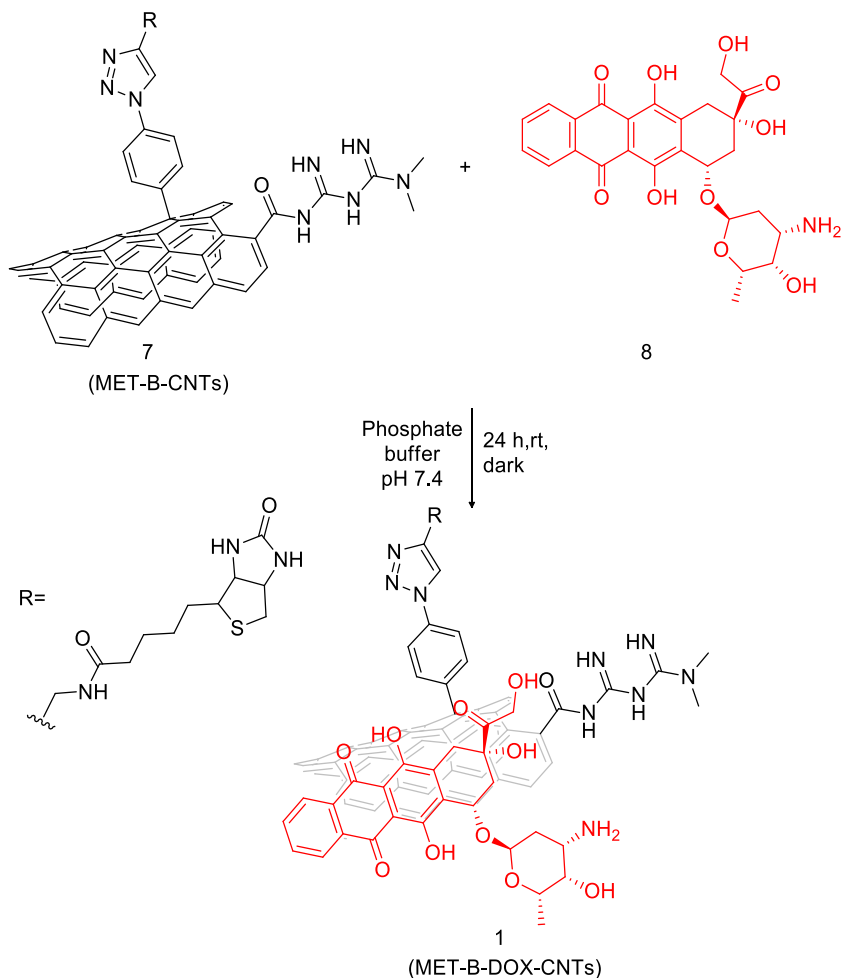
Figure 13. Decoration of MET-B-CNTs to afford the DDS 1.

Complete characterization of DDS **1** is reported in in **Errore. L'origine riferimento non è stata trovata.**, pg 78. DOX loading provided by the supramolecular functionalization is 41% wt. Content of biotin, metformin and doxorubicin are respectively 0.17, 1.2 and 0.75 mmol/g of material on MET-B-CNTs.

1.3.2 Choosing the tumor models: in vitro evaluation of biological properties.

A series of in vitro assays were designed in order to assess the biological behavior of our DDS. We aimed to define the maximum *in vitro* tolerated dose, IC_{50}, toxicity of each fragment, and efficacy toward certain tumor cells. Two cell lines were selected for this study: I) human breast cancer MCF-7 cells, and 2) 4T1 murine cell line as aggressive model of triple-negative breast cancer. Both cell lines are reported to respond to DOX, to be OxPhos dependent and to overexpress biotin receptors.[63,76–78] The evaluation *in vitro* of such models prepares the field for the succeeding *in vivo* experiments, which will be further discussed.

A series of *in vitro* tests were performed to assess the effective biological activity of MET-CNTs, i.e. to assess the effect of the nanocarrier in comparison with each component and adduct **1**. **Figure 14**shows, as expected, that cells were sensitive to free MET at high concentration (ID_{50} for all cell lines around 450 µg/mL corresponding to 3.7 mM concentration).
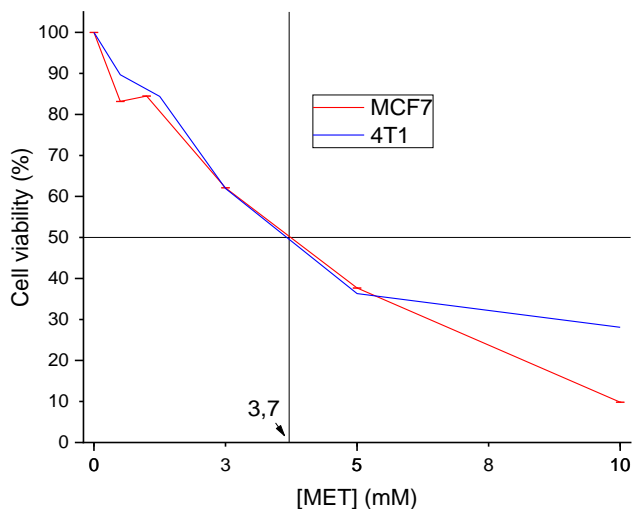
Figure 14. MTT viability assays of MCF-7 and 4T1 cells incubated with different concentrations of MET.

The toxicity of each component of DDS **1** and of DDS **1** itself was, then, evaluated.

Ox-CNTs (**Figure 15**, blue line) were found to be non-toxic for MCF-7 even at concentration of 40 µg/mL, while 4T1 cells showed a modest inhibition of growth at highest concentration. Different toxicity was found for MET-CNTs (**Figure 15**, green line) on the two cells line: MCF-7 cells were found to be more sensitive with and apparent IC_{50} of 20 µg/mL of CNTs, corresponding to 5.1 µg/mL of MET (0.04 mM, almost 100 times more effective with respect to the free MET), but with a cytostasis pattern of drug action. On the contrary, 4T1 cells showed no apparent increase of toxicity with respect to MET-CNTs. Opposite results were obtained for MET-B-CNTs (**Figure 15**, red line): not any increased toxicity was reached on MCF-7 cells, whereas an increase of toxicity around 30% was obtained on 4T1 cells. This result suggests that the internalization in 4T1 cells might be biotin-mediated. However, at least a blocking experiment is needed to confirm this hypothesis. Finally, with complete DDS **1,** the effect on viability of MCF-7 and 4T1 was remarkable. With MCF7 cells, the IC_{50} was 0.7 µg/mL (**Figure 15**, pink line) which is aligned with the IC_{50} = 0.66 previously reported for a DDS not conjugated with MET (corresponding to 0.25 µg/mL of DOX). In 4T1 cells the IC_{50} was higher (IC_{50} = 4 µg/mL of **1**) corresponding to 1.6 µg/mL of DOX and 0.62 µg/mL of MET. In summary, the results reported in **Figure 15** demonstrated that:

I.   CNTs are well tolerated by these two cancer cells;

II.   MCF7 and 4T1 cells show a different sensitivity against MET-CNTs, 4T1 cells being almost insensitive to MET-CNTs;

III.   biotin increases cytotoxicity of MET-CNTs toward murine 4T1 cells, but does not toward human MCF7 cancer cells, suggesting that uptake of MET-CNTs in 4T1 cells might be favored by the presence of biotin linked onto CNTs surface;

IV.   both 4T1 and MCF7 cell lines show a similar sensitivity toward the complete DDS **1**.

Based on these results, we chose to perform *in vivo* pilot studies of biodistribution and efficacy on 4T1 tumor bearing mice. 4T1 is a murine tumor, which allows the use of

immunocompetent mice, therefore enabling to highlight the role of an intact immune system of the biodistribution and metabolic profile of our DDS. In modern oncology, with immunotherapy grown as the fourth pillar in the fight of cancer, the role of the immune system can no longer be ignored when investigating a new drug or a new drug delivery system. 4T1 is also a syngeneic and aggressive model for triple negative breast cancer, a type of cancer that lacks viable clinical options, once patients stop responding to first line chemotherapy.
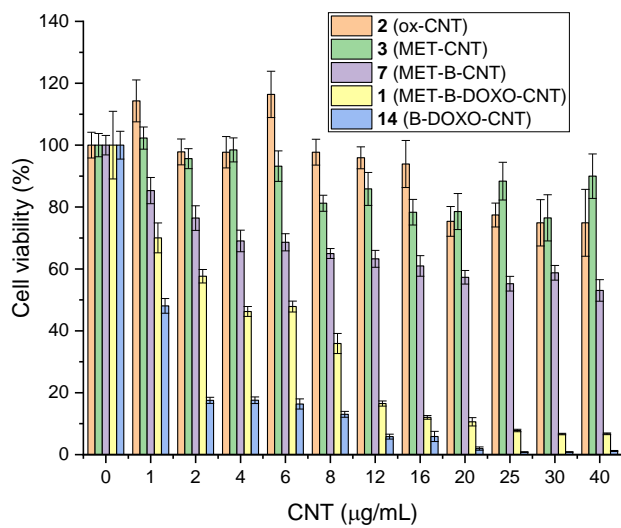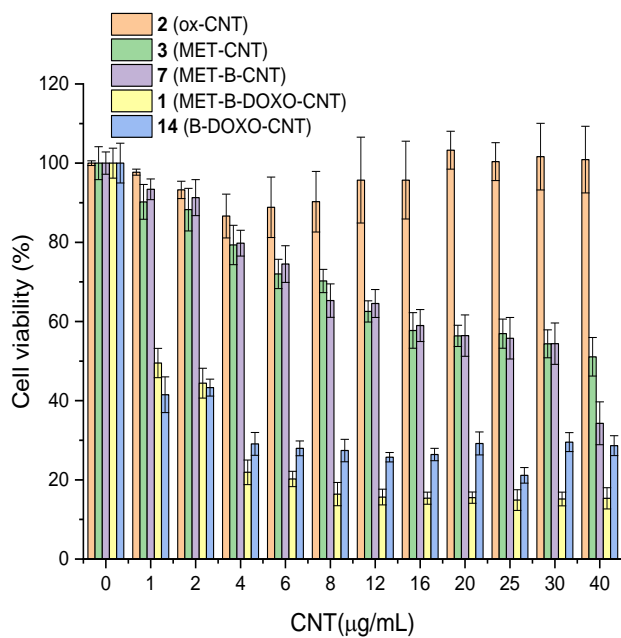
Figure 15. MTT vitality assays of MCF-7 (top) and 4T1 tumor cell lines incubated with different concentrations of **2** (blue), **3** (green), **7** (red), **1** (pink) and B-DOX-CNTs **14** (black).

1.4 Conclusions of Chapter 1

In the first part of the present work, the chemistry of MWCNTs was exploited to synthesize a multimodal DDS bearing a cytotoxic and an antimetabolic drug. The oxidation process, together with the selection of tubes by length, provides a material highly dispersible in water or polar solvents like DMF and THF. The insertion of carboxylic groups opens the route to functionalization using coupling reactions; this was used to load the antimetabolic drug, Met, with high yield and reproducibility. Then, using orthogonal synthetic approaches, which involved formation of both covalent and supramolecular bonds, a selector, biotin, and the cytotoxic drug, DOX, were loaded to complete the drug delivery system. A stepwise characterization protocol (that involved TEM, elemental analysis, ICP-AES, TGA-MS, infrared and UV-vis spectroscopies) allowed the precise quantification of each component. *In vitro* assays were carried out using carefully chosen tumor models to evaluate the toxicity of each component and of the complete DDS. The Ox-CNTs **2** were confirmed to be well tolerated, moderate toxicity was found for Met-CNTs **3** and a biotin receptor mediated internalization was evidenced for 4T1 tumor cell line. By comparison with the free DOX, DDS **1** showed a higher efficacy with a lower IC_{50}. These results encouraged to move on and consider the possibility to extend the study to *in vivo* models. Thanks to the collaboration with the Cancer Systems Imaging Department of MD Anderson Cancer Center of Houston, the biodistribution and the efficacy of DDS **1** in 4T1 tumor bearing mice were studied, and the results will be presented in the next chapter.

2.1 Preface

The second part of this work was focused on the study of the pharmacokinetics and efficacy *in vivo*. Thanks to the collaboration with Prof. David Piwnca-Worms, Chair of the Department Cancer System Imaging at the University of Texas MD Anderson Cancer Center, I had the opportunity to spend 7 months in Houston as visiting PhD student under the supervision of Federica Pisaneschi PhD. In MD Anderson Cancer Center I performed the labeling of our DDS using different radiometals learning how to handle the radioactive material. Moreover, my american Tutors, due to their knowledge of tumor biology, pointed out some critical aspects of the work, such as the evaluation of the target engagement on OxPhos, suggesting elegant experiments to elucidate the question.

2.2 Introduction

2.2.1 In vivo studies

Several different biological properties can be determined through *in vitro* essays: cytotoxicity, cellular uptake, internalization mechanism, and biological pathway exploited for the activity. However, such tests do not take into account the complexity of living organism: biological parameters such as pharmacokinetic and metabolism can change completely the performance observed in the *in vitro* tests.

The evaluation of the properties of DDS **1** was completed with a series of *in vivo* tests:

- Study of the biodistribution via PET/CT with radiolabeled DDS.
- Study of target engagement using [^{18}F]FAZA PET/CT imaging of hypoxia.
- Small pilot study of efficacy.

All the studies were carried out on immunocompetent 4T1 tumor bearing mice. The possibility to use xenograft model was excluded considering that recent studies have

demonstrated the importance of the immune system in the transport and delivery of CNTs.[79,80]

2.2.2 Pharmacokinetic

Different techniques are available for the study of biodistribution of CNTs-based nanocarriers, and they can be divided in two groups: direct and indirect detection.

Direct detection involves techniques for the direct visualization of the CNTs, it is time consuming and gives only a semi-quantitative estimation of the set down dose. It is complicated by the difficulty to visualize CNTs in the tissues unless they occur in agglomerates. Light and electron microscopy are popular methods for the observation of CNTs in tissues, generally are used to support other indirect techniques and to verify the macroscopic interaction of the material with the tissue.[81] Raman spectroscopy is also used to measure the typical inelastic laser light scattering and it is able to detect both individual and agglomerated nanotubes. However, even though the specificity is high, the sensitivity is not always sufficient. A detection limit of 0.04 μg/ml blood (0.2% of the dose/g) and 0.2 μg/ml (1% of the dose/g) in homogenized and solubilized tissues has been reported.[82–84] Another useful technique is the detection of near infrared fluorescence; CNTs, after laser excitation, can emit at 700-900 nm or around 1100-1400 nm. These wavelengths fall in the "biological transparency windows" due to low optical scattering, low autofluorescence and low absorption from hemoglobin and water in tissues.[40,85]

Indirect detection exploits some intrinsic characteristics of CNTs like NIR absorption or fluorescence, alternatively CNTs surface can be modified to add some tag which can be visualized in the tissues. The use of tags increases the sensitivity (especially with the radiolabeling), but, at the same time, adds an important parameter to be considered, the stability of the labeling. This must be determined in harsh and biological-like conditions.

Radiolabeling of CNTs is one of the best strategies to follow the biodistribution after administration. Many different radiotracers exist and are used as probes for the detection of CNTs. The best strategy is to include ^{13}C or ^{14}C in the carbon skeleton. The inclusion in the atomic structure prevents any possible problem of stability, the pharmacokinetic is detected as *C/^{12}C isotope ratio mass spectroscopy. The use of ^{14}C is able to bring the detection limit in the range of pg of material/g of tissue.[86] Also ^{125}I-modified CNTs have been used, however the size and the nature of iodine made the I-C bond more labile than the C-C bond, increasing the risk of the detachment of the radioactive tag.[87,88]Ultimately , it is possible to modify the CNTs surface by covalently binding a bifunctional chelator for labeling with radiometals. This approach has the advantage to be applied at a late stage of a synthetic procedure for the modification of CNTs, but, at the same time, introduces concerns about the stability of the complex itself. Such structures usually possess a remarkable stability *ex situ*, but they may be susceptible to modification by the complex *in vivo* milieu.[82] Nevertheless this approach was used several times to study the biodistribution of chemically modified CNTs. Ligands like diethylene-triamine-penta-acetic-acid dianhydride (DTPA) or 1,4,7,10-tetraazacyclododecane-1,4,7,10-tetraacetic acid (DOTA) have been used to bind, via a co-ordination bond, In-111, [34,44,89,90] Cu-64,[91] and Y-86 [47,92]. In case of labeling with positron (β$^+$) emitters, the biodistribution can be followed using positron emission tomography/computed tomography (PET/CT).

2.2.3 Positron emission tomography (PET)

PET is a noninvasive imaging technique that provides physiological information upon administration of radioactive compounds (radiotracers), detection of gamma radiation, and reconstruction of the distribution of the radiotracer. It is based on detecting two time-coincident high-energy photons from the emission of a positron-emitting radioisotope.[93] As the radionuclide decays, it ejects a positron from its nucleus, which

travels a short distance before being annihilated with an electron to release two 511 keV γ rays 180° apart that are detected by the PET scanner (**Figure 16**).
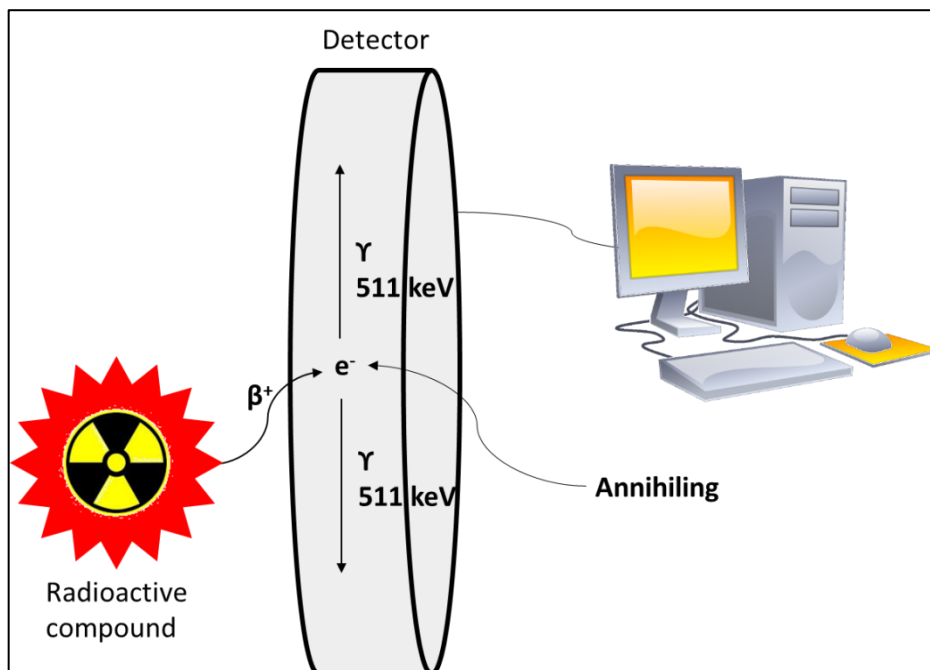
Figure 16. Schematic representation of processes occurring during PET imaging.

After sufficient acquisition time, the data are reconstructed using computer-based algorithms to yield images of the radiotracer's location within the organism.[94] Combining PET imaging with the anatomical imaging delivered by X-ray computed tomography (CT) or magnetic resonance imaging (MRI) provides the synergistic combination of information about the biochemical fate of the radiotracer (from PET) with morphological information (from CT or MRI). The technique has a high sensitivity, it is not invasive as the labeled compound is virtually massless, also allows to follow the initial pharmacokinetic by dynamic scanning as well as the biodistribution at different time-point. An increase of interest toward this technique has been registered after the introduction of radiometals. Traditional PET was confined using radioisotopes such ^{18}F,

[15]O, ^{13}N and ^{11}C whose short half-lives were perfect to study the kinetic of small molecules with rapid clearance. However, they were inefficient in the study of slow clearance targeting agent such as protein, antibodies and nanoparticles. Radiometals, such as Zr-89, Y-86, and Cu-64, display longer half-lives, matching the longer blood circulation times of macromolecules.[94]

2.2.4 Target engagement and ^{18}F-FAZA imaging of hypoxia.

In medicinal chemistry, target engagement is the study of the interaction of a drug with its target. This can be measured directly, or via biomarkers that enable a direct correlation between target engagement and a certain biological phenomenon. Ideally an assay of target engagement would not only verify the extent of the desired drug-target interaction, but also help to determine the drug dose that produces efficacy at fractional target occupancy while limiting side effects that might be caused by complete occupancy. Moreover it should provide information about the off target interactions correlating the toxicity with the *in vivo* selectivity.[95]

In our study, we tried to assess target engagement of Metformin by reading the hypoxic state of the tumor cells via PET/CT with [^{18}F]-fluoroazomicyn arabinoside (^{18}F-FAZA) (**Figure 17**), a known reporter of hypoxia. The method was validated by Gammon et al. and others with different Complex-1 inhibitors.[96,97]
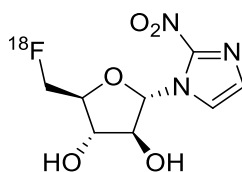
Figure 17. Structure of ^{18}F-FAZA

OxPhos dependent cells tend to be hypoxic because of the over activation of the electron transport chain that eventually overrun the cell's oxygen supply.[98–100] These

cells are likely to trap hypoxia reporters such as FAZA. FAZA trapping mechanism in hypoxic cells is well established. After injection, FAZA equally distributes in normal tissues and tumor (until the compound maintains the oxidized form (**Figure 17**) it is able to pass through cells membrane accordingly to a dynamic equilibria). If the tumor is in a hypoxic state, the subcellular micro-environment is reductive. Intracellular reductase converts the nitroimidazole moiety to hydroxylamine and more reduced nitrogen species, which are eventually trapped by conjugation with intracellular thiols, particularly glutathione GSH.
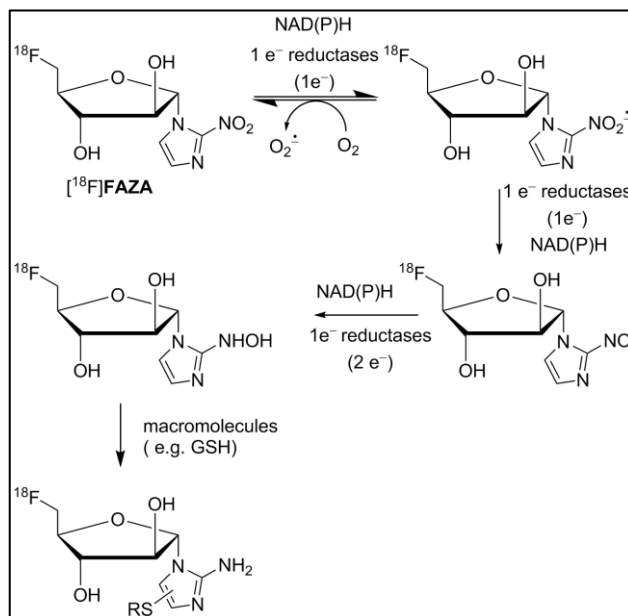
Figure 18. [^{18}F]FAZA reduction mechanism.

These conjugates lose the ability to pass the cellular membrane and the tracer accumulates in the tumor. As a result, the tumor/muscle ratio is greater than 1.

In the presence of an OxPhos inhibitor such as metformin, the electron transport chain is virtually shut down and this translates into re-oxygenation of the tumor mass and, as

a result, loss of FAZA trapping. FAZA can therefore be used as a pharmacodynamic marker for target engagement of OxPhos Inhibitors.

The experiment is generally designed as follow:

1) On day 0, a first PET/CT scan is registered to quantify the hypoxic state in the tumor measured as the tumor/muscle ratio at baseline.

2) Mice are treated with the OxPhos inhibitor after the PET/CT session.

3) On day 1, another [18F]FAZA PET/CT scan is registered.

If the inhibitor goes on target, the hypoxia state is reverted and a more oxidative micro-environment is restored, as a result, the retention of [18F]FAZA decreases and the tumor to muscle ratio measured should be closer to 1.

2.3 Discussion

2.3.1 Synthesis of modified DDS for the pharmacokinetic studies

The biodistribution of DDS **1** was studied using PET/CT and, accordingly with the expected long blood circulation time and with the need to follow the excretion pathway of the system, radiometals were chosen for the labeling. Two different radiometals have been selected for the pharmacokinetic studies: Ga-68 for the short term biodistribution and for the initial kinetic, Cu-64 for long term biodistribution. Of course, the use of radiometals required the introduction on the DDS **1** of proper ligands. NOTA and DOTA were selected to bind respectively gallium and copper ($logk_{LM}$ for the two complexes are 31 and 22.7, respectively).[94] The two ligands were anchored to the system modifying the original synthetic procedure. To achieve this goal, compound **7** was reacted with nitroacetamide **9**, via "Machetti-De Sarlo" reaction,[101,102] yielding adduct **10** with a high loading of protected-amine groups (1.4 mmol/g based on TGA-MS analysis) (**Figure 19**). Then Boc-protecting groups were cleaved under

acidic conditions, and the free amine groups in material **11** were titrated via a semiquantitative Kaiser test (0.129 mmol/g) (see experimental section).[44,103]
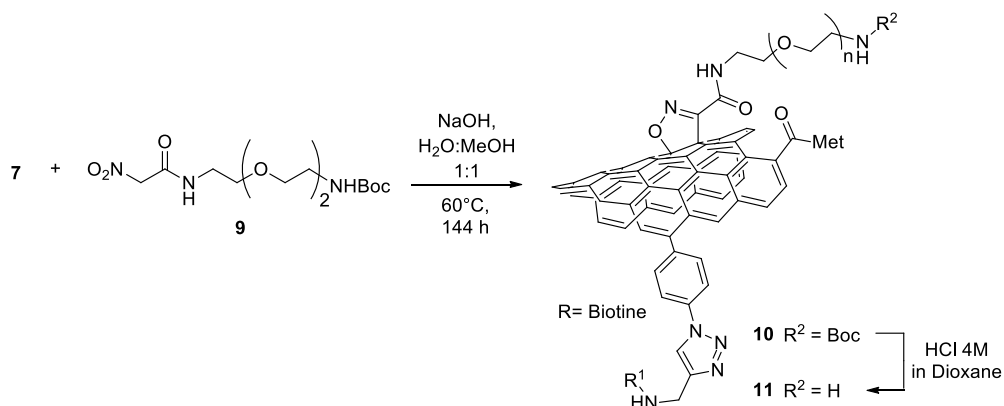
***Figure 19**. Amino decoration of CNTs via "Machetti-De Sarlo" reaction of nitroacetamide **9**.*

Finally, DOTA or NOTA, were bound to CNTs through coupling with the primary amino group. DOTA tri-*tert*-butyl ester was first activated with *N*-hydroxysuccinimide and coupled to compound **11** with a loading of 0.1 mmol/g (TGA-MS), then *tert*-butyl group were cleaved with TFA to restore the chelating ability of the ligand.   NOTA-NCS (Macrocyclics™) was directly coupled to compound **11** with a loading of 0.01 mmol/g (Kaiser test[103]). As for DDS **1**, the last step was the loading and quantification of DOX, following the procedure described above, to obtain DOTA-DDS **12** and NOTA-DDS **13**, respectively (**Figure 20**).
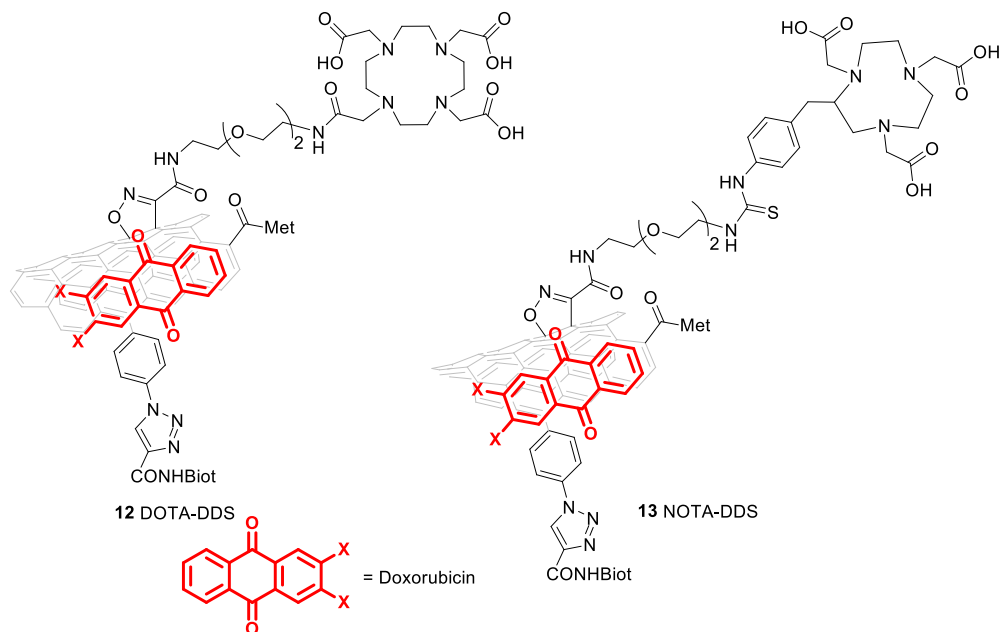
Figure 20. DOTA-CNT (12) construct on the left and NOTA-CNT construct (13) on the right.

2.3.2 Radiolabeling of CNTs-adduct

Radiolabeling using radiometals is a common technique to study the biodistribution of big molecules like proteins and antibodies, nevertheless, as discussed above, only few examples are reported with nanotubes.[104–106] Therefore a new protocol for the labeling of CNTs-adducts was developed starting from classical condition used in the labeling of protein and peptides.

2.3.3 Labeling of DOTA-DDS 12 with Cu-64

*The labeling of the DOTA-CNT with Cu-64 was performed at pH 5.6 in sodium acetate buffer 0.1 M and 37°C for 30 or 60 minutes, with a labeling efficiency higher than 95% (based on Instant Thin Layer Chromatography "ITLC", **Figure 21**). The reaction afforded a material ([^{64}Cu]12) with a high specific activity (814 GBq/g) and a radiochemical yield (RCY) non-decay corrected of 80%. The stability of the complex in PBS was evaluated at 37 °C and the probe was stable up to 48 h. (*

Table 1).

Chelated metal after:	4 h	24 h	48 h
64Cu-DOTA-CNTs	99%	100%	100%

Table 1. [64]Cu**12** complex shelf stability in PBS solution at 37°C.

Since the amount of complexed DOX can be influenced under the labeling reaction conditions, the decrease of complexed DOX was assessed by placing DDS-**12** in the same reaction condition used for the labeling. Aliquots of volume were then collected after 10, 20, 30 and 60 minutes, diluted and the absorbance at 480–490 nm was measured. De-complexation of DOX was about 18% after 1 h of incubation which is believed to have a negligible effect on efficacy, considering the high loading of the drug on the nanotube surface. (see experimental section).
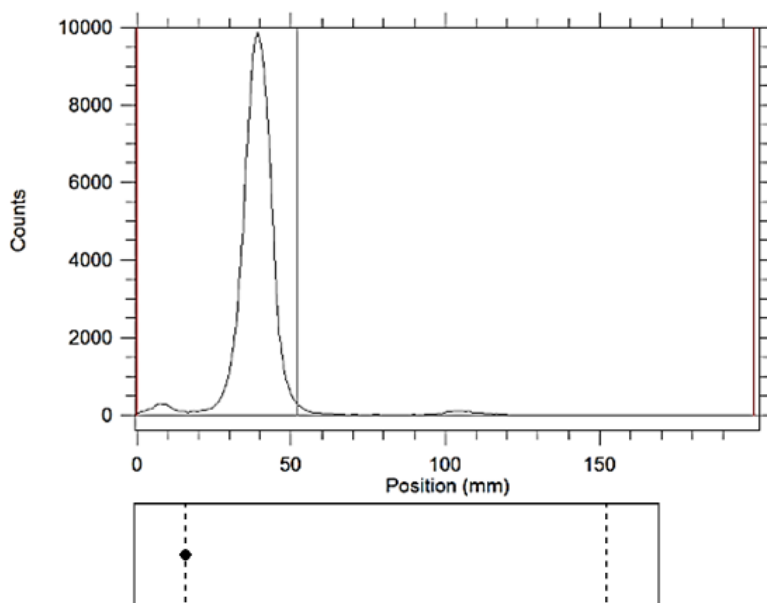
Figure 21. Quality control performed with radioactive ITLC on the labeling reaction of material **12** with [64]Cu.

2.3.4 Labeling of DOTA-DDS 12 with Ga-68

Since DOTA is also reported to be able to chelate Ga-68, a series of experiments was carried out to evaluate the feasibility with our DOTA-CNTs **12**. Classical conditions for the formation of the complex DOTA with Ga-68 are reported in **Table 2**.

Ga solution	Quantity MBq	pH		T °C	t min
Ga in 0.1 M HCl	27-28	4 (1M HEPES)		95	10

Table 2. Commonly used condition for the labeling with Ga-68 and DOTA.[107]

Taking into account that we have DOX on the system the possibility to use such high temperature was excluded *a priori* and the limit set at 37°C (tolerated temperature by the system). Other parameters were varied to find the better condition for the labeling and the results were listed below. Firstly, conditions close to what reported in the literature were tried (**Table 3** entry from 1 to 2a). However, under these conditions only traces of chelated metal were found after 20 minutes of reaction. Such unsatisfying results, together with the increased lability of DOX under these conditions, led us to rapidly abandon this procedure in favor of less acidic pH. The switch to a less acidic buffer (sodium acetate at pH 5.6) immediately increased the amount of complexed radiometal (**Table 3**, entry 3 to 5). At the same time the time-dependent nature of the process was evidenced with a net increase of the yield after prolonged reaction time (**Table 3**, entry 3b). On the other hand, the scale-up of the reaction resulted in a decreased yield (**Table 3**, entry 6). As expected, a positive effect on reaction yield was obtained increasing the amount of DOTA-CNTs **12**, which led to the 50 – 70 % of complexed metal (**Table 3**, entry 8 to 18). Despite the good results obtained under these conditions the amount of free radiometal is still too high to perform any pharmacokinetic study. Different protocols are described in the literature to purify the crude labeled material, McDevitt and coworkers reported the possibility to use size exclusion chromatography.[108] However this technique, which was found to be suitable

on ultra-short SWCNTs, did not give good results on our materials, probably due to the difference in dimension with the reported tubes.

Entry	Ga MBq	CNTs µg/µL	Total Vol. µL	Time min	Buffer NaOAc	Chelated Ga %[*]	Chelated Ga % post sep.[**]	Yield not D.C.
1	24	0.02	250	10	pH 4	0	-	-
1a	24	0.02	250	20	pH 4	11	-	-
2	10	0.15	250	10	pH 4	0	-	-
2a	10	0.15	250	20	pH 4	11	-	-
3	5.5	0.15	250	10	pH 5.6	61	-	-
3a	5.5	0.15	250	20	pH 5.6	61	-	-
3b	5.5	0.15	250	30	pH 5.6	70	-	
4	24	0.15	250	10	pH 5.6	51	-	-
4a	24	0.15	250	20	pH 5.6	56	-	-
5	18	0.2	250	10	pH 5.6	50	-	-
6	5	0.2	2500	10	pH 5.6	27	-	-
7	24	0.25	150	10	pH 5.6	54	-	-
8	18	0.43	175	10	pH 5.6	40-60	-	-
9	18	0.43	175	10	pH 5.6	68	91	17
10	11	0.43	175	10	pH 5.6	58	85	13
11	5.6	0.43	175	10	pH 5.6	70	95	23
12	22	0.43	175	10	pH 5.6	55	85	13
13	9	0.43	175	10	pH 5.6	70	95	27
14	33	0.41	925	10	pH 5.6	65	97	12
15	19	0.19	775	10	pH 5.6	72.5	97	12
16	14	0.23	320	10	pH 5.6	50	94	20
17	7	0.23	320	10	pH 5.6	60	93.5	19
18	9.4	0.43	175	10	pH 5.6	64	100	5

Table 3. Labeling condition investigated for the labeling of DOTA-CNTs 12 with Ga-68. Ga-68 was provided as [68]GaCl$_3$ in HCl solution 0.1 M. [*]Chelated metal in the crude mixture after quench with ETDA 0.1 M; [**] Chelated metal after purification via centrifugation cycles.

Alternatively, as suggested by Prato and coworkers,[109] a good compromise between improvement of purity and loss of material can be reached using centrifugation cycles. After several attempts the following protocol was defined:

- Quench with 0.01 M EDTA in PBS 2.4 folds the reaction volume.

- 3 min centrifuge, then remove the supernatant and add PBS.

- 3 min centrifuge, then remove the supernatant and add PBS.

- 3 min centrifuge, then remove the supernatant and recover the labeled CNTs.

The procedure allows to obtain labeled CNTs with purity ranging from 93.5 to 97 % with RCY not d.c. around 20% (**Table 3**, entry 9 to 17). Increasing the number of centrifuge cycle is possible to reach the purity of 100%, but this goes to detriment of the RCY which falls to 5% (**Table 3**, entry 18). Experimentally it was observed that the use of more concentrated EDTA solution (0.1 M) causes loss of radioactivity: the reason can be found in the $logK_{ML}$ of EDTA-Ga complex which is slightly greater than $logK_{ML}$ of DOTA-Ga leading to trans-chelation with the excess of EDTA. In summary the results reported in **Table 3** suggest that:

1. The labeling with Ga-68 using DOTA-decorated CNTs can be successfully done using *ad hoc* conditions: pH 5.6, T 37°C, 10 min and CNTs conc. of 0.43 mg/mL with a maximum volume of 925 μL.

2. Centrifuge cycles are a good tool to purify the crude mixture.

3. The use of concentrated EDTA ($\geq$ 0.1 M) in the work-up causes the loss of radioactivity.

4. Three centrifugation cycles are the best compromise to obtain labeled CNTs with good purity and RCY.
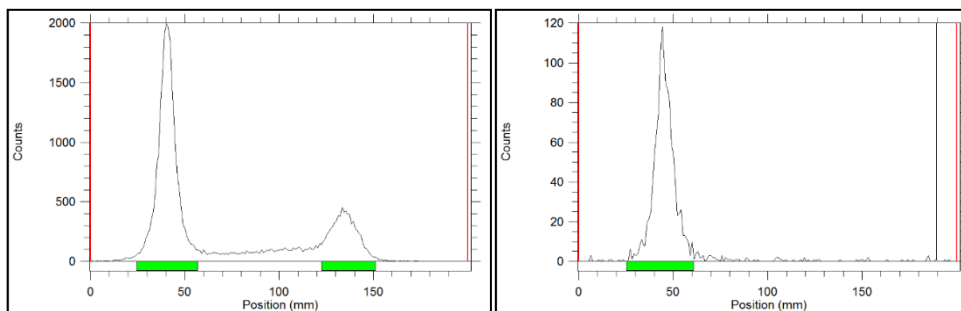
Figure 22. Quality control via radioactive ITLC on the labeling reaction of material **12** with Ga-68: on the left crude mixture and on the right after repeated centrifugation cycles.

2.3.5 Labeling of NOTA-DDS 13 with Ga-68

Given the low radiochemical yields obtained, which would have prevented the feasibility of the *in vivo* studies, NOTA-CNT **13** was used for the labeling with Ga-68. This ligand is able to provide high metal loading even in mild conditions, because the $logK_{ML}$ with gallium is ten-fold higher than DOTA.[94] Labeling of NOTA-CNT to afford [^{68}Ga]**13** complex proceeded at 95–100% at 37 °C and pH 5.6 after 10 minutes (ITLC quality control **Figure 23**). The final RCY (non-decay corrected) was 65% (see experimental section).
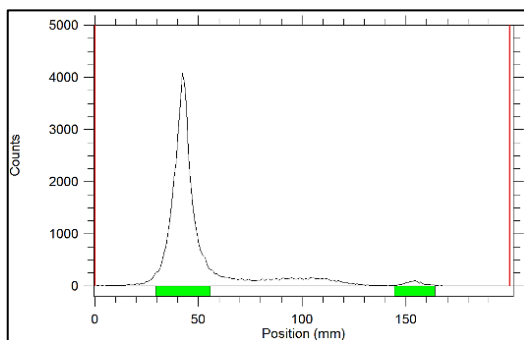

Figure 23. Quality control via radioactive ITLC on the labeling reaction of material **13** with [68]Ga.

2.3.6 Radiosynthesis of [^{18}F]FAZA 14

The radiosynthesis of [^{18}F]FAZA was performed on General Electric Medical System (GEMS) TracerLab FX$_{FN}$ automated synthesis module, following a procedure reported in the literature (**Figure 24**).[110,111] Such equipment allows to complete the full synthesis included the semipreparative HPLC purification in short time (50 minutes) providing high radiochemical yield (≥ 27% not decay corrected) and purity (greater than 99%). Moreover the use of an automatic module strongly reduces the exposure time to the radiation accordingly with the ALARA (As Low As Reasonably Achievable) principles.[112]

The synthesis starts from the commercial precursor 1-(2,3-diacetyl-5-tosyl-(α-D-arabinofuranosyl)-2-nitroimidazole, the tosylate group is replaced by the [^{18}F]fluoride in a nucleophilic substitution, then the hydroxy groups were deprotected under basic condition. After quench with KH$_2$PO$_4$ solution the product was purified via semipreparative HPLC (C18 column) recovering the pure [^{18}F]FAZA.
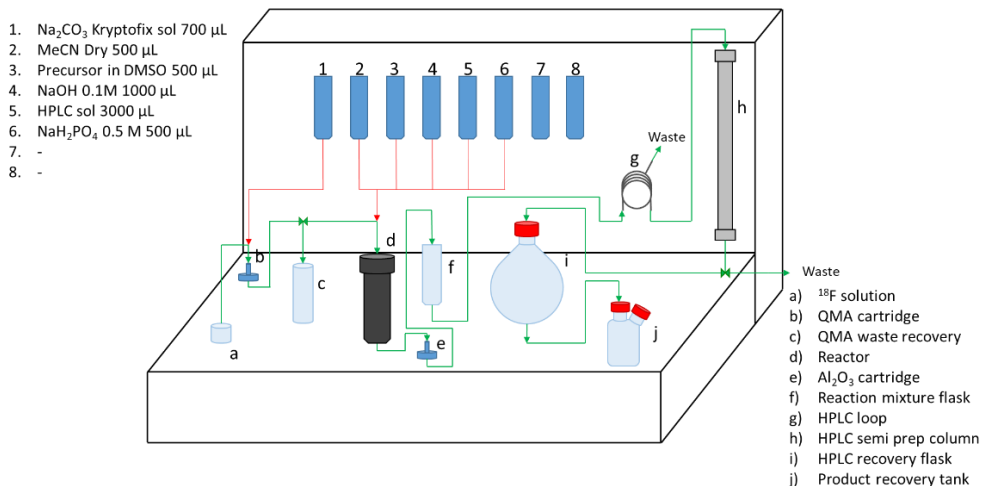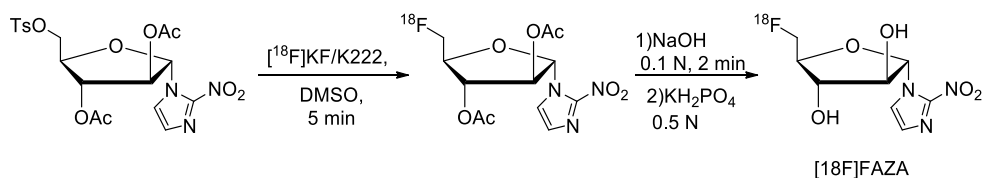
Figure 24. Schematic representation of GE tracerlab equipped for the [18F]FAZA synthesis. Green line indicates the radioactivity flow and the red line the flow of other reagents.

2.3.7 Metabolism of Labeled CNTs

One of the concerns about new drugs and DDS is their stability in living organisms. The study of metabolism of a certain molecule *in vivo* is necessary to assess if any transformation occurs after administration. This is usually done by HPLC analysis of blood and urine samples. The presence of a radioactive tag allows the identification of

traces of material, using a gamma counter detector, with high sensitivity and the chromatographic separation allows to identify any possible metabolite. However, the assess of the metabolism of CNTs is not so trivial; the impossibility to run CNTs on the chromatographic column denies application of HPLC for analysis of possible metabolites. We resolved to analyze our biological samples by ITLC analysis. This enables clear assessment of the stability of the radiometal complex, but did not provide information on the integrity of the DDS.

The *in vivo* stability of [^{64}Cu]**12** and [^{68}Ga]**13** complexes was measured 1.5 h post injection (**Table 4**). Blood and urine samples were analyzed by radio-TLC in order to assess the amount of circulating free metal. Only 11±14 % (n=4) and the 24±6 % (n=3) of free metal were found respectively in blood and urine for [^{64}Cu]**12**. [^{68}Ga]**13** showed a lower stability with 37±17 % (n=3) of free metal in blood. These data indicate a stability in line with other CNT-radiometal complexes reported in the literature.[44,94] More importantly, the high stability of [^{64}Cu]**12** validates the use of PET/CT to assess the biodistribution of the nanomaterial.

[64]Cu	Blood % of chelated metal	Urine % of chelated metal
Mouse 1	100	-
Mouse 2	100	83
Mouse 3	72	71
Mouse 4	83	75
Mean	88.75	76.33
stdv	11.90	4.99

[64]Ga	Blood % of chelated metal
Mouse 1	70
Mouse 2	57
Mouse 3	43
mean	56.67
stdv	11.03

Table 4. Percentage of chelated metal in blood and urine of [64]Cu**12** and [68]Ga**13**, measured by radioactive ITLC.

2.3.8 Biodistribution and PET imaging

The *in vivo* biodistribution of the nano-materials was evaluated by PET/CT at short and long-time points, with the short-live isotope Ga-68 and long-lived isotope Cu-64 respectively. A second study was then performed to elucidate the impact of the injection methods on the distribution of the materials. For the first study, seven Balb/c mice were inoculated with 4T1 cells in the right mammary fat-pad. Two weeks post inoculation, when tumors were palpable, the cohort of mice was divided into two groups: the first group (n=3) was imaged with [^{68}Ga]**13** and the second group (n=4) with [^{64}Cu]**12**. Both probes were injected intravenously (*i.v*). For the first group, the PET/CT protocol comprised a dynamic PET scan of the first 10 min, followed by 15 min of whole-body CT scan. The same protocol was applied for 1.5 h and 3 h time points. The second group was imaged following an analogous PET/CT protocol, and adding 24h and 48h time points.

The biodistribution profile at early time points suggests an early renal clearance (5% ID/cc) probably of the free metal. Radioactivity in the heart, used as estimation of the amount of radiopharmaceutical in the blood pool, was less than 10% ID/cc after 3 h, proving the modestly fast blood clearance already observed by others. The higher uptakes are in the liver (30% ID/cc) and lungs (15% ID/cc), confirming a behavior commonly observed for nanoparticles.[82] The uptake in the liver might be caused by Kupffer cells retention, but proof lays beyond the scope of this study. In addition, McDavitt *et al.* demonstrated that liver sinusoidal endothelium plays a crucial role in the CNTs retention and decomposition.[90] The spleen (9% ID/cc) also retained significant activity, while minimal retention was observed into the muscles. Tumor uptake was around 1.5% ID/cc and might be the result of the enhanced permeability and retention effect (EPR) plus a small contribution of the biotin. The net biotin contribution may be studied in the future with CRISPR biotin knock-out mice or biotin blocking studies. No

radioactivity was observed in the mice cranial cavity, suggesting that the CNTs are not able to cross an intact blood-brain barrier.
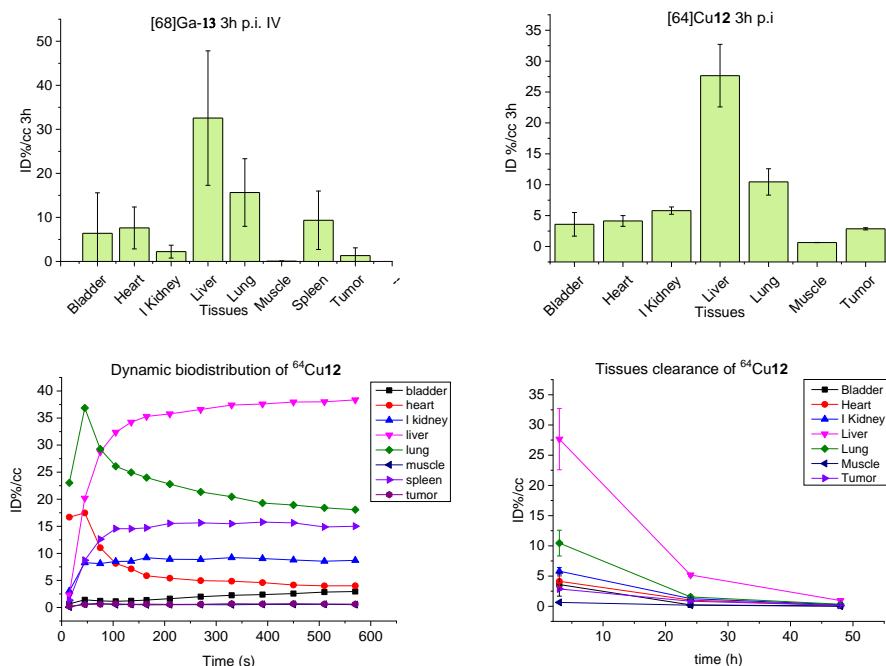
Figure 25. Biodistribution 3h post-injection for [^{64}Cu]**12** (a) and [^{68}Ga]**13** (b); probe retention in the tissues (calculated from PET/CT of ROI) of [^{64}Cu]**12** (c) and its clearance (d).

The 3h post-injection biodistribution was confirmed by the [^{64}Cu]**12** imaging, (**Figure 25**) excluding any metal or ligand dependent effect. The Cu-64 labeled material was taken up mainly in the liver and lungs, similarly to what seen for the Ga-68 labeled CNT; its retention was also similar in the bladder, kidneys and muscles. The blood clearance was fast, with less than 5% in the heart after 3h. The tumor uptake was slightly higher (around 3%). After 24 h, the radioactivity in the tissues dramatically decreased, the activity in all the organs examined was five time lower, with the liver and lungs going from 27% and 10% to 5% and 1.5%, respectively. The tumor uptake remained constant (≈1% ID/cc) for the first 24 hours. At 48h post-injection, the body clearance was almost complete, with activity decreasing to less than 1% in all the main organs. Tumor uptake

was also reduced. Radioactivity was found in the feces, suggesting an hepato-biliary excretion. As an experimental observation, mice looked scruffy after the imaging sessions, but they completely recovered within 2 days, suggesting a good tolerability of the nanomaterial.

2.3.9 Biodistribution with different injections methods

Nine Balb/c mice were inoculated with 4T1 cells in the right mammary fat-pad three weeks prior the imaging session. The cohort was divided in three groups and injected with compound [^{64}Cu]**12**: intravenously (IV), intraperitoneally (IP) and subcutaneously (SC). The PET/CT images were recorded 3 h later by a 10 min PET scan followed by a whole-body CT, 24 and 48 hours images were also acquired. The biodistribution profile with the IV injection was the same to that shown above, with higher uptakes in liver and lungs, and in tumor the retention of the CNTs was 2.7% ID/cc. These results documented day-to-day and batch-to-batch reproducibility. Administration via subcutaneous injection completely changed the pharmacokinetics: diffusion occurred through the lymphatic system, which was reached after a slow permeation from the site of injection. Our experiment showed that labeled-DDS, SC injected, remained at the injection site even after 24 h (**Figure 26**). After 3 hours, only a small amount of the injected material distributed to the organs. The SC administered CNTs were mainly sequestered by the liver (8.5% ID/cc), followed by kidney (3.4% ID/cc), spleen (2.8% ID/cc) and bladder (1.5% ID/cc); the uptake in the lungs was only 1.1% ID/cc. Surprisingly the tumor uptake was around 1.9 % ID/cc suggesting that it was not affected by the reduced circulating material. The extremely low amount in the heart (1.1% ID/cc) and the absence of radioactivity in the muscles confirmed that only a small amount elapsed in the blood circulation.

PET/CT imaging
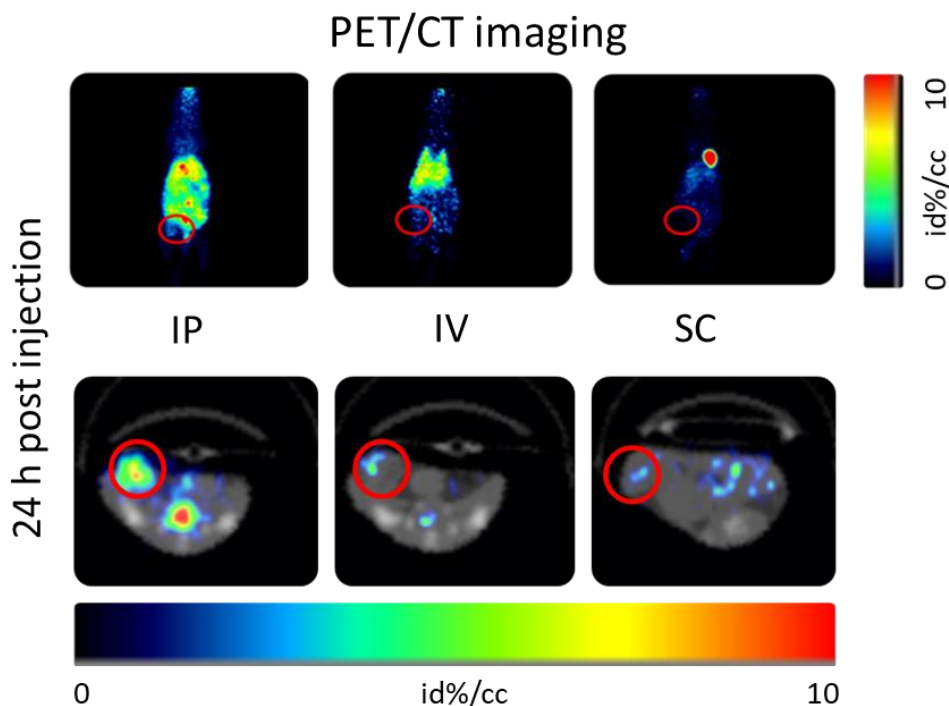
Figure 26. Whole PET imaging 24 h post injection using [64]Cu12 material and different types of injection: subcutaneous (SC), intravenous (IV) and intraperitoneal (IP); red circle indicates tumor position.

The injection in the peritoneal cavity gave a third biodistribution profile, with a strongly reduced lung uptake (3.1 % ID/cc, around 6 times less than with the IV delivery); liver trapping was partially avoided (13.1 ID %/cc) (**Figure 27**). Slightly higher activity was observed in spleen (7.7 %), kidneys (5.9 %) and bladder (3.4 %), suggesting a concomitant renal excretion of the labeled material. The retention in muscles was, as for the other type of injections, close to zero, the tumor showed the highest uptake among all the injection and Bio-D experiments, with an average ID %/cc close to 7%. However, the variance in the data of the IP series is higher than the IV series, as shown by error bars on the tumor uptake, thus reducing its statistical relevance. On the contrary, in the lungs, the difference is undeniable, and the IP injection strongly limited the off-target uptake.

Tissues	IP ID%/cc	STDV
Lung	3,07	0,80
Heart	2,33	0,88
Liver	13,12	4,03
Spleen	7,66	3,23
L Kidney	5,91	2,26
Bladder	3,43	0,87
Muscle	0,50	0,34
Tumor	7,00	3,98

Table 5.[64Cu]**12** retention in different tissues with intraperitoneal injection, mean value and standard deviation (n=3).

Activity after 24 hours proportionally decreased in all tissues as a result of probe excretion. Except for the SC injection, where most of the radioactivity remained trapped in the injection site, no sign of bioaccumulation was evidenced, neither in the IV nor in the IP administration.
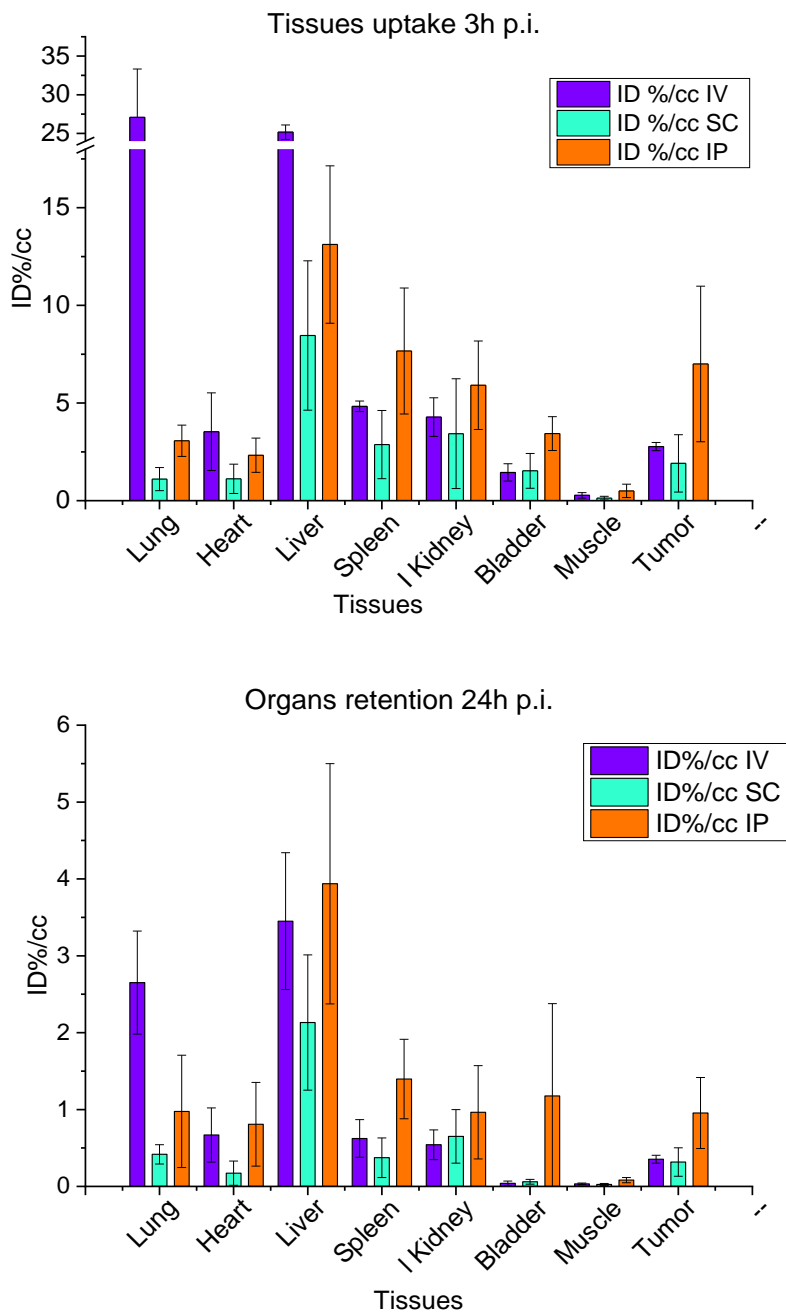
Figure 27. Biodistribution of [64Cu]12 (n=3) after 3h comparing different type of injection; c) Biodistribution of [64Cu]12 (n=3) after 24h comparing different type of injection.

2.3.10 In vivo efficacy evaluation

Fifteen Balb/c mice were inoculated with 10,000 4T1-FLUC cells in the left mammary fat-pad. Two weeks post cell inoculation, tumors were palpable, and the mice were randomly divided into three groups. Tumor sizes were measured via caliper and via bioluminescence imaging (BLI). Given the favorable biodistribution profile which maximizes tumor uptake, i.p. injections were chosen as method of administration of the DDS. The three groups were treated twice a week i.p. with: A) vehicle (PBS solution), B) DDS **1**, 5 mg/kg and C) combination of doxorubicin and metformin (2 mg/kg and 1.29 mg/kg, respectively). Measurements of tumor size with caliper and by BLI suggested that the group treated with compound **1** had an initially slower growth rate (after 2 weeks of treatment) with respect to vehicle and drug combination groups (the overlapping of error bars made these differences not statistically significant). The difference in average tumor size was visible until the third week of treatment when the first mice of vehicle groups reached end point. Between the second and the third week of treatment, an increase of the tumor growth-rate in group B brought the tumor to the size of group C. Within three weeks all mice treated with vehicle reached end-point (**Figure 28 A and B**). Treatment with the drug combination extended the life by 1 week and 2 days in 20% of the mice. The DDS-treated group showed the longest life expectation with the last mouse reaching end-point after 35 days (**Figure 28 C**). Although no long-term survivors were found, DDS **1** was able to increase the intermediate survival and showed improved efficacy compared to the unsupported drugs. During the treatment period, no side effects were observed in the mice treated with the nanotubes; on the contrary, mice treated with the combination of free drugs showed granulation at the injection site.
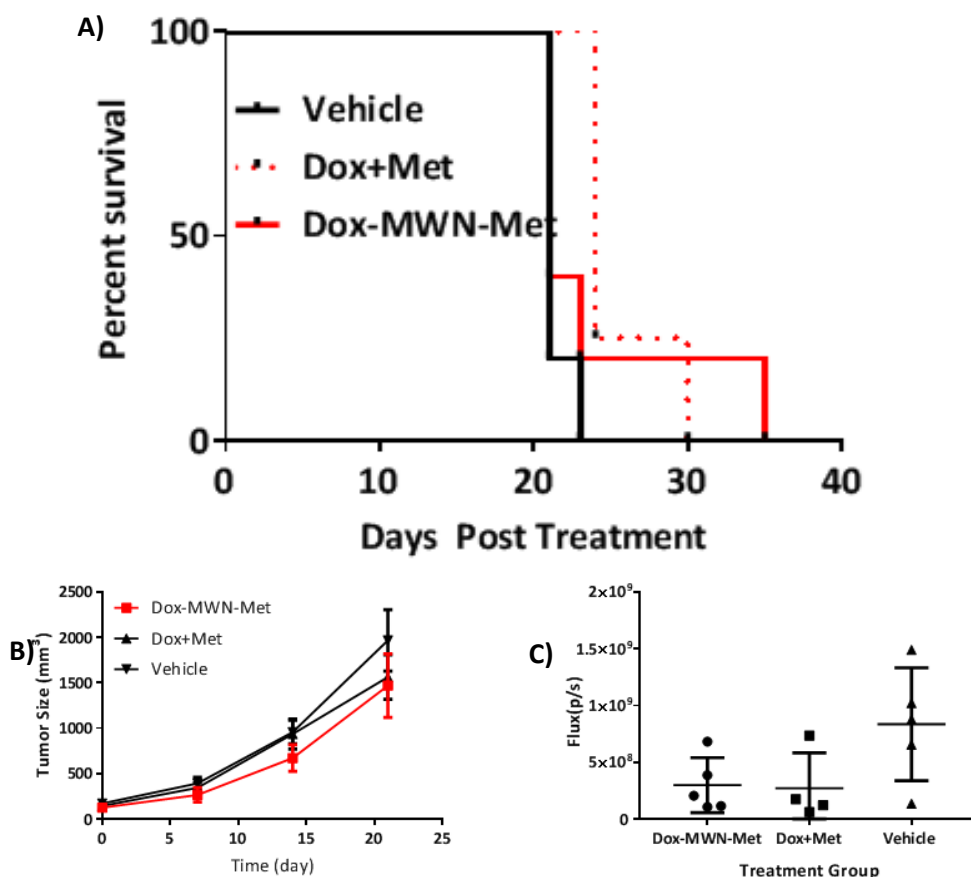
Figure 28. Tumor size comparison at different time points based on caliper measurement; b) BLI measurements of tumors after three weeks of treatment; c) survival curve of the three group of mice treated with vehicle, combination of drugs and DDS 1.

2.3.11 Study of target engagement with [^{18}F]FAZA

FAZA imaging of hypoxia was reported, as discussed above, to be a useful tool to identify hypoxic tumor. This characteristic can be also exploited to evaluate if metformin, inhibiting OxPhos, was able to reverse hypoxic tumor to a normal oxygenated state. Since the hypnotized mechanism of action of Met is, actually, to inhibit OxPhos, FAZA may confirm the target engagement on the 4T1 hypoxic tumor model. Nine Balb/c mice were inoculated with 10,000 4T1-FLUC cells in the left

mammary fat-pad. Three weeks post implantation, tumors were palpable, and the mice were randomly divided into three groups. Tumor sizes were measured via caliper and via bioluminescence imaging (BLI). Firstly, was evaluated FAZA uptake in the tumor, comparing 4T1 with historical data on the A375R melanoma model: the mean values for both cell lines are close, in 4T1 tumor the data are less dispersed than A375R.
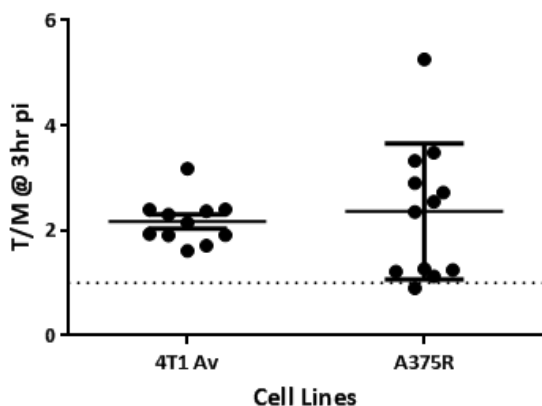

Figure 29. Comparison of baseline FAZA uptake on 4T1 and A375R tumor bearing mice.

The evaluation of target engagement was carried out as follows.

- Day O injection of [^{18}F]FAZA on each group and measurement of tumor to muscles ratio via PET imaging. Then mice were treated with vehicle, DDS **1** 5 mg/kg or metformin 250 mg/kg.

Day 1 injection of [^{18}F]FAZA on each group and measurement of tumor to muscles ratio via PET imaging.
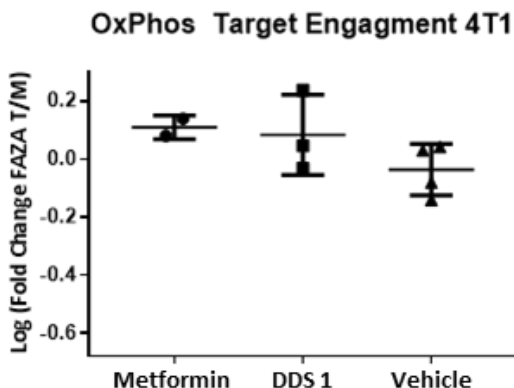
Figure 30. [18F]Faza tumor to muscle ratio at Day 1 .

Data were reported as the fold change of FAZA uptake, expressed as T/M, on Day 1 versus Day 0. A decrease in FAZA uptake, as expected in the event of target engagement, should yield a value <0. Vehicle treated mice should average around zero. As seen in **Figure 30** vehicle treated mice showed no variation in FAZA uptake, validating the experimental data. Unfortunately, neither unsupported Metformin or DDS 1 gave the expected reduction in FAZA uptake (**Figure 30**). The absence of FAZA reduction could be explained by multiple factors. On one hand, the absence of FAZA reduction with free Met did not allow us to validate the experimental protocol. This lack of effect is probably due to the time point chosen for the observation. Met, as most of small molecules, has a fast pharmacokinetic, the highest retention peak is reported after 2 hours, and the body clearance is almost completed after 5 hours through glomerular filtration.[113,114] All considered, it is unlikely that an effect could be seen 24h after administration, when the second PET/CT scan was performed. However, based on our previous pharmacokinetic studies, DD1 was known to have the highest uptake in the tumor 24h post treatment. The 24h time point seemed more logical for a direct comparison.

On the other hand, Met is linked onto DDS1 covalently and, in order to have an effect, it is supposed to be cleaved from the nanosupport and reach the mitochondria where it can exert its inhibitory activity. This might not happen, and the intact DDS1 is unlikely to be able to react the mitochondria and inhibit Complex-1 with its Met load.

Take home lesson is that drugs loaded on these supports need to have a clear release mechanism, otherwise are unlikely to work. This has been taken into account in the design of the second generation of DDS.

2.4 Conclusions of Chapter 2

The second part of this work was focused on the study of pharmacokinetic and *in vivo* efficacy of the multimodal DDS **1**. For these purposes the synthetic procedure for the preparation of the nanocarrier was modified to introduce the ligand necessary for the radiolabeling. The cycloaddition of nitro acetamides was found to be a useful reaction to decorate CNTs without using a metal catalyst. Such condition is particularly important in the preparation of substrates for the labeling with radiometals, because the presence of metal residues, even in traces, could affect negatively the radiolabeling. Using the amine group, introduced with the cycloaddition, DOTA or NOTA functionalized DDS were prepared. A strategy for the labeling using Cu-64 and Ga-68 was developed and fine-tuned, and the effect of the labeling reaction on the Dox, supramolecular loaded, was negligible. The biodistribution was studied on 4T1 tumor bearing mice as function of time and type of injection: intravenous injection provided the classical pharmacokinetic profile observed with nanoparticles, with liver being the main organ of accumulation. The comparison of different probes confirmed the reliability of the results obtained. Subcutaneous injection showed a low efficiency in the biodistribution with most of the tracer stacked in the site of injection, however tumor uptake comparable with the intravenous injection was observed. Surprisingly,

intraperitoneal administration provided a dramatic change in the pharmacokinetic: lung uptake was strongly reduced, also liver accumulation was reduced, and more important tumor uptake was increased.

The efficacy was evaluated on 4T1 tumor bearing mice: this challenging cancer model was selected because it was reported to respond to doxorubicin, to be OxPhos dependent and to overexpress biotin receptors. DDS **1** compared with combination of DOX and Met was able to extend survival of 1 week for the 20 % of mice treated. Even though this result could seem not impressive, it should be stressed that the tumor model is very aggressive and metastatic, generally hard to be treated even with immunotherapy.

Finally, target engagement of metformin with OxPhos Complex-1 using [^{18}F]Faza imaging of hypoxia was attempted, but not successful. This might be due to several facts: Met might not be released promptly from the nanosupport, or Met covalently bound to CNTs might not exert its inhibitory ability, or, finally, the timing of observation was not ideal, given that no FAZA reduction was observed in the group of mice treated with free metformin.

2.5 Summary and final consideration

Achieved goals:

- A multimodal DDS bearing two different drugs (doxorubicin and metformin) and a selector (biotin) was synthesized and characterized.
- The *in vitro* efficacy was studied toward two different cell lines.
- The DDS synthesized was modified to introduce two different ligands suitable for the labeling with Ga-68 and Cu-64
- The labeling protocol was finely-tuned and the effect of the labeling reaction on the DOX was evaluated.
- The pharmacokinetic was studied using PET/CT as function of the radiometal and the type of injection: intravenous, subcutaneous and intraperitoneal.
- The *in vivo* efficacy was evaluated.
- Target engagement on OxPhos dependent tumor *in vivo* was investigated.

Despite that nanomedicine applications of CNTs were extensively studied, there is still room available for further investigation. The results showed in this work sustain the biocompatibility of these materials after opportune functionalization and pose the basis for a second generation of CNTs aimed to overcome the critical issues encountered. We are currently working on the synthesis of a second generation of DDS bearing a highly toxic drug covalently bound to CNTs through a self-cleavable linker. The biocompatibility of our short OxCNTs will be further increased by surface modifications, and high-performance selectors will be loaded to greatly increase the selectivity of the system for selected tumor types. The drug release, the receptor mediated internalization and efficacy will be assessed *in vitro* before moving to the *in vivo* studies.

— Chapter 3 —

3.1 Experimental section

3.2 Materials and Methods

MWCNTs were purchased from Sigma-Aldrich, O.D. x L.= 6-9 nm x 5 μm, carbon > 95%, CoMoCat©, NOTA-NCS was purchased from Macrocyclics Inc. All the other reagents, whose synthesis is not described, were commercially available and have been used without any further purification, if not specified otherwise. R_f values are referred to TLC on silica gel plate (0.25 mm, Merck silica gel 60 F_{254}). NMR spectra were recorded on Varian Gemini 200 MHz or Varian Mercury 400 MHz at room temperature. Chemical shifts were reported in parts per million (ppm) relative to the residual solvent peak rounded to the nearest 0.01 for proton and 0.1 for carbon (reference: $CHCl_3$ [^{1}H:7.26, ^{13}C:77.0], DMSO [^{1}H:2.50, ^{13}C:39.7], MeOH [^{1}H:3.35, ^{13}C:49.3]. Coupling constants *J* were reported in Hz to the nearest 0.01 Hz. Peak multiplicity was indicated as follows s (singlet), d (doublet), t (triplet), q (quartet), m (multiplet) and br (broad signal). IR spectra were recorded on a Perkin-Elmer FT-IR 881 or Shimadzu FT-IR 8400s or Shimadzu IRAffinity-1s spectrometer. IR data are reported as frequencies in wavenumbers (cm^{-1}). Mass spectra were recorded on a Thermoscientific LCQ-Fleet. UV-Vis spectra were recorded on Varian Cary 4000 Uv-vis spectrophotometer using 1cm cell or a BioTeK Synergy H4 microplate reader. Fluorescence spectra were registered on a Jasco FP750 spectrofluorimeter using 1 cm cell. Thermogravimetric analysis (TGA) are run under N_2 atmosphere (50 or 100 mL min^{-1}) on an EXSTAR Seiko 6200 analyzer coupled with a ThermoStarTM GSD 301T (TGA-MS) for MS gas analysis of volatiles. Elemental analyses were performed with a Thermofinnigan CHN-S Flash E1112 analyzer. ICP analysis was made using an Optima 2000 Perkin Elmer Inductively Coupled Plasma (ICP) Dual Vision instrument after acidic mineralization. TEM images were acquired at the electronic microscopy center CNR Florence (CE.M.E.) with a Philip

CM12 with CRYO-GATAN UHRST 3500 technology, digital camera and EDAX microanalysis. Radio-TLCs were run on Instant Thin Layer Chromatography Medium (*i*TLC) chromatography paper (Agilent) and read on an AR-2000 radio-TLC Imaging Scanner (Bioscan Inc.). PET/CT images were recorded on a Bruker Albira PET/CT/SPECT Preclinical Imaging System and reconstructed using an iterative MLEM algorithm. Ga-68 and Cu-64 were acquired as HCl solutions from the MD Anderson Cyclotron Radiochemistry Facility (CRF).

3.3 Synthetic procedures

3.3.1 Oxidation of Multiwalled Carbon Nanotubes

Pristine nanotubes (500 mg) were dispersed in a 3:1 mixture of 95% sulfuric acid and 65% nitric acid (30 mL) and heated at 100°C under stirring for 30 minutes. The mixture was cooled at room temperature and quenched with 130 mL of milliQ water, the obtained solution was centrifuged at 1500 rcf (relative centrifugal force) for 30 minutes, the supernatant was removed, and the precipitate dispersed with milliQ water (130 mL) and centrifuged again. The CNT slurry recovered from centrifugation (still acidic) was filtered on a 0.2 μm polycarbonate membrane and washed with water until neutral pH of the filtered solution. The process provided 200 mg of oxidized material, elemental analysis: C 79.1%, N 0.15%, H 0.62% and O 20.3%. FT-IR showed the C=O absorption peak at 1700 cm^{-1}.

3.3.2 Separation of Oxidized Carbon Nanotubes by length

Bulk oxidized CNT (140 mg) were dispersed using ultrasound bath in milliQ water (280 mL) to obtain a 0.5 mg/mL solution. The solution was centrifuged at 10k rcf for 1h and supernatant and precipitate were collected. The supernatant was centrifuged again at 15k rcf for 1h providing a new precipitate and a new supernatant. The procedure was

repeated using the supernatant other 3 times using different G force (20, 25 and 30 K rcf) as reported in the figure 6. The supernatant of the 30 k rcf centrifuge was dried and 65 mg of material **2** were obtained, the length was measured with TEM (**Figure 31**) giving an average value of 130 nm accordingly with the literature.[68]
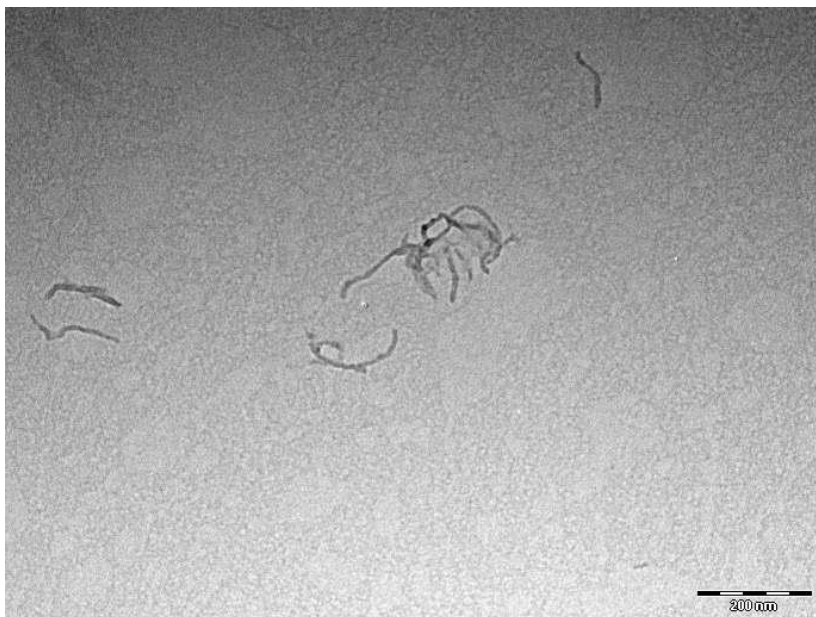

Figure 31. TEM image of short ox-MW-CNT 2.

3.3.3 Synthesis of MET-CNT (3)

Short ox-CNT (**2**) (35 mg) were dispersed in freshly distilled oxalyl chloride (10 mL) under nitrogen. Then the dispersion was stirred at reflux for 24 h, after that the oxalyl chloride was accurately removed under vacuum. The acyl chloride CNT directly dispersed in dry DMF (9.5 mL), using an ultrasound bath, metformin (170 mg) was added to the dispersion and the mixture stirred at 120 °C under nitrogen for 40 h. CNT-MET were recovered by filtration over a 0.2 μm nylon membrane washing several times with DMF and methanol to remove the unreacted metformin. Metformin loading ranged from 1.8 to 2 mmol/g as evaluated from elemental analysis on three different samples.

### 3.3.4 Synthesis of 4-azidoaniline (4)
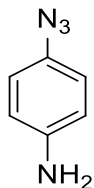
Compound **4** was synthesized from 4-bromoaniline in quantitative yield following a procedure reported in the literature.[115]

3.3.5 Synthesis of MET-N$_3$-CNT (6) (Tour reaction)

Material **3** (20 mg) was dispersed in dry DMF (2 mL) and sonicated for 15 minutes, then 4-azidoaniline (61.5 mg, 0.46 mmol) and isoamylnitrite (38.6 mg, 0.33 mmol) were added and the mixture stirred at 60°C under nitrogen for 24 h. CNT **5** was recovered by filtration on a 0.2 µm nylon membrane, washing with DMF until a colorless solution obtained and then with methanol to remove the unreacted materials. FT-IR peak at 2100 cm^{-1} confirmed the azide decoration (**Figure 46**).

3.3.6 Synthesis of biotin propargylamide (6)
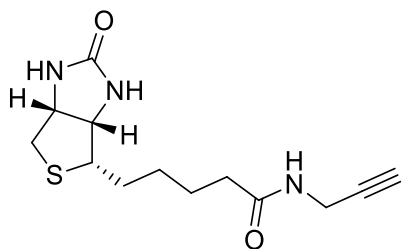
Compound **6** was synthesized accordingly to a procedure reported in literature with a yield of 90%.[37]
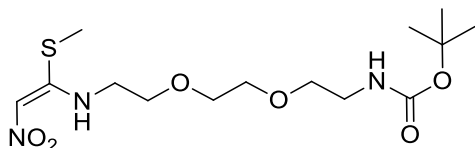
3.3.7 Synthesis of MET-B-CNT (7)

Compound **7** was synthesized from material **5** accordingly to a procedure previously reported. [37] The biotin content was evaluated measuring the sulfur content via ICP-AES, biotin was found to be 0.210 to 0.277 mmol/g on different samples.
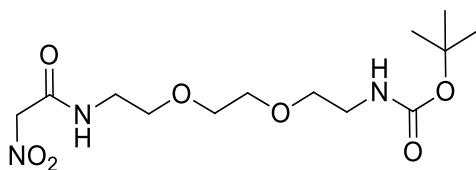
3.3.8 Synthesis (E)-tert-butyl (3-(nitromethylene)-7,10-dioxa-2-thia-4-azadodecan-12-yl)carbamate

1,1-*bis*(methylthio)-2-nitroethylene (798.4 mg, 4.83 mmol, 1.2 eq) and *p*-toluensulfonic acid monohydrate (34.7 mg, 0.202 mmol, 0.05 eq) were dissolved in 40 mL of ethanol and heated at 35 °C. The solution was added with tert-butyl (2-(2-(2-aminoethoxy)ethoxy)ethyl)carbamate (1,00 g, 4.03 mmol, 1 eq) dissolved in 13 mL of ethanol and the mixture stirred at 35 °C for 72 h. The resulting methyl thiol, developed during the reaction, was removed with a nitrogen flow bubbling through bleach. The solvent was, finally, removed under vacuum and the product recovered after flash chromatography on silica gel. R_f = 0.35 (dichloromethane/ethyl acetate 1:1). ^{1}H-NMR (200 MHz, CDCl$_3$): δ = 10.6 (bs, 1 H, N*H*), 6.57 (s, 1 H, C*H*NO$_2$), 5.5 (bs, 1 H, N*H*Boc), 3.69-3.51 (m, 10 H, 5 x C*H$_2$*), 3.30 (q, J = 6.3 Hz, 2 H, C*H$_2$*NHBoc), 2.44 (s, 3 H, C*H$_3$*S), 1.42 (s, 9 H, (C*H$_3$*)$_3$C) ppm. ^{13}C-NMR (50 MHz, CDCl$_3$): δ = 156.0 (s, *C*O$_2$*t*Bu), 106.6 (d, =*C*H), 79.1 (s, (CH$_3$)$_3$*C*), 70.7 (t, *C*H$_2$O), 70.3 (t, *C*H$_2$O), 70.2 (t, *C*H$_2$O), 68.6 (t, *C*H$_2$O), 44.2 (t, *C*H$_2$NH), 40.4 (t, *C*H$_2$NHBoc), 28.4 (q, 3 C, (*C*H$_3$)$_3$C), 14.4 (q, *C*H$_3$S) ppm. MS-ESI: 388 [M + Na]$^+$. HRMS-ESI: calculated for C$_{14}$H$_{27}$N$_3$O$_6$S 366.16933 [M + H]$^+$, positive ionization measured 366.16973 ± 0.0001 [M+H]$^+$.

3.3.9 Synthesis of tert-butyl (2-(2-(2-(2-nitroacetamido)ethoxy)ethoxy)ethyl)carbamate (9)

Compound **9** was synthesized accordingly to the literature with minor changes.[116] (E)-tert-butyl (3-(nitromethylene)-7,10-dioxa-2-thia-4-azadodecan-12-yl)carbamate (256 mg, 0.7 mmol, 1 eq) was dissolved in 700 μL of a 3 : 1 acetonitrile/water solution and heated at 30°C. Then a solution of mercury chloride (190.19 mg, 0.70 mmol, 1 eq, 1 mL of CH_3CN) was added dropwise and the mixture stirred at 30 °C for 48 h. The reaction mixture was than filtered over celite to remove the solid mercury salts and the product recovered after flash chromatography on silica gel. R_f = 0.32 (ethyl acetate/dichloromethane 2:1). ^{1}H-NMR (400 MHz, CD_3OD) δ 5.20 (s, 2H, CH_2NO_2), 3.66 (s, 4 H, OCH_2CH_2O), 3.63 (t, J = 5.2 Hz, CH_2O), 3.56 (t, J = 5.6 Hz, CH_2O), 3.48 (t, J = 5.2 Hz, CH_2NH), 3.26 (t, J = 5.6 Hz, CH_2NH), 1.36 (s, 9H, *(CH_3)$_3$C)* ppm. ^{13}C NMR (101 MHz, CD_3OD) δ 164.0 (s, C=O), 158.8 (s, C=O), 80.4 [s, (CH$_3$)$_3$*C*], 71.6 (t, *C*H$_2$O), 71.5 (t, *C*H$_2$O), 71.4 (t, *C*H$_2$O), 70.5 (t, *C*H$_2$O), 41.5 (t, *C*H$_2$NH), 41.1 (t, *C*H$_2$NH), 29.0 (q, 3 C, (*C*H$_3$)$_3$C) ppm. IR: 3695 (N-H), 2974 (C-H), 2931 (C-H), 2875 (CH), 1723 (s, C=O, carbamate), 1693 (s, C=O, amide), 1563 (s, N-O), 1603 (w, N-O), 1392, 1255, 1172 cm^{-1}. MS-ESI: positive ionization 358 [M + Na]$^+$, negative ionization 334 [M - H]$^-$. MS-ESI: positive ionization 358 [M + Na]$^+$, negative ionization 334 [M - H]$^-$. HRMS-ESI: calculated for $C_{13}H_{25}N_3O_7$ m/z = 358.15887 [M + Na]$^+$, positive ionization measured m/z = 358.15847 (± 0.0001) [M + Na]$^+$.

3.3.10 Synthesis of DDS 1

The loading of DOX was carried out following the procedure already reported.[37] For characterization see section **4.2**.

3.3.11 Synthesis of material 10

Material **7** (10 mg) and compound **9** were dispersed in a mixture of methanol and water 1:1 (1.2 mL) using an ultrasound bath (15 min). Then 12 μL of 4.24 M NaOH were added and the mixture stirred five days at 60°C. Material **10** was recovered after filtration on a 0.2 μm PC membrane washing with water and methanol to remove all the impurities. Loading of protected amine 1.40 mmol/g based on TGA-MS section **4.5** and **6**.

3.3.12 Synthesis of material 11

Material **10** (10 mg) was dispersed in 4 M HCl in dioxane sonicating for 5 min then the dispersion was stirred for 4 h at room temperature. The acid media was removed by precipitating the CNT in centrifuge (15 min at 1500 rcf) and pipetting the supernatant, then the material was re-dispersed in isopropanol and precipitated in centrifuge to remove any residue of HCl. Then to obtain the free amine group the material was dispersed in aqueous 0.01 M NaOH and precipitated in centrifuge using the program described above. Finally the material was washed with isopropanol to remove the NaOH solution and recovered. The amount of free amine group was evaluated with a semiquantitative Kaiser Test, section **4.4**.

3.3.13 Synthesis of DOTA-OSU 15
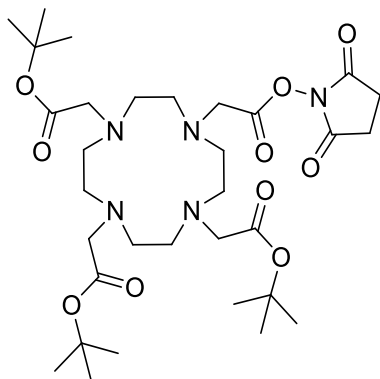
Tri-*tert*-butyl ester DOTA (40 mg, 0.0698 mmol, 1eq) was dissolved in 1 mL of dry acetonitrile, then 5 mg of *N*-hydroxi-succinimide (0.039 mmol, 1.1 eq) and HBTU 14.8 mg (0.039 mmol, 1.1 mmol) were added and the mixture stirred under nitrogen for 24 h. The product purified by flash chromatography on alumina gel (ethyl acetate: acetonitrile 4:1, *Rf* 0.8). Yield 30%. ^{1}H NMR (400 MHz, CDCl$_3$) δ = 3.6 to 2 ppm (serie of broad peaks 28H) and 1.44 ppm (s, 27H *t*-Bu).^{13}C NMR (101 MHz, CDCl$_3$) δ = 173.3 (3C, COO*t*Bu), 173.1 (COON), 169.8 (CON), 82.3 (3C, C$_q$), 55.9 (CH$_2$COON), 55.7 (3C,

CH$_2$COOtBu), 53.2 (2C, CH$_2$ succinimide), 38.7 (4C, CH$_2$N macrocycle) and 28.0 ppm (3C, CH$_3$ tBu). ESI-MS+ m/z= 692.50 [M+Na]$^+$. [117]

3.3.14 Synthesis of DDS 12

Material **11** and DOTA-OSU **15** in ratio 1.5:1 in weight were dispersed in dry, amine free, DMF (900 µL) under nitrogen and sonicated for 5 min. Then TEA was added, and the mixture stirred for 48 at room temperature under nitrogen. Then crude mixture was diluted with 5 mL of methanol and centrifuged for 15 min at 1500 rcf, the supernatant removed and replaced with 15 mL of fresh methanol. The procedure was repeated twice then the solid was washed with 40 mL of a 1:3 mixture of methanol/isopropanol and, finally, isopropyl ether. The products were characterized via TGA-MS. Then t-butyl groups were removed by suspending the product in a solution of trifluoroacetic acid/acetonitrile 2:1 (10 mg/mL conc.) and stirring at room temperature for 5 h. Then the solution was diluted with acetonitrile, filtered over PTFE membrane (0.2 µm pores), and washed firstly with methanol and then with phosphate buffer solution at pH 7.4 to neutralize the residual acidity. Finally, Doxorubicin was loaded as reported in point **2.1** and quantified as reported in point **4.2** and **4.6**.

3.3.15 *Synthesis of DDS 13*

DDS **13** was synthesized with the same protocol of DDS **12** with the exception that NOTA-Bn-NCS (Macrocyclics inc.) was used instead of compound **15**, and the doxorubicin was directly loaded on the coupling product . For characterization see point **4.2** and **4.6**.

3.3.16 Synthesis of DDS 14

DDS **14** was prepared according to a previously reported protocol[68] starting from short ox-CNT. For characterization see point **4.6**.

3.4 Radiochemistry

3.4.1 Formation of the ^{68}Ga-NOTA-CNTs-MET complex

^{68}Ga eluate (567 µCi, 200 µL) was buffered at pH 5.6 with sodium acetate buffer 1 M (35 µL), then CNTs-NOTA-Met (50 µL of 1.5 mg/mL solution) was added. The mixture was kept at 37°C for 10 minutes, quenched with 380 µL of PBS. Chelated metal 100%. Radioactive yield 65% not decay corrected.

3.4.2 Formation of the ^{68}Ga-NOTA-CNTs-MET-DOXO complex

Ga-68 eluate (0.05M in HCl, 370 µCi, 100 µL) was buffered at pH 5.6 with sodium acetate buffer 1M (35 µL), then material **13 (**83 µL of 1.5 mg/mL solution) was added. The mixture was kept at 37°C for 10 minutes, quenched with PBS (380 µL) and the efficiency of the labeling monitored by *i*TLC (PBS). [^{68}Ga]**13** was obtained with a 93.5% radiochemical purity and radioactive yield 60% (not decay corrected).

3.4.3 Formation of the [^{68}Ga]DOTA-CNTs-MET-DOXO complex

The standard complexation conditions required heating at 85°C due to the different size of Ga(III) ions respect to Cu(II),[94,107,118,105] a temperature not compatible with the presence of the DOX-CNT complex. For this reason, the procedure was modified lowering the temperature. Ga-68 eluate (0.05 M in HCl, 370 µCi, 100 µL) was buffered at pH 5.6 with sodium acetate buffer 1M (35 µL), then material **12**(50 µL of 1.5 mg/mL solution) was added. The mixture was kept at 37 °C for 10 minutes and quenched with PBS (380 µL) with an efficiency of 70%. The free metal was removed in centrifuge, the CNT were precipitated, and the supernatant replaced with fresh PBS 3 times, after purification the sample reached 95% of radiochemical purity with a radioactive yield 60% not decay correcte

3.4.4 *Formation of the [^{64}Cu]DOTA-CNTs-MET-DOX complex*

Cu-64 solution (0.1M in HCl, 1 mCi, 1 µL) was buffered at pH 5.6 with sodium acetate buffer 1M (50 µL), then material **12** (20 µL of 1.5 mg/mL solution in water) was added. The mixture was kept at 37°C for 30 minutes, quenched with 430 µL of PBS. Chelated metal 93.5%. Radioactive yield 77.2% not decay corrected.

3.4.5 Radiosynthesis of [^{18}F]FAZA

Starting material 1-(2,3-diacetyl-5-tosyl-(α-D-arabinofuranosyl)-2-nitroimidazole was purchased from ABX GmbH (Germany) and all other reagent were acquired from Sigma-Aldrich (Merk). Purification was performed using Luna C18 5 µm 250 mm x 10 mm semipreparative HPLC column. Radiochemical and UV purities were assessed by analytical HPLC using Econosyl C18 10 µm 250mm x 4.6 mm column. The HPLC method for quality control was: A) 10 mM NaH$_2$PO$_4$, B) MeCN; % B: 5 for 3 min, 5 to 90 in 12 min, 90 to 5 in 2 min, 5 for 3 min. [^{18}F]FAZA retention time was 10.0 min. [^{18}F]FAZA was obtained in 50 min, with 99% of purity and a radioactive yield of 27% not decay corrected.

3.5 Characterization of the synthesized compounds

3.5.1 General procedure for the quality control of the labeling reactions

The quality control was accomplished via Instant Thin Liquid Chromatography (*i*TLC), 1 to 3 µL of the reaction mixture were diluted with 100 µL of EDTA 0.1 M in PBS to chelate all the free metal, a 3-5 µL drop was eluted with PBS on *i*TLC paper and the strip read with the *i*TLC scanner. The radiolabeled CNT stay at baseline and the free metal move with the front of the solvent. The instrument displays the results as a chromatogram. The quantification was done integrating the area under the peaks.

3.5.2 *Quantification of Doxorubicin loading*

The quantification was made measuring the UV-Vis absorption (peak at 480-490 nm) of the non-loaded DOX after work-up, and back-calculating the concentration with a calibration curve, as reported in the literature.[119–121]

The calibration curve was built reading the absorbance of five solution at different concentration as reported in the table of **Figure 32**.

Conc. mg/mL	Abs
0,0015	0,024
0,006	0,093
0,012	0,183
0,024	0,353
0,048	0,714
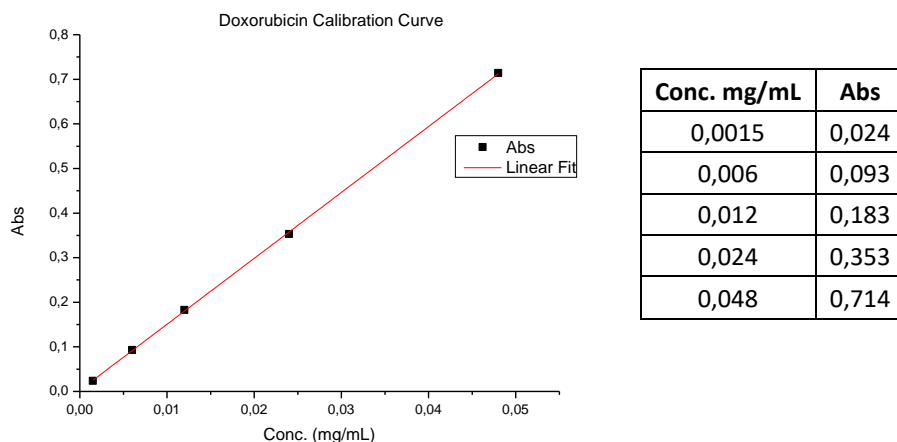
Figure 32. Calibration curve of doxorubicin used for the quantification of the loading of CNT, equation y=14.78488+0.00226, r^2=0.99985.
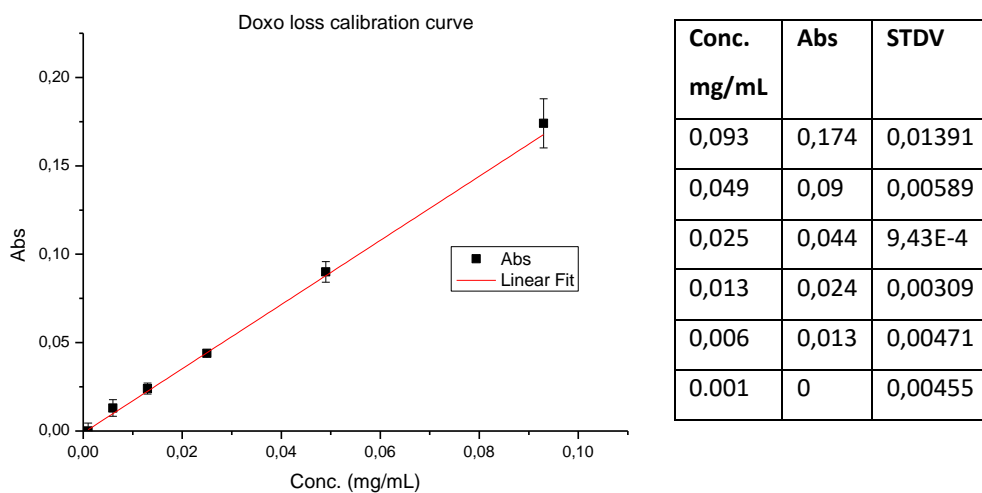
The solutions of work up were collected and dilute to known volume, then the absorbance was measured and the concentration back-calculated giving the amount of non-loaded DOX. The loading on the nanotube was calculated by difference between the non-loaded and the used DOX.

3.5.3 Doxorubicin loss during the labeling

The loss of doxorubicin during the labeling reaction was quantified by UV-Vis absorption spectroscopy. A stock solution of CNTs-MET-B-DOX **1** in PBS 1.5 mg/mL was prepared, then 200 µL of this solution were buffered at pH 5.6 with 400 µL of sodium

acetate buffer 1M and heated at 37°C for 1 h. Aliquots of 100 µL of the reaction solution were collected after 10, 20, 30 and 60 minutes and quenched with 100 µL of PBS. The nanotubes were precipitated in centrifuge and the absorbance of the supernatant was measured.
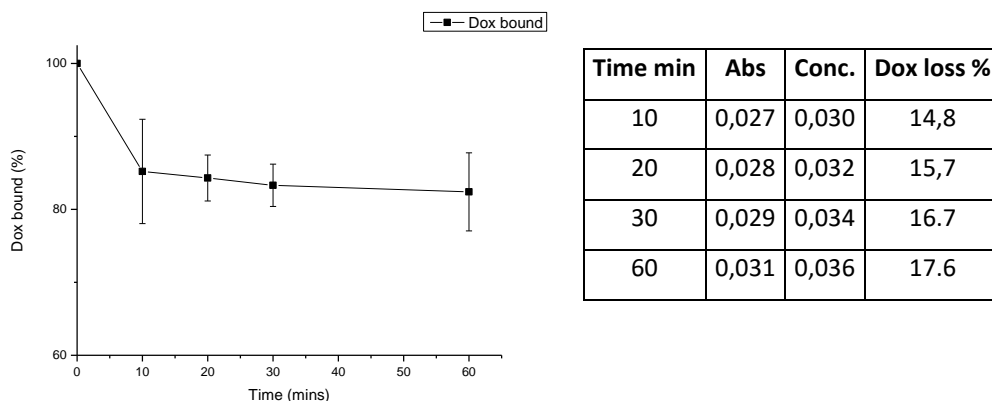

Conc. mg/mL	Abs	STDV
0,093	0,174	0,01391
0,049	0,09	0,00589
0,025	0,044	9,43E-4
0,013	0,024	0,00309
0,006	0,013	0,00471
0.001	0	0,00455

Figure 33. Doxorubicin UV-Vis calibration curve for DOXO loss experiment, equation: y=1.81497x0.00106, R^2=0.99548. Error bars, where not visible, are smaller than symbols.

DOX loss was quantified to be around 15 % during the reaction time, this loss should not affect the biodistribution, providing a pharmacokinetic profile similar to the original DDS.

Time min	Abs	Conc.	Dox loss %
10	0,027	0,030	14,8
20	0,028	0,032	15,7
30	0,029	0,034	16.7
60	0,031	0,036	17.6

Figure 34. Doxorubicin loss at pH 5.6 and 37°C at different time point.

3.5.4 Kaiser test[45,63]

The Kaiser test was carried out following a reported procedure. Three solutions were prepared:

    A.   500 mg of ninhydrin in 10 mL of ethanol.

    B.   80 mg of phenol in 20 mL of ethanol.

    C.   2 mL of 0.001 M potassium cyanide dilute to 100 mL with pyridine.

The calibration curve was built using a stock solution of L-valine 1.5 mg/mL in ethanol and taking different aliquots and adding different volumes of the reactive solutions:

A.   75 µL

B.   75 µL

C.   100 µL

The obtained solution was heated at 120°C for 10 minutes, then diluted to 0.5 mL of volume with milliQ water and absorbance at 580 nm of each solution was measured.

Kaiser test calibration curve
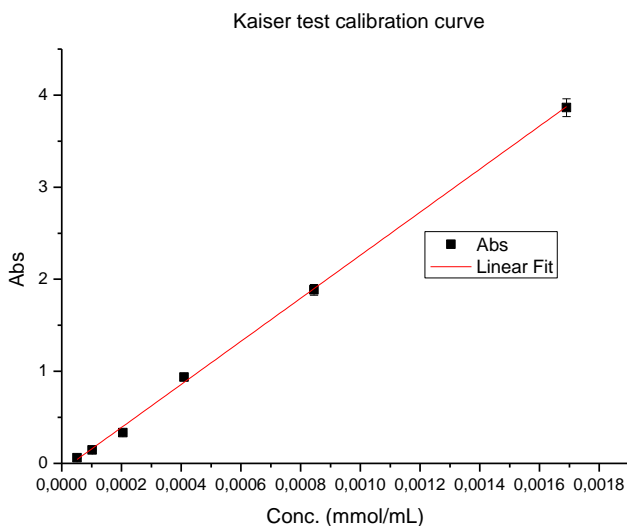
Vol. μL	mg	mmol	mmol/mL	Abs	STDV
66	0,099	0,000845	0,00169	3,864	0,09728
33	0,0495	0,000423	0,000845	1,885	0,05915
16	0,024	0,000205	0,00041	0,938	0,01127
8	0,012	0,000102	0,000205	0,333333	0,00862
4	0,006	5,12E-05	0,000102	0,146333	0,00764
2	0,003	2,56E-05	5,12E-05	0,060333	0,00493

Figure 35. UV-vis calibration curve Kaiser Test equation: y= 2338.3744x+0.02549, R2=0.98253. Error bars where not visible are smaller than symbols.

Measurements on Materials

Material	Abs	M	mmol	mmol/g of NH_2
11	0.099	7,75E-05	3,87677E-05	0.129
13	0.088	7.32E-05	3.66E-05	0.120

Table 6. Quantification of amine group on materials 11 and 13 through semiquantitative Kaiser-test.

3.5.5 General procedure to calculate the payload from TGA-MS spectra

The amount of payload was calculated from spectra using a graphical approach: the time-point for the weight loss due to the decoration was evidenced by the isobutene

peak in the MS spectrum, then it was measured as percentage directly from the TGA spectrum. From the weight loss % the mmol of the functionalities were calculated dividing by the molecular weight of the fragment and finally expressed as mmol/g of material. TGA spectra are reported in section **6.**

3.5.6 Characterization of final materials

Characterization of materials was accomplished using different techniques:

- metformin loading was evaluated measuring the increment of nitrogen content before and after functionalization using elemental analysis.
- Biotin functionalization was estimated measuring the increment of sulfur content using ICP-AES.
- Doxorubicin loading was estimated using UV-Vis as described above.
- DOTA was quantified by TGA-MS analysis.
- NOTA was quantified indirectly measuring the drop of free amine groups with the Kaiser Test.

Construct	Metformin mmol/g	Biotin mmol/g	Doxorubicin %wt	DOTA mmol/g	NOTA mmol/g
11	2.00	0.21	41.6	-	-
12	1.82	0.137	38.9	0.1	-
13	1.82	0.228	40	-	0.01
14	-	0.27	38.6	-	-

Table 7. Characterization of compounds **11** to **14.**

3.6 Biological studies

3.6.1 *In Vitro studies of toxicity*

Cytotoxic effects of CNTs loaded with metformin, doxorubicin, or both drugs, were evaluated by using the MTT method. MCF7 and 4T1 cancer cell lines were seeded in 96

multiwell plates and then treated with increasing concentration of CNTs for 48 hours at 37°C. After this time, cells were extensively washed with PBS and incubated in the presence of 0.5 mg/ml MTT dye (3-(4,5-dimethylthiazol-2-yl)-2,5-diphenyltetrazolium bromide) for 2 hours at 37°C. Insoluble crystals obtained were dissolved by adding DMSO to plate dishes. The absorbance of samples was quantified by using a microplate reader (Biorad) measuring the absorbance of samples at 570 nm. All experiments were carried out in triplicate. Data reported in the figure represent the mean values ± S.E.M.

### 3.6.2 *In Vivo* stability of [^{64}Cu]CNT-DOTA and [^{68}Ga]NOTA-CNT complexes.

Samples of blood and urine were collected 1.5 h after injection, samples of blood were diluted with 30 μL of PBS and 10 μL of the obtained solution dropped on the *i*TLC strip; urine samples were directly deposed (10 μL) on the strip. The *i*TLC strip were eluted with an EDTA 0.1M solution and then read to measure the amount of bound metal.

### 3.6.3 *PET/CT imaging of tumour bearing mice and analysis*

Mice were briefly anaesthetized (<5 min) using 1% to 2% isoflurane with O$_2$ as a carrier. Mice were injected *i.v., i.c.* or *i.p.* with of [^{64}Cu]**12** or [^{68}Ga]**13** in sterile phosphate-buffered saline (PBS) with a target of 3.7 MBq per mouse. Actual injected dose was calculated based on measuring the pre- and post-injection activity in the syringe with a dose calibrator (Capintec). Mice were then returned to their cages, quickly became ambulatory and could move freely, eat and drink *ad libitum* for ~45 min. Mice were then anaesthetized using 1% and 3% isoflurane, transferred to a pre-clinical PET/SPECT/CT system (Albira PET/SPECT/CT, Bruker) and maintained at 0.5% to 2% isoflurane with continuous monitoring of respiration during the acquisition. PET images were acquired for 10 min using a 15 cm FOV centered on the tumour; CT images were acquired for fusion using a 7 cm FOV also centered on the tumour. The same procedure was repeated for the 3h, 24h and 48 h PET/CT scans. The 10 min PET/CT dynamic scan

was recorded immediately after injection of the tracer, and then mice were allowed to awake and freely move around their cages until the 3 h time point. Images were reconstructed using MLEM and FBP for PET and CT, respectively, and automatically fused by the software. Image data were decay corrected to injection time (Albira, Bruker) and expressed as %ID/cc (PMOD, PMOD Technologies). Tumour-to-muscle ratios (T/M) were calculated by dividing the activity present in the tumour by the activity present in the muscle.
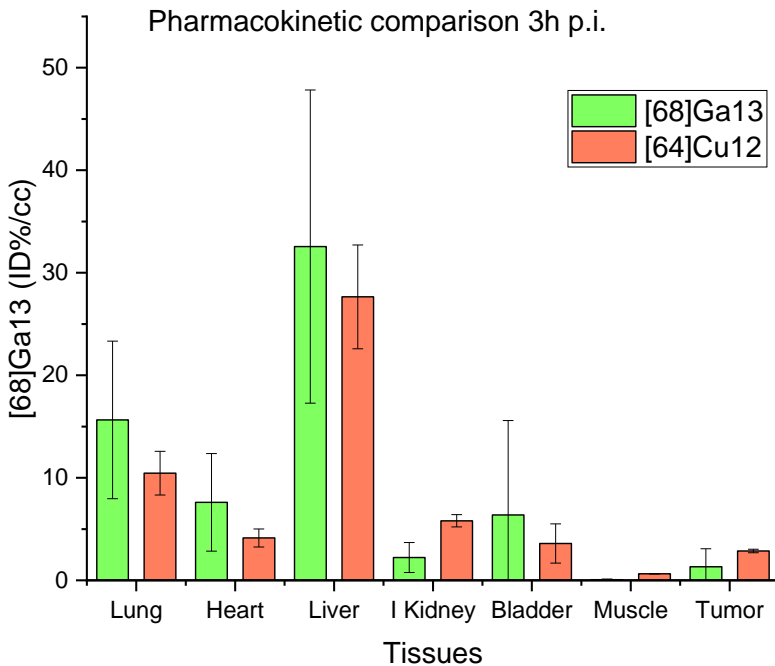
Figure 36. Biodistribution at 3 h post injection using the two different labelled materials and intravenous injection.
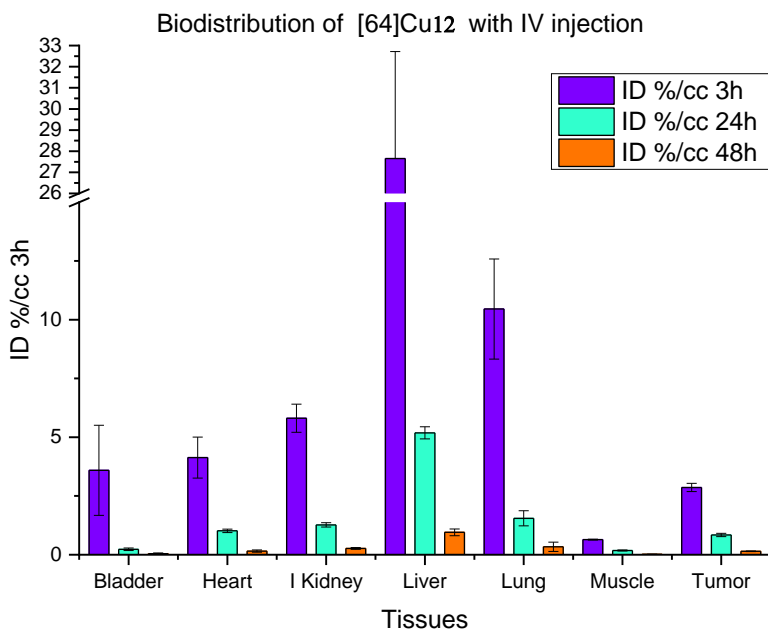
*Figure 37. Biodistribution at different time point of [64Cu]**12** after intravenous injection.*

3.6.4 *Treatment*

15 Balb/c mice (Taconic) were implanted with 10K 4T1 Fluc-GFP tumors using an orthotopic implantation procedure to create a syngeneic immunocompetent model of triple negative breast cancer. Two weeks subsequent to implantation mice were treated, ip, twice weekly with either vehicle (PBS (Sigma Aldrich)), metformin+ dox (2 mg/kg) or DDS **1** (5 mg/kg). Tumor long and short axis were measured weekly and tumor volume calculated at 0.5*(long axis x short axis^2) . 12 days post treatment mice were imaged for bioluminescence signal (IVIS SPECTRUM, Perkin Elmer).[cite any one of our other papers]. Mice reached

endpoint as defined by IACUC protocol 00001179 with tumor burden >= 1.5 or moribund status as determined by veterinary staff.
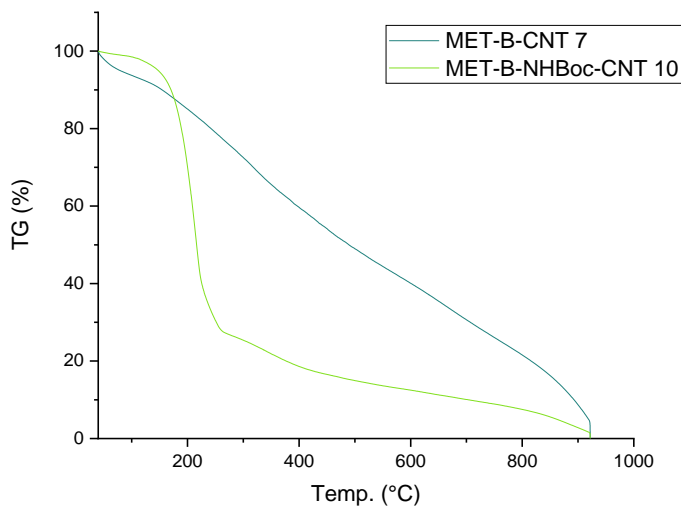
3.7 Supplementary Figures and Schemes

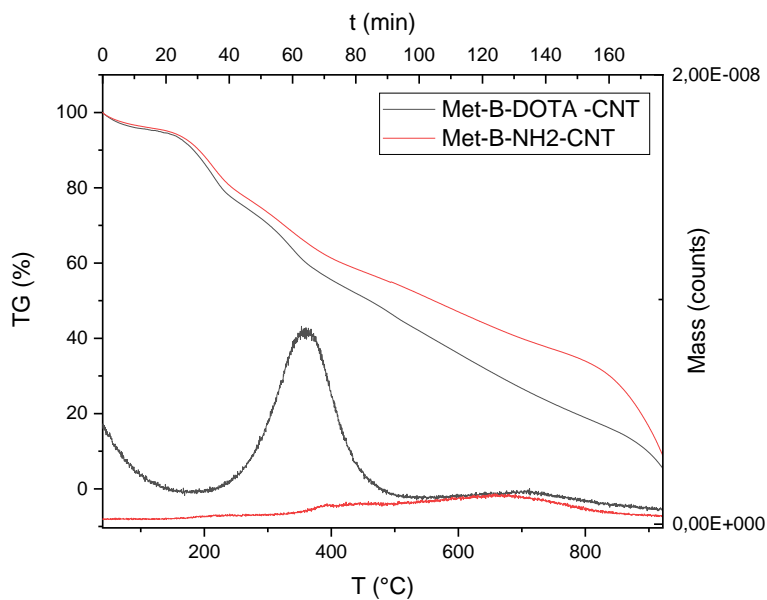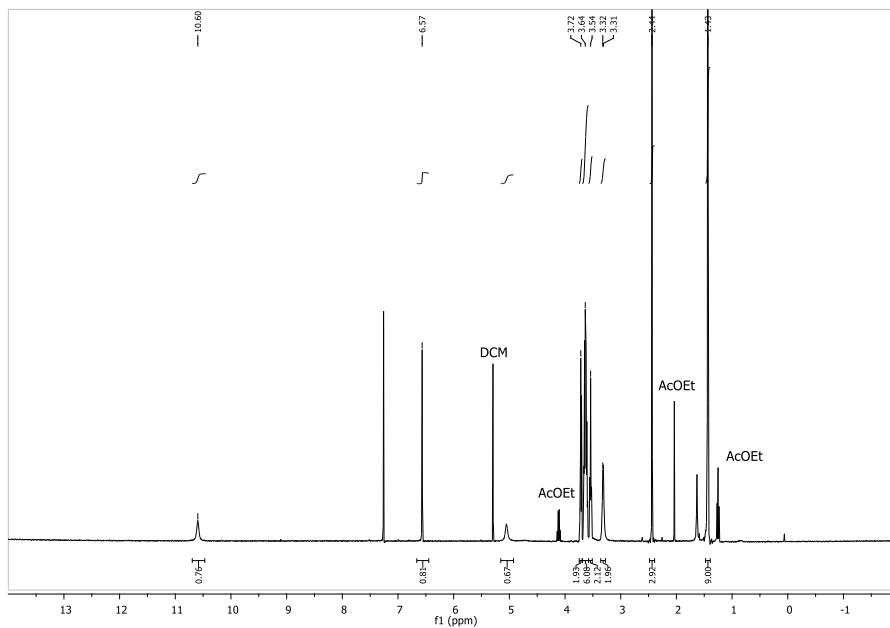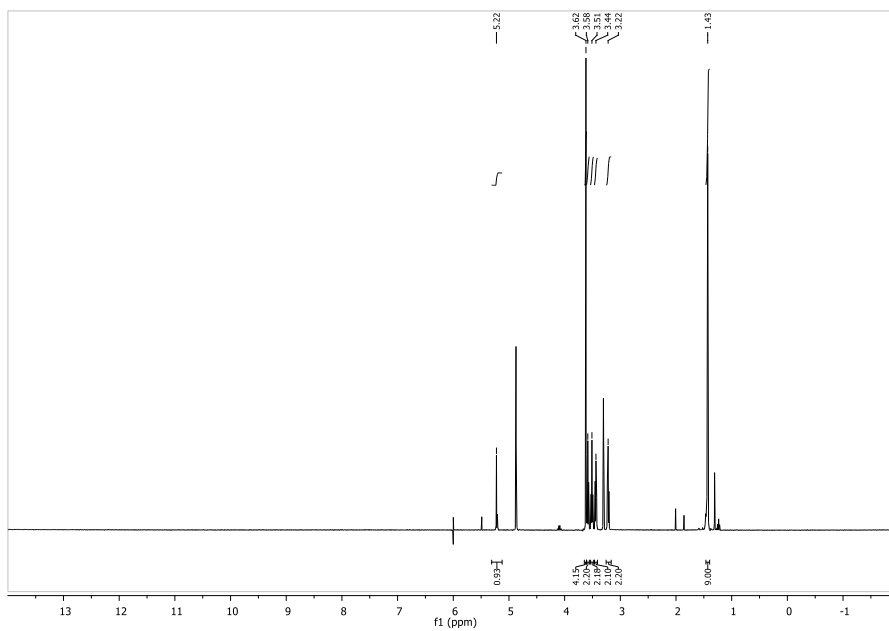*Figure 38*. TGA of material 7 (Red) and material 10 (Black).

Figure 39. TGA of CNT-DOTA-tertbutyl ester and material 11.

Figure 40. ¹H-NMR of (E)-tert-butyl (3-(nitromethylene)-7,10-dioxa-2-thia-4-azadodecan-12-yl)carbamate.
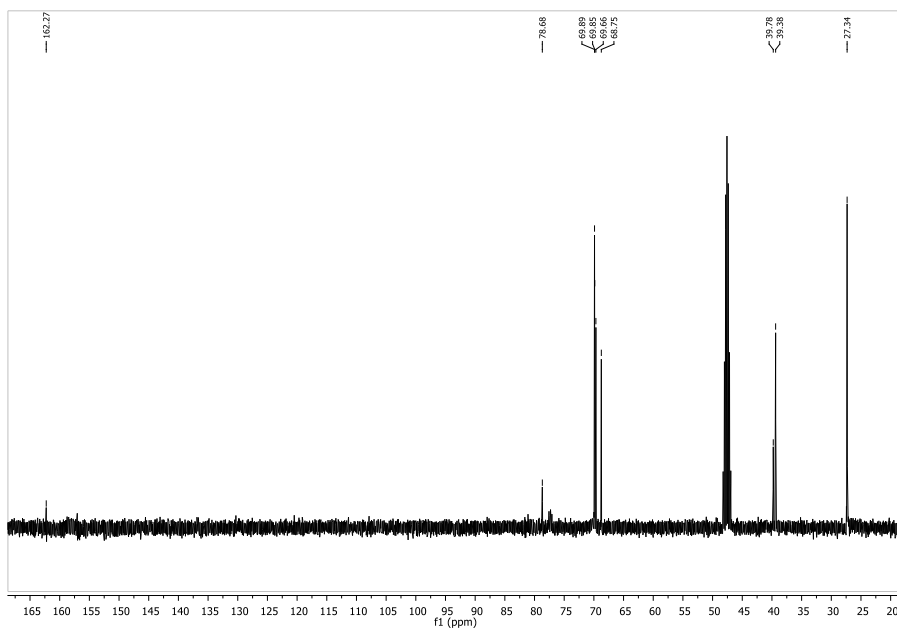

Figure 41. ¹H-NMR Compound **9**.

Figure 42. ^{13}C-NMR Compound **9**.
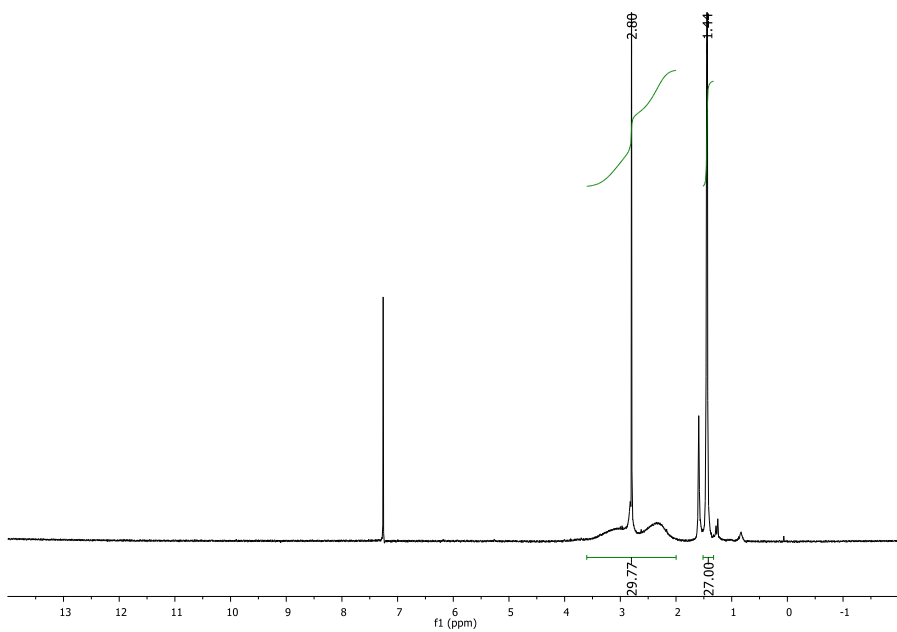
Figure 43. ^{1}H-NMR (400 MHz) of DOTA-OSU **15**.

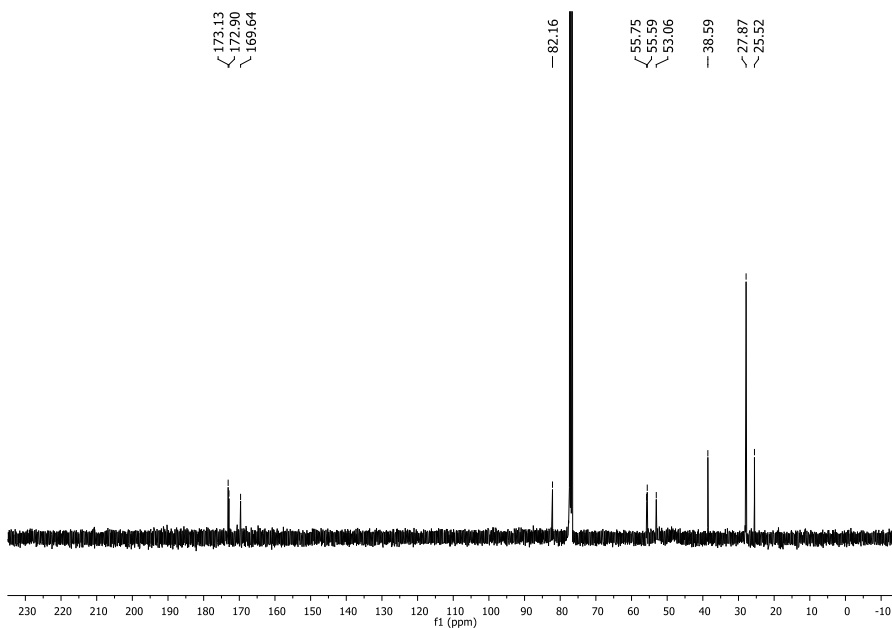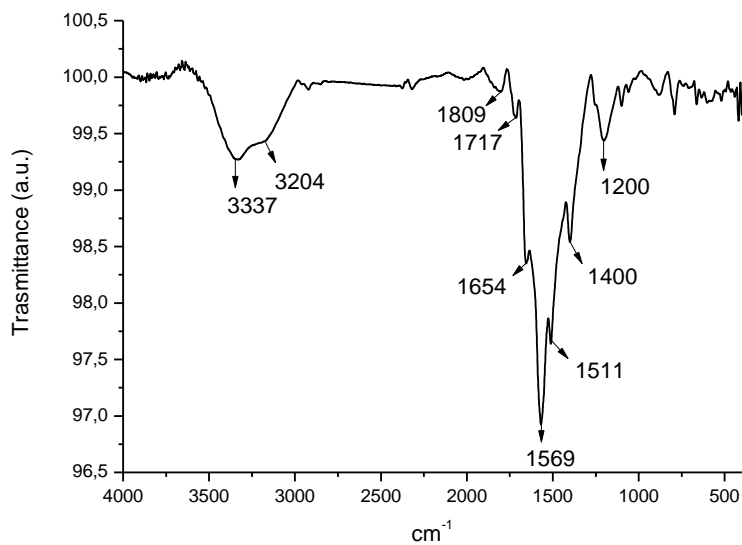***Figure 44.*** ^{13}C-NMR (100 MHz) of DOTA-OSU **15**.

Figure 45. FT-IR spectrum of CNT-Met adduct **3**.
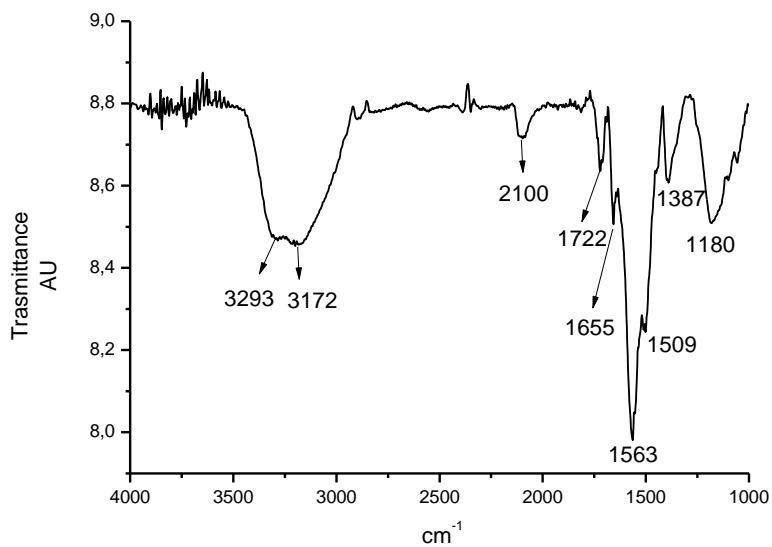
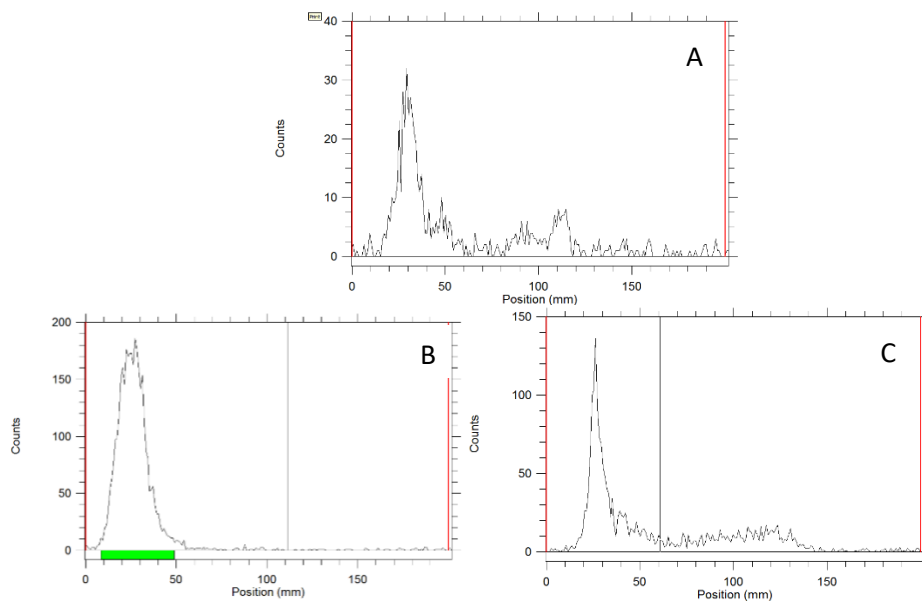*Figure 46*. FT-IR of CNT-Met-N$_3$ **6**.

Figure 47. Metabolism ITLC quality control of [64]Cu**12** materials in blood A,B and urine C, 1 h post injection.

References

(1)   Webster, T. J. *Int. J. Nanomedicine* **2006**, *1* (2), 115–116.

(2)   Iijima, S. *Nature* **1991**, *354* (6348), 56–58.

(3)   Tasis, D.; Tagmatarchis, N.; Bianco, A.; Prato, M. *Chem. Rev.* **2006**, *106* (3), 1105–1136.

(4)   Kumar, I.; Rana, S.; Cho, J. W. *Chem. - A Eur. J.* **2011**, *17* (40), 11092–11101.

(5)   Kumar, S.; Rani, R.; Dilbaghi, N.; Tankeshwar, K.; Kim, K.-H. *Chem. Soc. Rev.* **2017**, *46* (1), 158–196.

(6)   Corma, A.; Garcia, H.; Leyva, A. *J. Mol. Catal. A Chem.* **2005**, *230* (1–2), 97–105.

(7)   Hong, S. Y.; Tobias, G.; Al-Jamal, K. T.; Ballesteros, B.; Ali-Boucetta, H.; Lozano-Perez, S.; Nellist, P. D.; Sim, R. B.; Finucane, C.; Mather, S. J.; et al. *Nat. Mater.* **2010**, *9* (6), 485–490.

(8)   Fedeli, S.; Paoli, P.; Brandi, A.; Venturini, L.; Giambastiani, G.; Tuci, G.; Cicchi, S. *Chem. - A Eur. J.* **2015**, *21* (43), 15349–15353.

(9)   Tasis, D.; Tagmatarchis, N.; Bianco, A.; Prato, M.; Tasis, D.; Tagmatarchis, N.; Bianco, A.; Prato, M. **2006**, *106* (February), 1105–1136.

(10)   Wohlstadter, J. N.; Wilbur, J. L.; Sigal, G. B.; Biebuyck, H. A.; Billadeau, M. A.; Dong, L.; Fischer, A. B.; Gudibande, S. R.; Jameison, S. H.; Kenten, J. H.; et al. *Adv. Mater.* **2003**, *15* (14), 1184–1187.

(11)   Xiong, J.; Zheng, Z.; Qin, X.; Li, M.; Li, H.; Wang, X. *Carbon N. Y.* **2006**, *44* (13), 2701–2707.

(12)   Mooney, E.; Dockery, P.; Greiser, U.; Murphy, M.; Barron, V. *Nano Lett.* **2008**, *8* (8), 2137–2143.

(13)   Kumar, S.; Rani, R.; Dilbaghi, N.; Tankeshwar, K.; Kim, K. H. *Chem. Soc. Rev.* **2017**, *46* (1), 158–196.

(14)   Karousis, N.; Tagmatarchis, N.; Tasis, D. *Chem. Rev.* **2010**, *110* (9), 5366–5397.

(15)   Tromp, R. M.; Afzali, A.; Freitag, M.; Mitzi, D. B.; Chen, Z. *Nano Lett.* **2008**, *8* (2), 469–472.

(16)   Kim, U. J.; Furtado, C. A.; Liu, X.; Chen, G.; Eklund, P. C. *J. Am. Chem. Soc.* **2005**, *127* (44), 15437–15445.

(17)   Dresselhaus, M. S.; Dresselhaus, G.; Saito, R.; Jorio, A. *Phys. Rep.* **2005**, *409* (2), 47–99.

(18)   Kane, A. B.; Hurt, R. H.; Gao, H. *Toxicol. Appl. Pharmacol.* **2018**, No. June.

(19)   Grosse, Y.; Loomis, D.; Guyton, K. Z.; Lauby-Secretan, B.; El Ghissassi, F.; Bouvard, V.; Benbrahim-Tallaa, L.; Guha, N.; Scoccianti, C.; Mattock, H.; et al. *Lancet Oncol.* **2014**, *15* (13), 1427–1428.

(20)   Takagi, A.; Hirose, A.; Nishimura, T.; Fukumori, N.; Ogata, A.; Ohashi, N.; Kitajima, S.; Kanno, J. *J. Toxicol. Sci.* **2008**, *33* (1), 105–116.

(21)   Nagai, H.; Okazaki, Y.; Chew, S. H.; Misawa, N.; Yamashita, Y.; Akatsuka, S.; Ishihara, T.; Yamashita, K.; Yoshikawa, Y.; Yasui, H.; et al. *Proc. Natl. Acad. Sci.*

2011, *108* (49), E1330–E1338.

(22) Muller, J.; Delos, M.; Panin, N.; Rabolli, V.; Huaux, F.; Lison, D. *Toxicol. Sci.* **2009**, *110* (2), 442–448.

(23) Rittinghausen, S.; Hackbarth, A.; Creutzenberg, O.; Ernst, H.; Heinrich, U.; Leonhardt, A.; Schaudien, D. *Part. Fibre Toxicol.* **2014**, *11* (1), 1–18.

(24) Donaldson, K.; Poland, C. A.; Murphy, F. A.; MacFarlane, M.; Chernova, T.; Schinwald, A. *Adv. Drug Deliv. Rev.* **2013**, *65* (15), 2078–2086.

(25) Kagan, V. E.; Konduru, N. V.; Feng, W.; Allen, B. L.; Conroy, J.; Volkov, Y.; Vlasova, I. I.; Belikova, N. A.; Yanamala, N.; Kapralov, A.; et al. *Nat. Nanotechnol.* **2010**, *5* (5), 354–359.

(26) Sureshbabu, A. R.; Kurapati, R.; Russier, J.; Ménard-Moyon, C.; Bartolini, I.; Meneghetti, M.; Kostarelos, K.; Bianco, A. *Biomaterials* **2015**, *72*, 20–28.

(27) Mata, D.; Amaral, M.; Fernandes, A. J. S.; Colaço, B.; Gama, A.; Paiva, M. C.; Gomes, P. S.; Silva, R. F.; Fernandes, M. H. *Nanoscale* **2015**, *7* (20), 9238–9251.

(28) Russier, J.; Oudjedi, L.; Piponnier, M.; Bussy, C.; Prato, M.; Kostarelos, K.; Lounis, B.; Bianco, A.; Cognet, L. *Nanoscale* **2017**, *9* (14), 4642–4645.

(29) Pantarotto, D.; Briand, J.-P.; Prato, M.; Bianco, A. *Chem. Commun. (Camb).* **2004**, No. 1, 16–17.

(30) Lee, Y.; Geckeler, K. E. *Adv. Mater.* **2010**, *22* (36), 4076–4083.

(31) Kam, N. W. S.; Dai, H. *Phys. Status Solidi Basic Res.* **2006**, *243* (13), 3561–3566.

(32) Zhou, F.; Xing, D.; Wu, B.; Wu, S.; Ou, Z.; Chen, W. R. *Nano Lett.* **2010**, *10* (5), 1677–1681.

(33) Cherukuri, P.; Bachilo, S. M.; Litovsky, S. H.; Weisman, R. B. *J. Am. Chem. Soc.* **2004**, *126* (48), 15638–15639.

(34) McDevitt, M. R.; Chattopadhyay, D.; Kappel, B. J.; Jaggi, J. S.; Schiffman, S. R.; Antczak, C.; Njardarson, J. T.; Brentjens, R.; Scheinberg, D. A. *J. Nucl. Med.* **2007**, *48* (7), 1180–1189.

(35) Zhang Z. Zhang, and Y. Zhang, W. *Nanoscale Res. Lett.* **2011**, *6* (555), 1–22.

(36) Li, J.; Pant, A.; Chin, C. F.; Ang, W. H.; Ménard-Moyon, C.; Nayak, T. R.; Gibson, D.; Ramaprabhu, S.; Panczyk, T.; Bianco, A.; et al. *Nanomedicine Nanotechnology, Biol. Med.* **2014**, *10* (7), 1465–1475.

(37) Fedeli, S.; Brandi, A.; Venturini, L.; Chiarugi, P.; Giannoni, E.; Paoli, P.; Corti, D.; Giambastiani, G.; Tuci, G.; Cicchi, S. *J. Mater. Chem. B* **2016**, *4* (21), 3823–3831.

(38) Biagiotti, G.; Fedeli, S.; Tuci, G.; Luconi, L.; Giambastiani, G.; Brandi, A.; Pisaneschi, F.; Cicchi, S.; Paoli, P. *J. Mater. Chem. B* **2018**, *6* (14).

(39) Yang, S.; Guo, W.; Lin, Y.; Deng, X.; Wang, H.; Sun, H.; Liu, Y.; Wang, X.; Wang, W.; Chen, M.; et al. *J. Phys. Chem. C* **2007**, *111* (48), 17761–17764.

(40) Cherukuri, P.; Gannon, C. J.; Leeuw, T. K.; Schmidt, H. K.; Smalley, R. E.; Curley, S. A.; Weisman, R. B. *Proc. Natl. Acad. Sci.* **2006**, *103* (50), 18882–18886.

(41) OWENSIII, D.; PEPPAS, N. *Int. J. Pharm.* **2006**, *307* (1), 93–102.

(42) Yang, S.; Fernando, K. A. S.; Liu, J.; Wang, J.; Sun, H.; Liu, Y.; Chen, M.; Huang,

Y.; Wang, X.; Wang, H.; et al. *Small* **2008**, *4* (7), 940–944.

(43)   Liu, X.; Tao, H.; Yang, K.; Zhang, S.; Lee, S. T.; Liu, Z. *Biomaterials* **2011**, *32* (1), 144–151.

(44)   Lacerda, L.; Soundararajan, A.; Singh, R.; Pastorin, G.; Al-Jamal, K. T.; Turton, J.; Frederik, P.; Herrero, M. A.; Li, S.; Bao, A.; et al. *Adv. Mater.* **2008**, *20* (2), 225–230.

(45)   Wang, J. T. W.; Fabbro, C.; Venturelli, E.; Ménard-Moyon, C.; Chaloin, O.; Da Ros, T.; Methven, L.; Nunes, A.; Sosabowski, J. K.; Mather, S. J.; et al. *Biomaterials* **2014**, *35* (35), 9517–9528.

(46)   Singh, R.; Pantarotto, D.; Lacerda, L.; Pastorin, G.; Klumpp, C.; Prato, M.; Bianco, A.; Kostarelos, K. *Proc. Natl. Acad. Sci. U. S. A.* **2006**, *103* (9), 3357–3362.

(47)   Ruggiero, A.; Villa, C. H.; Bander, E.; Rey, D. A.; Bergkvist, M.; Batt, C. A.; Manova-Todorova, K.; Deen, W. M.; Scheinberg, D. A.; McDevitt, M. R. *Proc. Natl. Acad. Sci. U. S. A.* **2010**, *107* (27), 12369–12374.

(48)   Yang, S. T.; Luo, J.; Zhou, Q.; Wang, H. *Theranostics* **2012**, *2* (3), 271–282.

(49)   Chen, M.; Zeng, G.; Xu, P.; Zhang, Y.; Jiang, D.; Zhou, S. *Environ. Sci. Nano* **2017**, *4* (3), 720–727.

(50)   Kouznetsov, V. V.; Merchan-Arenas, D. R.; Tangarife-Castaño, V.; Correa-Royero, J.; Betancur-Galvis, L. *Med. Chem. Res.* **2016**, *25* (3), 429–437.

(51)   Thorn, Caroline; Oshiro, Connie; Marsh, Sharon; Hernandez-Boussard, Tina; McLeod, Howard; Klein, Teri; Altman, R. *Pharmacogenet Genomics* **2012**, *21* (7), 440–446.

(52)   Gabizon, a; Shmeeda, H.; Barenholz, Y. *Clin.Pharmacokinet.* **2003**, *42* (5), 419–436.

(53)   Fedeli, S.; Brandi, A.; Venturini, L.; Chiarugi, P.; Giannoni, E.; Paoli, P.; Corti, D.; Giambastiani, G.; Tuci, G.; Cicchi, S. *J. Mater. Chem. B* **2016**, *4* (21), 3823–3831.

(54)   Li, R.; Wu, R.; Zhao, L.; Wu, M.; Yang, L.; Zou, H. *ACS Nano* **2010**, *4* (3), 1399–1408.

(55)   Pistone, A.; Iannazzo, D.; Ansari, S.; Milone, C.; Salamò, M.; Galvagno, S.; Cirmi, S.; Navarra, M. *Int. J. Pharm.* **2016**, *515* (1–2), 30–36.

(56)   Mayer, M. J.; Klotz, L. H.; Venkateswaran, V. *Prostate Cancer Prostatic Dis.* **2015**, *18* (4), 303–309.

(57)   Dowling, R. J. O.; Niraula, S.; Stambolic, V.; Goodwin, P. J. *J. Mol. Endocrinol.* **2012**, *48* (3).

(58)   Hirsch, H. A.; Iliopoulos, D.; Tsichlis, P. N.; Struhl, K. *Cancer Res.* **2009**, *69* (19), 7507–7511.

(59)   Orecchioni, S.; Reggiani, F.; Talarico, G.; Mancuso, P.; Calleri, A.; Gregato, G.; Labanca, V.; Noonan, D. M.; Dallaglio, K.; Albini, A.; et al. *Int. J. Cancer* **2015**, *136* (6), E534–E544.

(60)   Iliopoulos, D.; Hirsch, H. A.; Struhl, K. *Cancer Res.* **2011**, *71* (9), 3196–3201.

(61) Peng, M.; Darko, K. O.; Tao, T.; Huang, Y.; Su, Q.; He, C.; Yin, T.; Liu, Z.; Yang, X. *Cancer Treat. Rev.* **2017**, *54*, 24–33.

(62) Yoo, S.; Hou, J.; Yi, W.; Li, Y.; Chen, W.; Meng, L.; Si, J.; Hou, X. *Sci. Rep.* **2017**, *7* (1), 1–9.

(63) Russell-Jones, G.; McTavish, K.; McEwan, J.; Rice, J.; Nowotnik, D. *J. Inorg. Biochem.* **2004**, *98* (10 SPEC. ISS.), 1625–1633.

(64) Ojima, I. *Acc. Chem. Res.* **2008**, *41* (1), 108–119.

(65) Fedeli, S.; Paoli, P.; Brandi, A.; Venturini, L.; Giambastiani, G.; Tuci, G.; Cicchi, S. *Chem. - A Eur. J.* **2015**, *21* (43), 15349–15353.

(66) Tuci, G.; Vinattieri, C.; Luconi, L.; Ceppatelli, M.; Cicchi, S.; Brandi, A.; Filippi, J.; Melucci, M.; Giambastiani, G. *Chem. - A Eur. J.* **2012**, *18* (27), 8454–8463.

(67) Scheibe, B.; Borowiak-Palen, E.; Kalenczuk, R. J. *Mater. Charact.* **2010**, *61* (2), 185–191.

(68) Sciortino, N.; Fedeli, S.; Paoli, P.; Brandi, A.; Chiarugi, P.; Severi, M.; Cicchi, S. *Int. J. Pharm.* **2017**, *521* (1–2), 69–72.

(69) Bahr, J. L.; Tour, J. M. *Chem. Mater.* **2001**, *13* (11), 3823–3824.

(70) Price, B. K.; Tour, J. M. *J. Am. Chem. Soc.* **2006**, *128* (39), 12899–12904.

(71) Schmidt, G.; Gallon, S.; Esnouf, S.; Bourgoin, J. P.; Chenevier, P. *Chem. - A Eur. J.* **2009**, *15* (9), 2101–2110.

(72) Lomeda, J. R.; Doyle, C. D.; Kosynkin, D. V.; Hwang, W.-F.; Tour, J. M. *J. Am. Chem. Soc.* **2008**, *130* (48), 16201–16206.

(73) M??nard-Moyon, C.; Fabbro, C.; Prato, M.; Bianco, A. *Chem. - A Eur. J.* **2011**, *17* (11), 3222–3227.

(74) Salice, P.; Fabris, E.; Sartorio, C.; Fenaroli, D.; Figà, V.; Casaletto, M. P.; Cataldo, S.; Pignataro, B.; Menna, E. *Carbon N. Y.* **2014**, *74* (2), 73–82.

(75) Biagiotti, G.; Langè, V.; Ligi, C.; Caporali, S.; Muniz-Miranda, M.; Flis, A.; Pietrusiewicz, K. M.; Ghini, G.; Brandi, A.; Cicchi, S. *Beilstein J. Nanotechnol.* **2017**, *8* (1), 485–493.

(76) Simões, R. V.; Serganova, I. S.; Kruchevsky, N.; Leftin, A.; Shestov, A. A.; Thaler, H. T.; Sukenick, G.; Locasale, J. W.; Blasberg, R. G.; Koutcher, J. A.; et al. *Neoplasia* **2015**, *17* (8), 671–684.

(77) Dennison, J. B.; Molina, J. R.; Mitra, S.; Gonzalez-Angulo, A. M.; Balko, J. M.; Kuba, M. G.; Sanders, M. E.; Pinto, J. A.; Gomez, H. L.; Arteaga, C. L.; et al. *Clin. Cancer Res.* **2013**, *19* (13), 3703–3713.

(78) Vineberg, J. G.; Wang, T.; Zuniga, E. S.; Ojima, I. *J. Med. Chem.* **2015**, *58* (5), 2406–2416.

(79) Smith, B. R.; Ghosn, E. E. B.; Rallapalli, H.; Prescher, J. A.; Larson, T.; Herzenberg, L. A.; Gambhir, S. S. *Nat. Nanotechnol.* **2014**, *9* (6), 481–487.

(80) Andón, F. T.; Digifico, E.; Maeda, A.; Erreni, M.; Mantovani, A.; Alonso, M. J.; Allavena, P. *Semin. Immunol.* **2017**, *34* (September), 103–113.

(81) Købler, C.; Poulsen, S. S.; Saber, A. T.; Jacobsen, N. R.; Wallin, H.; Yauk, C. L.;

Halappanavar, S.; Vogel, U.; Qvortrup, K.; Mølhave, K. *PLoS One* **2015**, *10* (1), e0116481.

(82) Jacobsen, N. R.; Møller, P.; Clausen, P. A.; Saber, A. T.; Micheletti, C.; Jensen, K. A.; Wallin, H.; Vogel, U. *Basic Clin. Pharmacol. Toxicol.* **2017**, *121*, 30–43.

(83) Liu, Z.; Davis, C.; Cai, W.; He, L.; Chen, X.; Dai, H. *Proc. Natl. Acad. Sci.* **2008**, *105* (5), 1410–1415.

(84) Ingle, T.; Dervishi, E.; Biris, A. R.; Mustafa, T.; Buchanan, R. A.; Biris, A. S. *J. Appl. Toxicol.* **2013**, *33* (10), 1044–1052.

(85) Welsher, K.; Sherlock, S. P.; Dai, H. *Proc. Natl. Acad. Sci.* **2011**, *108* (22), 8943–8948.

(86) Czarny, B.; Georgin, D.; Berthon, F.; Plastow, G.; Pinault, M.; Patriarche, G.; Thuleau, A.; L'Hermite, M. M.; Taran, F.; Dive, V. *ACS Nano* **2014**, *8* (6), 5715–5724.

(87) Deng, X.; Yang, S.; Nie, H.; Wang, H.; Liu, Y. *Nanotechnology* **2008**, *19* (7), 075101.

(88) Lin, Z.; Zhang, H.; Huang, J.; Xi, Z.; Liu, L.; Lin, B. *Toxicol. Res.* **2013**, *3* (6), 497–502.

(89) Mulvey, J. J.; Villa, C. H.; McDevitt, M. R.; Escorcia, F. E.; Casey, E.; Scheinberg, D. A. *Nat. Nanotechnol.* **2013**, *8* (10), 763–771.

(90) Alidori, S.; Bowman, R. L.; Yarilin, D.; Romin, Y.; Barlas, A.; Mulvey, J. J.; Fujisawa, S.; Xu, K.; Ruggiero, A.; Riabov, V.; et al. *Nat. Commun.* **2016**, *7*, 12343.

(91) Liu, Z.; Cai, W.; He, L.; Nakayama, N.; Chen, K.; Sun, X.; Chen, X.; Dai, H. *Nat. Nanotechnol.* **2007**, *2* (1), 47–52.

(92) McDevitt, M. R.; Chattopadhyay, D.; Jaggi, J. S.; Finn, R. D.; Zanzonico, P. B.; Villa, C.; Rey, D.; Mendenhall, J.; Batt, C. A.; Njardarson, J. T.; et al. *PLoS One* **2007**, *2* (9), e907.

(93) Vaquero, J. J.; Kinahan, P. *Annu. Rev. Biomed. Eng.* **2015**, *17* (1), 385–414.

(94) Wadas, T. J.; Wong, E. H.; Weisman, G. R.; Anderson, C. J. *Chem. Rev.* **2010**, *110* (5), 2858–2902.

(95) Simon, G. M.; Niphakis, M. J.; Cravatt, B. F. *Nat. Chem. Biol.* **2013**, *9* (4), 200–205.

(96) Chang, E.; Liu, H.; Unterschemmann, K.; Ellinghaus, P.; Liu, S.; Gekeler, V.; Cheng, Z.; Berndorff, D.; Gambhir, S. S. *Clin. Cancer Res.* **2015**, *21* (2), 335–346.

(97) Seth T. Gammon1, Federica Pisaneschi, Madhavi L. Bandi, Melinda G. Smith, Yuting Sun, Yi Rao, Florian Muller, Franklin Wong, John De Groot, Jeffrey Ackroyd, Osama Mawlawi, Michael A. Davies, Y.N. Vashisht Gopal, M. Emilia Di Francesco, J. R. M. and D. P.-W. *Sci. Rep.* **2018**, *under revi*.

(98) Sancho, P.; Barneda, D.; Heeschen, C. *Br. J. Cancer* **2016**, *114* (12), 1305–1312.

(99) Sancho, P.; Burgos-Ramos, E.; Tavera, A.; Bou Kheir, T.; Jagust, P.; Schoenhals, M.; Barneda, D.; Sellers, K.; Campos-Olivas, R.; Graña, O.; et al. *Cell Metab.*

2015, *22* (4), 590–605.

(100) Morandi, A.; Indraccolo, S. *Biochim. Biophys. Acta - Rev. Cancer* **2017**, *1868* (1), 1–6.

(101) Guideri, L.; De Sarlo, F.; Machetti, F. *Chem. - A Eur. J.* **2013**, *19* (2), 665–677.

(102) Biagiotti, G.; Cicchi, S.; De Sarlo, F.; Machetti, F. *European J. Org. Chem.* **2014**, *2014* (35), 7906–7915.

(103) Kaiser, E.; Colescott, R. L.; Bossinger, C. D.; Cook, P. I. *Anal. Biochem.* **1970**, *34* (2), 595–598.

(104) Morgat, C.; Hindié, E.; Mishra, A. K.; Allard, M.; Fernandez, P. *Cancer Biother. Radiopharm.* **2013**, *28* (2), 85–97.

(105) Wu, N.; Kang, C. S.; Sin, I.; Ren, S.; Liu, D.; Ruthengael, V. C.; Lewis, M. R.; Chong, H. S. *J. Biol. Inorg. Chem.* **2016**, *21* (2), 177–184.

(106) Yang, S.-T.; Wang, Y.-W.; Liu, J.-H.; Wang, H. *J. Radioanal. Nucl. Chem.* **2013**, *295* (2), 1181–1186.

(107) Pellegrini, P. A.; Howell, N. R.; Shepherd, R. K.; Lengkeek, N. A.; Oehlke, E.; Katsifis, A. G.; Greguric, I. *Molecules* **2013**, *18* (6), 7160–7178.

(108) Mulvey, J. J.; Villa, C. H.; McDevitt, M. R.; Escorcia, F. E.; Casey, E.; Scheinberg, D. A. *Nat. Nanotechnol.* **2013**, *8* (10), 763–771.

(109) Al-Jamal, K. T.; Nunes, A.; Methven, L.; Ali-Boucetta, H.; Li, S.; Toma, F. M.; Herrero, M. A.; Al-Jamal, W. T.; Tena Eikelder, H. M. M.; Foster, J.; et al. *Angew. Chemie - Int. Ed.* **2012**, *51* (26), 6389–6393.

(110) Melsens, E.; De Vlieghere, E.; Descamps, B.; Vanhove, C.; Kersemans, K.; De Vos, F.; Goethals, I.; Brans, B.; De Wever, O.; Ceelen, W.; et al. *Radiat. Oncol.* **2018**, *13* (1), 1–8.

(111) Peeters, S. G.; Zegers, C. M.; Yaromina, A.; Van Elmpt, W.; Dubois, L.; Lambin, P. *Q. J. Nucl. Med. Mol. Imaging* **2015**, *59* (1), 39–57.

(112) Gopal B. Saha. **2004**, 208.

(113) Gong, L.; Goswami, S.; Giacomini, K. M.; Altman, R. B.; Klein, T. E. *Pharmacogenet. Genomics* **2012**, *22* (11), 820–827.

(114) Wilcock, C.; Bailey, C. J. *Xenobiotica* **1994**, *24* (1), 49–57.

(115) Andersen, J.; Madsen, U.; Björkling, F.; Liang, X. *Synlett* **2005**, No. 14, 2209–2213.

(116) Chittari, P.; Rajappa, S. *Helv. Chim. Acta* **1991**, *74* (5185).

(117) Li, C.; Winnard, P. T.; Takagi, T.; Artemov, D.; Bhujwalla, Z. M. *J. Am. Chem. Soc.* **2006**, *128* (47), 15072–15073.

(118) Kilian, K. *Reports Pract. Oncol. Radiother.* **2014**, *19*, S13–S21.

(119) Ren, J.; Shen, S.; Wang, D.; Xi, Z.; Guo, L.; Pang, Z.; Qian, Y.; Sun, X.; Jiang, X. *Biomaterials* **2012**, *33* (11), 3324–3333.

(120) Ji, Z.; Lin, G.; Lu, Q.; Meng, L.; Shen, X.; Dong, L.; Fu, C.; Zhang, X. *J. Colloid Interface Sci.* **2012**, *365* (1), 143–149.

(121) Huang, H.; Yuan, Q.; Shah, J. S.; Misra, R. D. K. *Adv. Drug Deliv. Rev.* **2011**, *63*

(14–15), 1332–1339.

(122) Kroto, H. W.; Heath, J. R.; O'Brien, S. C.; Curl, R. F.; Smalley, R. E. *Nature* **1985**, *318* (6042), 162–163.

(123) Novoselov, K. S.; Raimond, J. M.; Brune, M.; Computation, Q.; Martini, F. De; Monroe, C.; Moehring, D. L.; Knight, P. L.; Plenio, M. B.; Vedral, V.; et al. *Science (80-.).* **2004**, *306* (5696), 666–669.

(124) Saeed, K.; Park, S. Y.; Lee, H. J.; Baek, J. B.; Huh, W. S. *Polymer (Guildf).* **2006**, *47* (23), 8019–8025.

(125) Dirian, K.; Herranz, M. Á.; Katsukis, G.; Malig, J.; Rodríguez-Pérez, L.; Romero-Nieto, C.; Strauss, V.; Martín, N.; Guldi, D. M. *Chem. Sci.* **2013**, *4* (12), 4335.

(126) Wong, B. S.; Yoong, S. L.; Jagusiak, A.; Panczyk, T.; Ho, H. K.; Ang, W. H.; Pastorin, G. *Adv. Drug Deliv. Rev.* **2013**, *65* (15), 1964–2015.

(127) Campidelli, S.; Ballesteros, B.; Filoramo, A.; Díaz, D. D.; De La Torre, G.; Torres, T.; Rahman, G. M. A.; Ehli, C.; Kiessling, D.; Werner, F.; et al. *J. Am. Chem. Soc.* **2008**, *130* (34), 11503–11509.

(128) Strom, T. A.; Dillon, E. P.; Hamilton, C. E.; Barron, A. R. *Chem. Commun.* **2010**, *46* (23), 4097–4099.

(129) Lutz, J. F. *Angew. Chemie - Int. Ed.* **2007**, *46* (7), 1018–1025.

(130) Fedeli, S.; Brandi, A.; Venturini, L.; Chiarugi, P.; Giannoni, E.; Paoli, P.; Corti, D.; Giambastiani, G.; Tuci, G.; Cicchi, S. *J. Mater. Chem. B* **2016**, *4*, 3823–3831.

(131) Tuci, G.; Luconi, L.; Rossin, A.; Baldini, F.; Cicchi, S.; Tombelli, S.; Trono, C.; Giannetti, A.; Manet, I.; Fedeli, S.; et al. *Chempluschem* **2015**, *80* (4), 704–714.

(132) Choi, W.; Lahiri, I.; Seelaboyina, R.; Kang, Y. S. *Crit. Rev. Solid State Mater. Sci.* **2010**, *35* (1), 52–71.

(133) Muleja, a. a.; Mbianda, X. Y.; Krause, R. W.; Pillay, K. *Carbon N. Y.* **2012**, *50* (8), 2741–2751.

(134) Hamilton, C. E.; Ogrin, D.; McJilton, L.; Moore, V. C.; Anderson, R.; Smalley, R. E.; Barron, A. R. *Dalton Trans.* **2008**, No. 22, 2937–2944.

(135) Fareghi-Alamdari, R.; Haqiqi, M. G.; Zekri, N. *New J. Chem.* **2016**, *40* (2), 1287–1296.

(136) Methot, J. L.; Roush, W. R. *Adv. Synth. Catal.* **2004**, *346* (9–10), 1035–1050.

(137) Xu, S.; He, Z. *RSC Adv.* **2013**, *3* (38), 16885–16904.

(138) Xiao, Y.; Sun, Z.; Guo, H.; Kwon, O. *Beilstein J. Org. Chem.* **2014**, *10* (1), 2089–2121.

(139) Denton, R. M.; An, J.; Adeniran, B. *Chem Commun* **2010**, *46* (entry 7), 3025–3027.

(140) Denton, R. M.; Tang, X.; Przeslak, A. *Org. Lett.* **2010**, *12* (20), 4678–4681.

(141) Buonomo, J. A.; Aldrich, C. C. *Angew. Chemie - Int. Ed.* **2015**, *54* (44), 13041–13044.

(142) Kosal, A. D.; Wilson, E. E.; Ashfeld, B. L. *Angew. Chemie - Int. Ed.* **2012**, *51* (48), 12036–12040.

(143)   Tang, X.; An, J.; Denton, R. M. *Tetrahedron Lett.* **2014**, *55* (4), 799–802.

(144)   Wu, B.; Kuang, Y.; Zhang, X.; Chen, J. *Nano Today* **2011**, *6* (1), 75–90.

(145)   Esumi, K.; Ishigami, M.; Nakajima, A.; Sawada, K.; Honda, H. *Carbon N. Y.* **1996**, *34* (2), 279–281.

(146)   Shaffer, M. S. P.; Fan, X.; Windle, a. H. *Carbon N. Y.* **1998**, *36* (11), 1603–1612.

(147)   Iannazzo, D.; Mazzaglia, A.; Scala, A.; Pistone, A.; Galvagno, S.; Lanza, M.; Riccucci, C.; Ingo, G. M.; Colao, I.; Sciortino, M. T.; et al. *Colloids Surfaces B Biointerfaces* **2014**, *123*, 264–270.

(148)   Castelaín, M.; Martínez, G.; Merino, P.; Martín-Gago, J. Á.; Segura, J. L.; Ellis, G.; Salavagione, H. J. *Chem. - A Eur. J.* **2012**, *18* (16), 4965–4973.

(149)   Georgakilas, V.; Otyepka, M.; Bourlinos, A. B.; Chandra, V.; Kim, N.; Kemp, K. C.; Hobza, P.; Zboril, R.; Kim, K. S. *Chem. Rev.* **2012**, *112* (11), 6156–6214.

(150)   Fedeli, S.; Paoli, P.; Brandi, A.; Venturini, L.; Giambastiani, G.; Tuci, G.; Cicchi, S. *Chem. - A Eur. J.* **2015**, *21* (43), 15349–15353.

(151)   Sharma, R.; Baik, J. H.; Perera, C. J.; Strano, M. S. *Nano Lett.* **2010**, *10* (2), 398–405.

(152)   Wu, H. C.; Yu, J. Q.; Spencer, J. B. *Org. Lett.* **2004**, *6* (25), 4675–4678.

(153)   Swartz, W. E.; Ruff, J. K.; Hercules, D. M. *J. Am. Chem. Soc.* **1972**, *94* (15), 5227–5229.

(154)   Zhang, X.; Liu, H.; Hu, X.; Tang, G.; Zhu, J.; Zhao, Y. *Org. Lett.* **2011**, *13* (13), 3478–3481.

(155)   Ha-Thi, M.-H.; Souchon, V.; Hamdi, A.; Métivier, R.; Alain, V.; Nakatani, K.; Lacroix, P. G.; Genêt, J.-P.; Michelet, V.; Leray, I. *Chem. - A Eur. J.* **2006**, *12* (35), 9056–9065.

(156)   Andersen, J.; Madsen, U.; Björkling, F.; Liang, X. *Synlett* **2005**, No. 14, 2209–2213.

(157)   McConnell, I.; Li, G.; Brudvig, G. W. *Chem. Biol.* **2010**, *17* (5), 434–447.

(158)   Leegwater, J. A. *J. Phys. Chem.* **1996**, *100* (34), 14403–14409.

(159)   Chen, S.; Zhao, X.; Chen, J.; Chen, J.; Kuznetsova, L.; Wong, S. S.; Ojima, I. *Bioconjug. Chem.* **2010**, *21* (5), 979–987.

— Chapter 4 —

— Chapter 5 —

Side-Projects

5.1 Nanostructured carbon materials decorated with organophosphorus moieties: synthesis and application

Introduction

The term of carbon nanomaterial (CNMs) comprises many different allotropic species of carbon, fullerene, carbon nanotubes and graphene being the most studied and used. Since their discovery [2,122,123], they have become very attractive for researchers, due to their peculiar physical and chemical proprieties such as chemical and thermal stability, electronic conductivity, and their nanometric dimensions that prompted their application in chemistry of materials [124] Furthermore, their functionalization with an increasing number of molecular moieties [3,125] has extended their use in new fields ranging from biology [126] to catalysis. Despite such variability, the classes of reactions most used for their functionalization are the same and limited in number. The Tour reaction[127] is one of the most used synthetic approach for the functionalization of CNTs and G. In this reaction, an aniline derivative is transformed into a diazonium salt that, upon decomposition, affords a radical species, responsible for the functionalization of the graphitic surface.[71] A useful alternative to this approach is the reaction of azido derivative with CNMs: the high temperature required for the process decomposes the azido group to a reactive nitrene species that reacts with the graphitic surface to form an aziridine ring. [128] Finally, the use of the CuAAC reaction, [129] between an azide group and a terminal alkyne, has revealed a practical synthetic approach for the decoration of CNMs with a variety of molecular moieties.[130,131] In this work, we present our results in the functionalization of oxidized MWCNTs **4** and multilayer graphene platelets(GPs) **5** [132] using amino- or azido-functionalized triphenylphosphine oxides **1** and **2** and the terminal alkyne **3** (see **figure 1**).
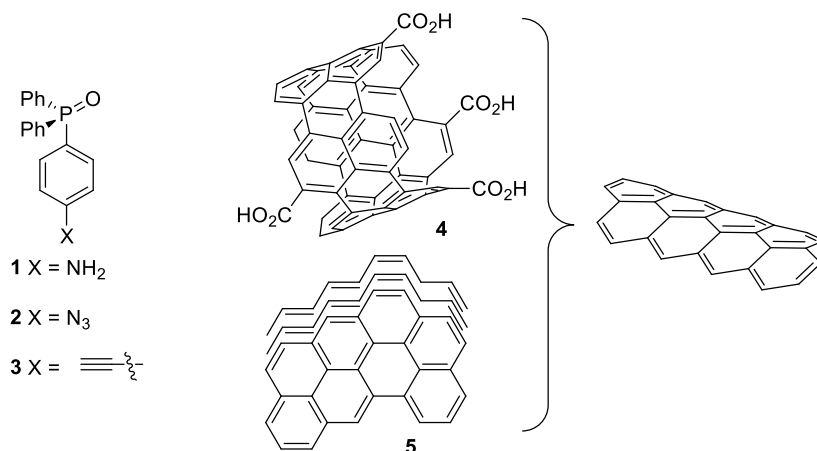
Figure 1. Structure of phosphine oxide derivatives **1**-**3**, of ox-MWCNTs **4** and of GPs **5**.

Such work led to the production of phosphine oxide substituted CNMs. A limited number of works describe the introduction of phosphorous moieties onto CNMs. Muleja et al synthesized a MWCNTs-TPP system modifying the nanotube with the introduction of a phenyl bromide group via diazonium coupling and then of the phosphinating reagent. [133] Hamilton et al. described the functionalization of carbon nanotube with triphenyl phosphine oxide (TPPO) using the carboxylic group, introduced with the oxidation, to covalently link the TPPO. [134] Only one example describes the functionalization of a graphene based material with a phosphine. The authors report the synthesis, characterization and test of palladium nanoparticles supported on phosphine decorated graphene oxide.[135] The interest in the introduction of a phosphine oxide group in CNMs is due to its ability to promote a wide varieties of chemical transformation.[136] Phosphines have found large application in organocatalytic processes[137,138] and, recently, also triphenyl phosphine oxide (TPPO) have found similar application.[139–142] Despite their utility, very few examples of heterogeneous catalysts are described. One example was reported by Tang, who developed a phosphine oxide derivative linked to a polystyrene resin. [143] For this reason, a new class of phosphine oxide functionalized CNMs can be of interest. Not to say of the wide possibilities offered

by the production of metal nanohybrid upon complexation of metal nanoparticles or metal ions by the phosphine functionalities.[144]

Results and Discussion

The CNMs substrates used for this study are oxidized MWCNTs **4** and GPs **5**. The oxidation of pristine MWCNTs [145,146] afforded an easily dispersible material and removed any possible metal impurities present in the starting substrate. GPs were used as example of easily accessible and low cost graphitic material (see experimental section). The first functionalization studied was the reaction of (4-aminophenyl) diphenylphosphine oxide (**1**) with the two substrates **4** and **5** (figure 2).

4 ox-MWCNTs
5 GPs

6 ox-MWCNTs-PO
7 GPs-PO
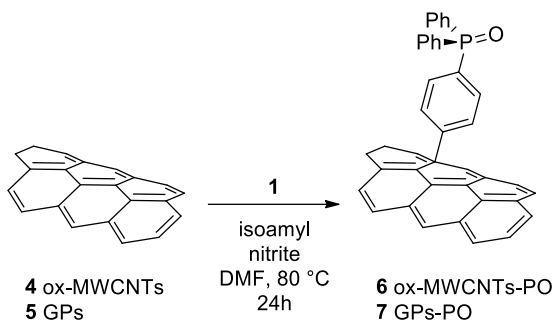
Figure 2. The Tour reaction applied on CNMs **4** and **5**.

This reaction was carried out using the well described Tour protocol [147,148]: the nanomaterials and **1** were dispersed in DMF, then isopentyl nitrite was added and the mixture kept at 80°C for 24 h. The ox-MWCNTs derivative **6** was isolated through filtration over a 0.2 μm PTFE membranes followed by repeated washings with different solvents to remove excess reagents, while the GPs **7** was recovered after several cycles of centrifugation and dispersion.

Subsequently, substrates **4** and **5** were reacted with the azido derivative **2** (**Figure 3**).
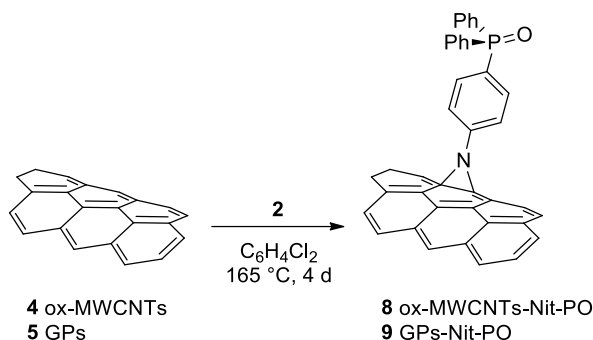
Figure 3. The [1+2] nitrene cycloaddition on CNMs **4** and **5**.

The mixture of the reagents in dichlorobenzene was kept in the ultrasound bath for 25 min, to obtain a homogeneous dispersion, and subsequently stirred at 165°C for four days. [128,4,149] Again, CNTs derivative **8** was more easily isolated by filtration and repeated washing for complete removal of the excess reagents while GPs-Nit-PO derivative **9** was recovered using cycles of centrifugation and re-dispersion of the carbon material in a 1:1 isopropyl ether-isopropanol solution.

The decoration of the carbonaceous substrates, **4** and **5**, with (4-ethynylphenyl) diphenyl phosphine oxide (**3**), via the CuAAC reaction, required their previous modification with the introduction of azido groups. For this purpose, CNMs **4** and **5** were reacted with 4-azido aniline **10** following, again, the Tour protocol affording compounds **11** and **12** (figure 4). [150]

The successful decoration of NMs **11** and **12** was confirmed by elemental analysis and IR spectroscopy (see experimental section figure 19 and 20) and, finally, they were reacted with compound **3** to afford the functionalized compounds **13** and **14** (**figure 4**).
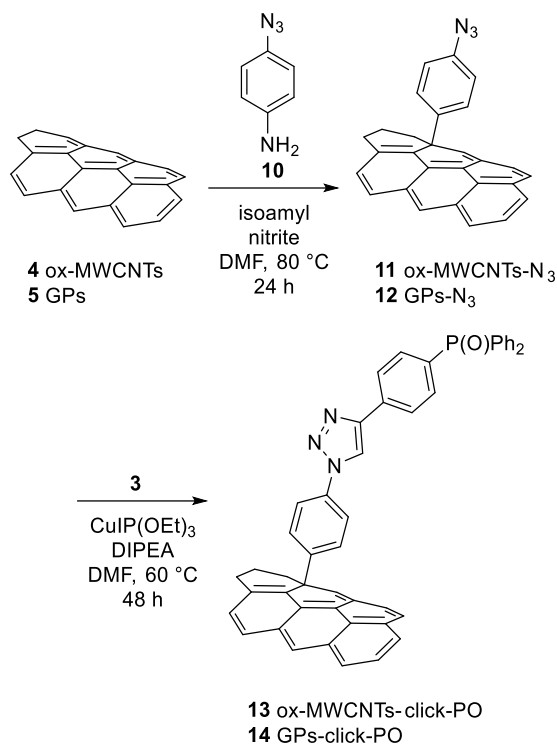
Figure 4. The Tour reaction with 4-azido aniline (**10**) on CNMs **4** and **5**.and the subsequent CuAAC reaction.

The characterization of each material produced was performed via elemental analysis, Inductively Coupled Ion Plasma Atomic Emission Spectroscopy (ICP-AES) analysis, IR and Raman spectroscopy, XPS analysis. Elemental and ICP analyses were useful for the determination of the loading after each chemical transformation. For example, the % content of nitrogen in compounds **8** (1.32 %) and **9** (0.42 %) suggested a loading degree for **8** (0.58 mmol/g) and **9** (0.3 mmol/g). The values obtained for **11** and **12** indicated a functionalization degree of 1.63 mmol/g and 0.075 mmol/g, respectively. The presence of the azido group in **11** and **12** was confirmed by the signal at 2118 cm^{-1} in the FT-IR spectra (see supporting material, figures S9 and S10). The ICP-AES was used to determine the amount of phosphorus in the complex matrix. The samples were

previously mineralized by treatment with nitric acid and a hydrogen peroxide solution at high temperature in microwave. The data obtained are reported in **Table 1**.

Entry	Compound	ICP-AES P %	mmol/g P
1	**4**	-	-
2	**5**	-	-
3	**6**	1.26	0.40
4	**7**	0.27	0.09
5	**8**	1.81	0.58
6	**9**	0.61	0.20
7	**13**	0.85	0.27
8	**14**	0.06	0.02

Table 1: ICP-Analysis results and P loading.

From the data reported in Table 1 it is evident the higher reactivity of Ox-MWCNTs **4** (entries 3, 5 and 7) respect to GPs **5** (entries 4, 6 and 8) as it was expected considering the different nature of the two substrates.[151] For both series of reactions, the higher efficiency was found for the nitrene cycloaddition (entries 5 and 6) followed by the Tour reaction (entries 3 and 4). The decoration using the CuAAC reaction (entries 7 and 8) revealed the less efficient. To be noted that this is not due to a poor content in the azido component (se data for compounds **11** and **12**) but to the low reactivity found in the CuAAC step. To be noted is the good agreement for the loading values obtained with the elemental analysis (see earlier) and with the ICP AES analysis for compound **8** and **9** (table 1, entry 5 and 6). X-ray photoelectron spectroscopy analysis showed the presence of the P (V) atoms in all the samples considered. The samples for the analysis where prepared by dispersion of 1 mg of substance in 1 mL of isopropanol and the dispersion was drop casted on a cleaned glass support. The spectra of all TPPO

decorated materials were recorded and all showed a signal at a binding energy of 132.8 eV, where the two components $2p^{3/2}$ and $2p^{1/2}$, compatible with a phosphine oxide species, can be observed (see figure 5).
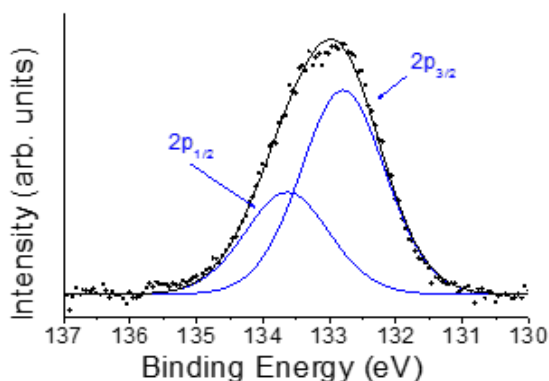

Figure 5. Fitting of the XPS spectrum characteristic of P collected on GPs-Nit-PO **9** showing the two components ($2p_{1/2}$ and $2p_{3/2}$) relative to the phosphine oxide group (for XPS spectra of the other compounds see supporting info)

Raman spectroscopy analyses were performed on the most functionalized samples, compound **8** and **9** (**figure 6**). Generally, CNMs show two main bands in their Raman spectra: one at $\approx$ 1580 cm^{-1} (G band) related to sp^2 graphitic domain and the second at $\approx$ 1360 cm^{-1} (D band) attributed to the amorphous carbon or deformation vibrations of a hexagonal ring.[133] Raman spectra of ox-MWCNTs **4** (**figure 3**, bottom) showed the D and G bands centered at 1320 and 1607 cm^{-1}, respectively, [67] while for compound **8** the band were at 1312 and 1590 cm^{-1}. Despite the ox-MWCNTs **4** already showed an intense D band (I_D/I_G = 2.57), the functionalization further increased the D band intensity, so that the I_D/I_G for compound **8** raised to 3.58. The Raman characterization of the GPs **5** (**figure 2**, top) showed the D and G bands at 1320 and 1580 cm^{-1} with a visible shoulder at 1610 cm^{-1}, while at 2640 cm^{-1} is visible the overtone band 2D typical of graphene. This latter band, sharp and intense in monolayer graphene, is broadened

confirming the high number of layers of the GPs. Upon functionalization The GPs-Nit-PO **9** spectrum showed the same bands with no significant differences respect to **5**.
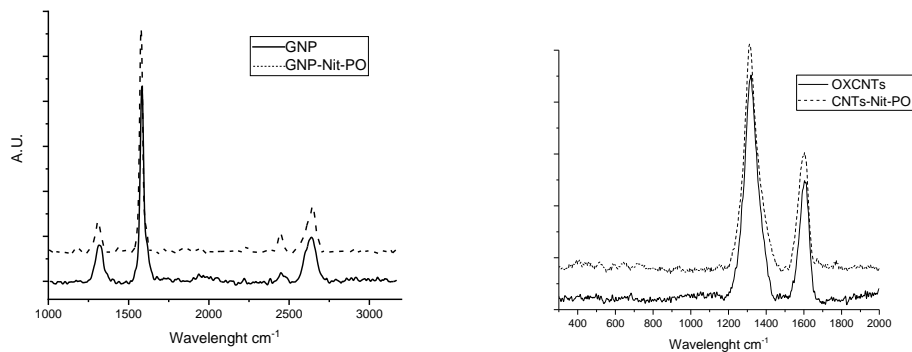
Figure 6. Raman spectra: GPs **5** vs GPs-Nit-PO **9** (top), ox-MWCNTs **4** vs ox-MWCNTs-Nit-PO **8** (bottom).

TEM images of functionalized CNM are shown in figure 3. No significant difference can be found in the morphology of the materials. In particular, as confirmed by the Raman analysis, the GPs present a multilayer structure and no further exfoliation of the multilayer GPs was observed.
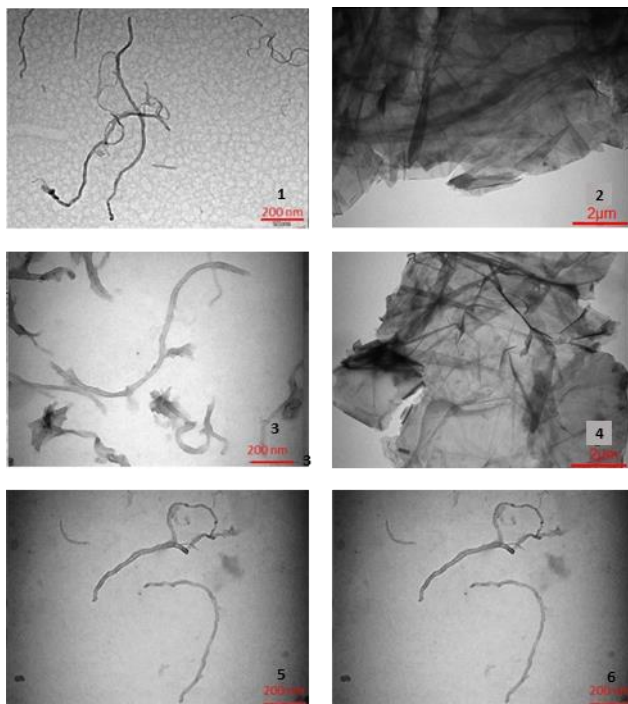
Figure 7. TEM images of ox-MWCNTs **4** (1), ox-MWCNTs-PO **6** (2), ox-MWCNTs-Nit-PO **8** (3), GPs **5** (4) GPs-PO **7** (5), GPs-Nit-PO **9** (6).

A useful extension of these synthetic approaches is the chance to reduce efficiently the P=O moiety to the corresponding phosphine. The phosphorus-phosphorus, trichlorosilane mediated oxygen transfer protocol, developed by Hamilton [134] and Wu [152], was used with compound **6**. The reaction was carried out in a Pyrex tube, heating for 48 h a degassed solvent solution of compound **6**, trichlorosilane and triethyl phosphite as final oxygen acceptor. The reduction of the phosphine oxide moiety was followed by XPS analysis and confirmed by FT-IR spectroscopy.
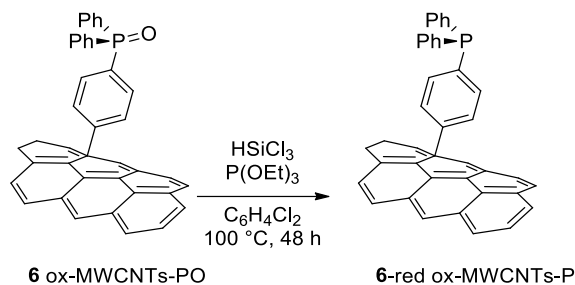
Figure 8. Reduction of phosphine oxide **6** to the corresponding phosphine 6-red.

Figure 9 shows the XPS spectra registered on starting material **6** (t = 0), and of the reaction product after 24 h and after 48 h. The XPS analysis of the starting material showed only the peak at binding energy 132.8 eV (related to presence the phosphine oxide group), after 24 h a new peak, related to the reduced phosphorus atoms, appeared at 130.8 eV, accordingly with value reported by Swartz et al.[153] After 48 h the peak at 130.8 eV is the main one showing that the reaction is almost complete.
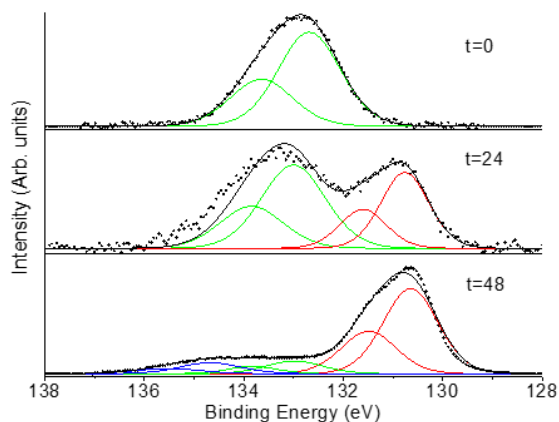
Figure 9. XPS analysis of samples from the reduction reaction of compound **6**: starting material (top), after 24 h (middle), after 48 h (bottom).

The FT-IR spectroscopy confirmed the reduction of the phosphine oxide group with the disappearance of the band at 1114 cm^{-1} related to the P=O stretching vibration (experimental section, figure 12, 13, 14).

The most functionalized material, compound **8**, was finally tested as organocatalyst in a Staudinger Ligation of carboxylic acids and azides being inspired by work of Ashfeld and co-workers.[142] In this work the reaction between a carboxylic acid and an organic azide, to afford the corresponding amide, is catalyzed by PPh$_3$ (10% mole). The process is general and affords high yields. The catalytic cycle is guaranteed by the presence of PhSiH$_3$ that reduces the triphenylphosphine oxide formed to the starting phosphine. In our experiments we substituted triphenylphosphine with the reduced form of compound **8**, **8**-red (**figure 10**).
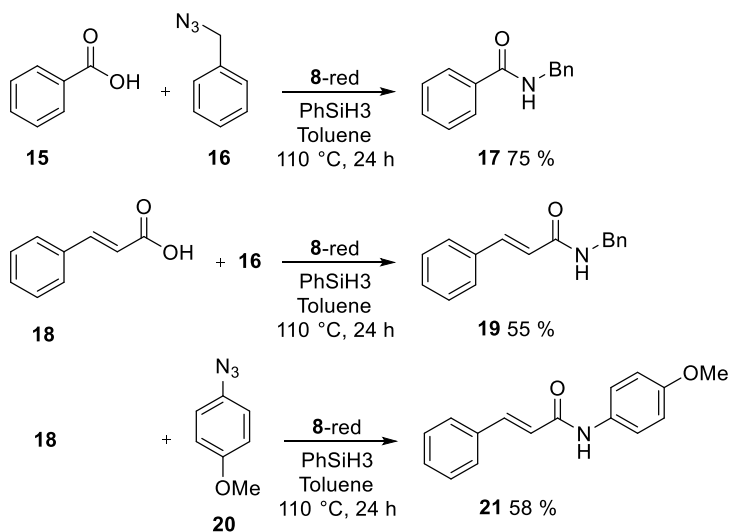
Figure 10. The Staudinger ligation reaction performed with benzoic (**15**) or cinnamic acid (**18**), and benzyl azide (**16**) or 4-MeOC$_6$H$_4$N$_3$ (**20**) and compound **8**-red as catalyst.

As a matter of fact, the reaction reported in figure 10 were successful and afforded the expected amides **17** and **19** and **21** in acceptable yields. For a correct comparison with the higher yields reported for the reaction performed in homogeneous phase (94 %, 95 % and 80%, respectively) it should be stressed that in these experiments the amount of phosphine used is one order of magnitude lower (1% calculated on the basis of the P loading in compound **8**). Further experiments aimed to evaluate the action of the

catalyst in new reaction cycles revealed a fast degradation of the efficiency: the yield of amide **17** dropped to 30 % and 20% in the second and third cycles while no conversion was observed in the second cycle for amide **19**. The yield of compound **21** was 48% in the second cycle.

Conclusion

In conclusion, we developed a simple procedure for the covalent decoration of oxidized multi-walled carbon nanotubes and graphene-based materials with three different TPPO derivatives. Materials were completely characterized by FT-IR, Raman, XPS spectroscopy and TEM, the loading of phosphorus were quantified by ICP-AES. The higher loading was obtained with the nitrene cycloaddition on CNTs but good results were also obtained with graphene. The reduction of adduct to the correspondent TPP was also investigated, the reduction was confirmed by XPS, whose spectra showed the complete disappearing of the phosphine oxide peak and the presence of the intense phosphine peak in 48 h. The possibility to use the TPP group for further modification as binding of Pd nanoparticles, oxidation to phosphine sulfide and selenide are actually under investigation in our laboratory. More significantly, we have explored the ability of one of these materials (the one with the highest loading in phosphine oxide moiety, compound **8**) as heterogeneous catalyst in a Staudinger ligation reaction. Despite the process is still to be optimized, concerning the yield and the recycling of the catalyst, the very low amount of phosphine oxide employed make this approach promising for the development of efficient nanostructured materials useful in organo-catalysis.

Experimental

Materials

MWCNTs were purchased from Sigma-Aldrich reagent, O.D. x L.= 6-9 nm x 5 μm, carbon > 95%, CoMoCat©. GPs were supplied from Nanesa in dry powder or water paste, C:O ratio 44:1, carbon > 97%, average flake thickness 10 nm (30 layers), average lateral size

10-50 μm. All the other reagents, whose synthesis is not described, were commercially available and have been used without any further purification, if not specified otherwise. Rf values are referred to TLC on silica gel plate (0.25 mm, Merck silica gel 60 F_{254}). NMR spectra were recorded on Varian Gemini 200 MHz or Varian Mercury 400 MHz at room temperature. Chemical Shifts were reported in parts per million (ppm) relative to the residual solvent peak rounded to the nearest 0.01 for proton and 0.1 for carbon (reference: $CHCl_3$ [^1H:7.26, ^{13}C:77.2], DMSO [^1H:2.5, ^{13}C:39.5], MeOH [^1H:3.35, ^{13}C:49.3]. Coupling constants J were reported in Hz to the nearest 0.01 Hz. Peak multiplicity was indicated as follows s (singlet), d (doublet), t (triplet), q (quartet), m (multiplet) and br (broad signal). IR spectra were recorded on a Perkin-Elmer FT-IR 881 or Shimadzu FT-IR 8400s spectrometer. IR data are reported as frequencies in wavenumbers (cm^{-1}). UV-Vis spectra were recorded on Varian Cary 4000 Uv-vis spectrophotometer using 1cm cell. Fluorescence spectra were registered on a Jasco FP750 spectrofluorometer using 1cm cell. Raman spectra were measured by a Renishaw RM2000 instrument, equipped with a diode laser emitting at 785 nm. Elemental analyses were performed with a Thermofinnigan CHN-S Flash E1112 analyzer. ICP analysis were made using an Optima 2000 Perkin Elmer Inductively Coupled Plasma (ICP) Dual Vision instrument after acidic mineralization. TEM images were acquired at the electronic microscopic center CNR Florence (CE.M.E.) with a Philip CM12 with CRYO-GATAN UHRST 3500 technology, digital camera and EDAX microanalysis.

Synthesis of (4-aminophenyl)diphenylphosphine oxide 1 and (4-ethynylphenyl)diphenylhosphine oxide 3

Compounds **1**[154] and **3**[155] were synthesized by literature procedures in 64% and 72% yield, respectively.

Synthesis of (4-azidophenyl)diphenylphosphine oxide 2

A solution of (4-aminophenyl)diphenylphosphine oxide **1** (1.06 g, 3.61 mmol) in acetone (10 mL), H_2SO_4 (2.7 mL) and H_2O (14.4 mL) was added with a solution of $NaNO_2$ (0.368 g, 5.33 mmol) in H_2O (2.2 mL) at 0°C. After stirring for 1.5 h at 0°C, a solution of NaN_3 (0.4 g, 6.13 mmol) in H_2O (2 mL) was added dropwise at 0°C. The resulting suspension was stirred for 1.5 h at 0°C and at room temperature for 15 h. After the completion of the reaction, the mixture was extracted with EtOAc (100 mL). The combined organic extracts were washed with brine, dried over anhydrous $MgSO_4$, filtered, and evaporated *in vacuo* to afford azide **2** as an off-white solid (1.09 g, 96%). Mp. 119-121 °C. ^{1}H NMR (500 MHz, chloroform-*d*) δ 7.76 – 7.61 (m, 6H), 7.60 – 7.53 (m, 2H), 7.52 – 7.44 (m, 4H), 7.17 – 7.05 (m, 2H). ^{13}C NMR (126 MHz, Chloroform-*d*) δ 143.98 (d, *J* = 3.0 Hz), 133.85 (d, *J* = 10.8 Hz), 132.29 (d, *J* = 105.0 Hz), 132.08 (d, *J* = 3.2 Hz), 132.01 (d, *J* = 10.1 Hz), 128.80 (d, *J* = 106.9 Hz), 128.58 (d, *J* = 12.1 Hz), 119.10 (d, *J* = 13.0 Hz). ^{31}P NMR (202 MHz, chloroform-*d*) δ 28.61. Elemental analysis: calculated for $C_{18}H_{14}N_3OP$: C 67,71; H 4,42; N 13,16%. Found: C 67,66; H 4,48; N 13,22%

Synthesis of *p*-azido aniline 10

Compound **10** was synthesized from 4-bromoaniline in quantitative yield following a procedure reported in literature.[156]

Oxidation of CNTs

A 100 mL flask was added with CNTs 500 mg and 40 mL of a 3:1 solution of 96% sulfuric acid/65% nitric acid. The mixture was stirred at reflux for 30 min, diluted with fresh water in ice bath and the acidic solution removed by centrifugation (10 min at 1400 rcf). The solid was dispersed with water and centrifuged 30 min at 1400 rcf. The solid was again dispersed with water and filtered over a 0.2 µM PC membrane and washed until neutral pH of the filtered solution was obtained. Purified Ox-MWCNTs were collected. Yield 39% (194.6 mg). FT-IR: 3431, 1704, 1224 cm^{-1}. Elemental analysis C 77,72; H 0,84; N 0,19%.

Synthesis of CNTs-Tour-PO (6)

A 5 mL flask was added with CNTs (10 mg, 0.83 mmol) and amino phosphine oxide **1** (54.3 mg, 0.185 mmol and 2.5 mL of anhydrous DMF. The mixture was kept in ultrasound bath for 10 min, under inert atmosphere, and 19.3 mg (0.165 mmol) of isopentyl nitrite were added. The mixture was stirred at 80°C under nitrogen for 16 h. The dispersion was diluted with a 1:1 solution of isopropanol:di-isopropyl ether and centrifuged for 15' at 1400 rcf. The supernatant solution was removed and the solid was washed by 5 cycles of dispersion in fresh solvent and centrifugation (4 times with a 2:1 isopropanol:di-isopropyl ether solution and once with a 1:1 solution of the same solvents. The product was finally recovered and dried to afford 15 mg of a black powder. ICP-AES analysis: phosphorus 1.255%, 0.41 mmol/g. FT-IR (KBr): 3328, 1724, 1579, 1384, 1154 and 1116 cm^{-1}.

Synthesis of GPs-Tour-PO (7)

A 5 mL flask was added with GPs 11.6 mg (0.95 mmol) , amino phosphine oxide **1** (54.3 mg, 0.185 mmol) and 2.5 mL of anhydrous DMF. The mixture was kept in an ultrasound bath for 30 min, under inert atmosphere, then 19.3 mg (0.165 mmol) of isopentyl nitrite were added and the mixture was stirred at 80°C under nitrogen for 16h. The dispersion was diluted with isopropanol and centrifuged for 15 min at 1400 rcf. The supernatant was removed and the solid was washed by cycle of dispersion in fresh methanol and centrifugation (six times). The product was recovered and dried to afford 12.5 mg. ICP-AES analysis: phosphorus 0.275%, 0.087 mmol/g.

Synthesis of OX-MWCNTs-Nitrene-PO (8)

A 50 mL flask was added with CNTs (10 mg) and 20 mL of 1,2-dichlorobenzene. The mixture was kept in an ultrasound bath for 30'. Azido phosphine oxide **2 (**39 mg 0.12 mmol) was added and the dispersion sonicated again for 10'. The resulting dispersion

was kept at 165°C under vigorous stirring for 4 days. The mixture was filtered through a 0.2 μm pore PTFE membrane and thoroughly washed with a solution of diisopropyl ether and isopropanol 1:1. The product was recovered and dried to afford 13.3 mg of a black powder. Elemental analysis C 76.07, H 1.12 and N 0.82 %. ICP-AES phosphorus 1.807%, 0.583 mmol/g. FT-IR (KBr): 3312, 1718, 1559, 1164 e 1114 cm^{-1} P=O stretching.

Synthesis of GPs-nitrene-PO (9)

A 50 mL flask was added with GPs (11.5 mg) and 20 mL of 1,2-dichlorobenzene. The mixture was kept in ultrasound bath for 30'. Azido phosphine oxide **2** (39 mg, 0.12 mmol) was added and the mixture sonicated again for 10'. The dispersion was kept at 165°C under vigorous stirring for 4 days. The mixture was, then, diluted with isopropanol and centrifuged 15' at 1400 rcf. The supernatant was removed, and the precipitate was washed by 5 cycles of dispersion and centrifugation (5' in ultrasound bath and centrifugation for 15' at 1400 rcf), with a solution of di-isopropyl ether and isopropanol 1:1. The product was recovered and dried to afford 13.1 mg. Elemental analysis C 90.36 %, H 0.58 and N 0.42%. ICP-AES 0,61 % of phosphorous. FT-IR (KBr): 1195 e 1181 cm^{-1} P=O stretching.

Synthesis OX-MWCNTs-N$_3$ (11)

A 10 mL flask was added with CNTs (50 mg), **10** (122.96 mg, 0.91 mmol), dry DMF (5.2 mL) and the mixture was sonicated with an ultrasound bath (10 min). The dispersion was added with isopentyl nitrite 97.62 mg (0.83 mmol) was added and stirred at 60°C for 24 h. The suspension was filtered over a 0.2 μm PTFE membrane, and the solid was washed with DMF and acetone until colorless solution obtained. CNTs-Azide were recovered with acetone and dried to afford 50.5 mg of a black powder. FT IR (KBr): 2118 nm N$_3$ stretching. Elemental analysis C 66.94 %, H 3.83 % and N 7.00 %. Azide loading based on elemental analysis 1.63 mmol/g.

Synthesis of GPs-N$_3$ (12)

A 25 mL flask was added with GPs (33 mg), **10 (**82 mg 0.61 mmol), 1,2-dichlorobenzene (2.64 mL) and dry DMF (5.2 mL). The mixture was dispersed with ultrasound bath. Isopentyl nitrite (63.9 mg, 0.54mmol) was added and the mixture was stirred at 60°C for 24 h. The suspension was filtered over a 0.2 µm ptfe membrane and the solid was thoroughly washed with DMF and Acetone until a colorless solution was obtained. Material was recovered with acetone and dried to obtain 32.5 mg of a black powder. FT IR (KBr) 2119 nm N$_3$ stretching. Elemental analysis C 97.7 %, H 0.15 % and N 0.31 %. Azide loading based on elemental analysis 0.075 mmol/g.

Synthesis of CNTs-Click-PO (13)

A 25 mL flask was added with **11** (30 mg, 0.049 mmol of azide), phosphine oxide **3** (17.75 mg, 0,059 mmol, 1.2 eq) of copper iodide triethyl phosphite (3.49 mg, 0.0098 mmol, 0.2 eq) and 8.5 mL of degassed dry DMF. The mixture dispersed with an ultrasound bath under inert atmosphere. After dispersion, DIPEA 18.35 mg (0.142 mmol, 2.9eq) was added and the dispersion stirred at 60°C for 48 h. The suspension was filtered over a 0.2 µm PTFE membrane and the solid was thoroughly washed with DMF and acetone until a colorless solution was obtained. The material was recovered and dried to afford 28.2 mg of a black powder. FT-IR (KBr) 3105, 2103, 1722, 1658, 1579, 1386, 1170 e 1118 cm^{-1}. ICP AES analysis: phosphorus 0.847%.

Synthesis of GPs-Click-PO (14)

A 25 mL flask was added with **12 (**28.5 mg, 0.0023 mmol of azide), phosphine oxide **3** (1 mg, 0.0027 mmol, 1.2 eq) copper iodide triethyl phosphite (0.162 mg, 0.00045 mmol, 0.2 eq) and degassed 1,2-dichlorobenzene (8.5 mL). The mixture was dispersed with an ultrasound bath. DIPEA (1 mg, 0.0078 mmol, 2.9 eq) was added and the reaction mixture was stirred at 60°C for 48 h. The suspension was diluted with acetone and centrifuged (10' at 1500 rcf) to remove 1,2-dichlorobenzene then the solid was

dispersed in DMF and filtered over a 0.2 μm PTFE membrane. The solid was washed with DMF and acetone until colorless solution obtained. The material was recovered and characterized to afford 28.7 mg of a black powder. ICP AES analysis: phosphorus 0.057%.

General procedure for the reduction of PO

A Pyrex tube was added with carbonaceous substrate (5 mg), degassed 1,2-dichlorobenzene (1 mL) and the mixture was dispersed with an ultrasound bath. The mixture was then added with triethyl phosphite (387.6 mg, 2.33 mmol) and trichlorosilane (134.2 mg, 0.99 mmol) and the reaction left 48h at 100°C under vigorous stirring. The material was washed by repeated dispersion and centrifugation cycles (10' at 1400 rcf): one cycle with isopropanol to remove the reaction solvent, three times with 1M aqueous sodium hydroxide, three times with aqueous hydrogen chloride 0.1M, three times with methanol and three times with isopropyl ether. The reduction was checked by XPS spectroscopy.

General procedure for the Staudinger ligation.

A pirex tube was added with phosphine decorated CNTs (**8**-red, 5 mg) degassed dry toluene (1 mL), carboxylic acid (0.19 mmol, 1 eq), a solution of benzyl azide (0.19 mmol) in 0.5 mL of degassed toluene and phenyl silane (21 mg,0.19 mmol, 1 eq) and the reaction stirred at 110°C under nitrogen atmosphere for 22 h. The catalyst was recovered by centrifugation (2X 15 min. at 1500 rcf) and dispersion with toluene 20 mL. The solution was evaporated under vacuum giving the crude product, the amide was recovered after flash chromatography (silica) using a mixture of hexane:ethyl acetate 1:1.

N-Benzylbenzamide (**17**): R_f = 0.48 (hexane:ethyl acetate 1:1), yield 75%. Spectral data already reported in literature.[142]

N-phenylcinnamamide (**19**): R$_f$ =0.77 (hexane:ethyl acetate 1:1), yield 55%. Spectral data already reported in literature.[142]

N-phenylcinnamamide (**21**): R$_f$ =0.64 (hexane:ethyl acetate 1:1), yield 58%. Spectral data already reported in literature.[142]

XPS Measurements

The chemical composition of the near surface sample portion was obtained by means of X-ray Photoelectron Spectroscopy (XPS). The experiments were carried out in an ultrahigh vacuum (UHV, 10-9 mbar) system equipped with a VSW HAC 500 hemispherical electron-energy analyzer using a non-monochromatic Mg Kα X-ray source operating at 120 W power (10 kVx10 mA). The samples were introduced in the UHV system via a loadlock under an inert gas (N_2) flux. Survey and high-resolution spectra (C1s, O1s, P2p) were acquired in the constant analyzer energy mode (CAE) at pass energy Epas = 22 eV with a step size of 1.0 and 0.1 eV, respectively. The peaks were fitted using CasaXPS software employing Gauss-Lorentz curves after subtraction of a Shirley-type background. Binding Energy (BE) scale was calibrated taking as reference the position of aliphatic C1s component (adventitious carbon) at 284.8 ± 0.1 eV.
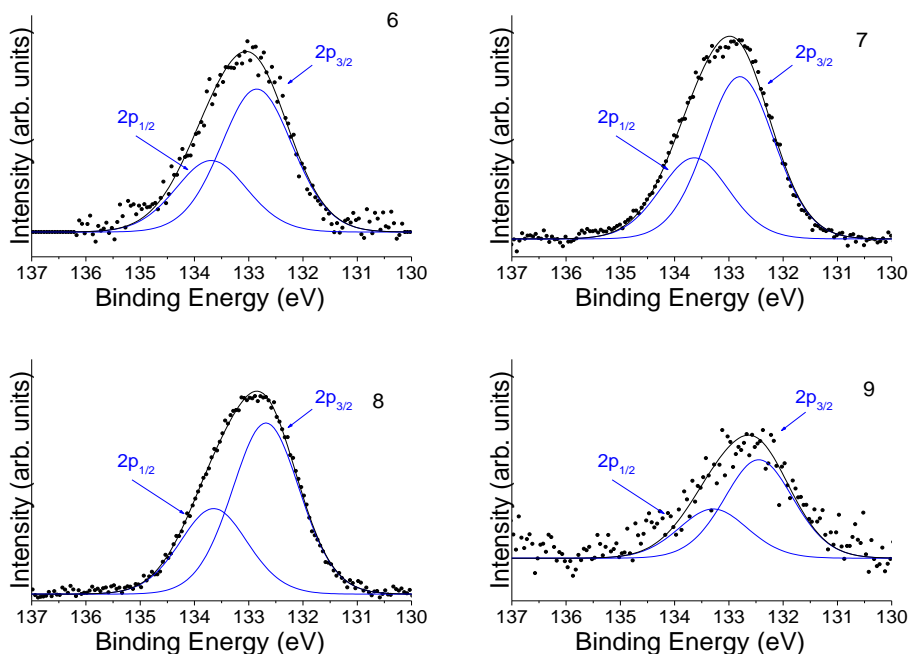
Figure 11. XPS spectra of compounds **6**, **7**, **8**, e **9**, all signals are at 132.8 eV.
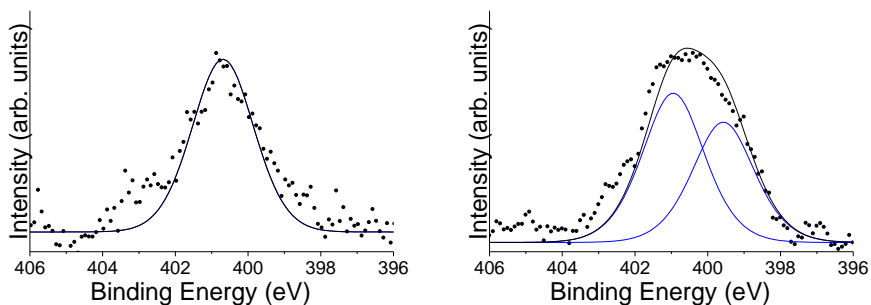
Figure

12. XPS spectra of compounds 6 on the left and 7 on the right, the binding energy of 400.7 eV, which evidence the presence of the nitrogen in both samples.

FT-IR SPECTRA

IR spectra were recorded on a Perkin-Elmer FT-IR 881 or Shimadzu FT-IR 8400s spectrometer. All the spectra were recorded in KBr pellets with a concentration of substances of 1mg in 100 mg and under nitrogen atmosphere to remove the noise.
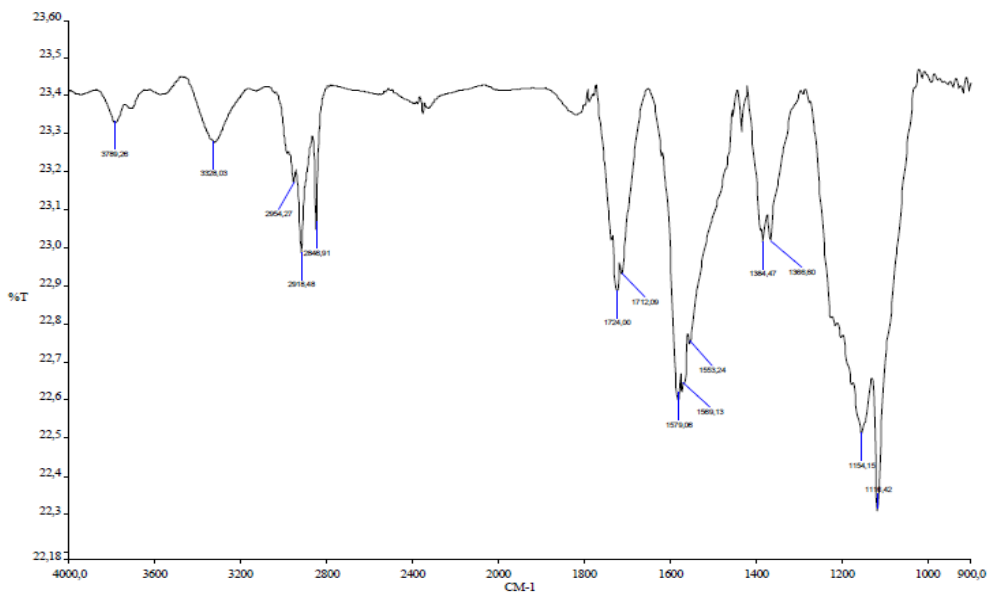
Figure 13. FT-IR Spectrum of Ox-MWCNTs-Tour-PO (6).
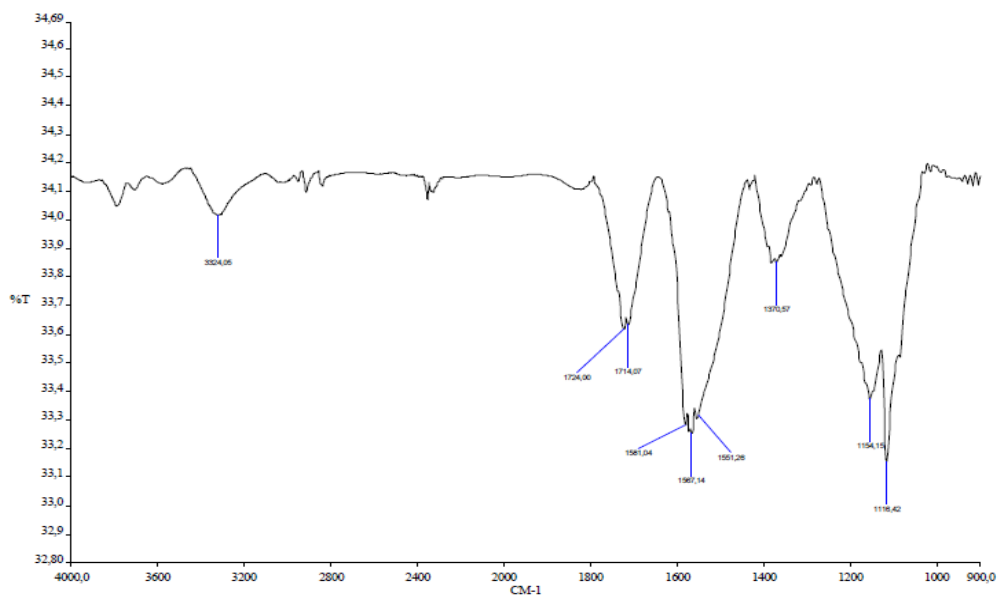
Figure 14. FT-IR Spectrum of CNT-Nit-PO (8).
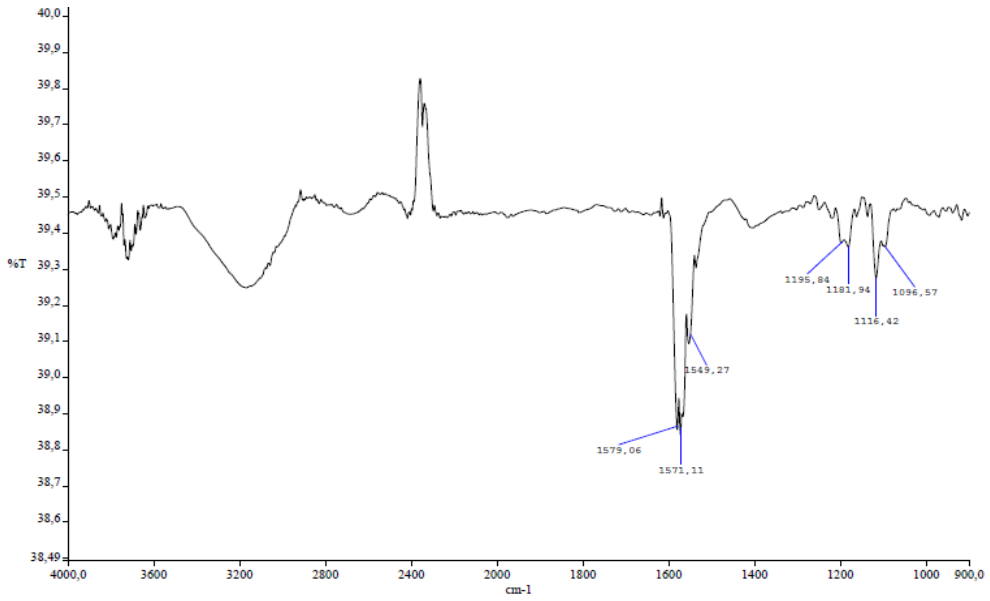
Figure 15. FT-IR spectrum GNP-Nit-PO (9).
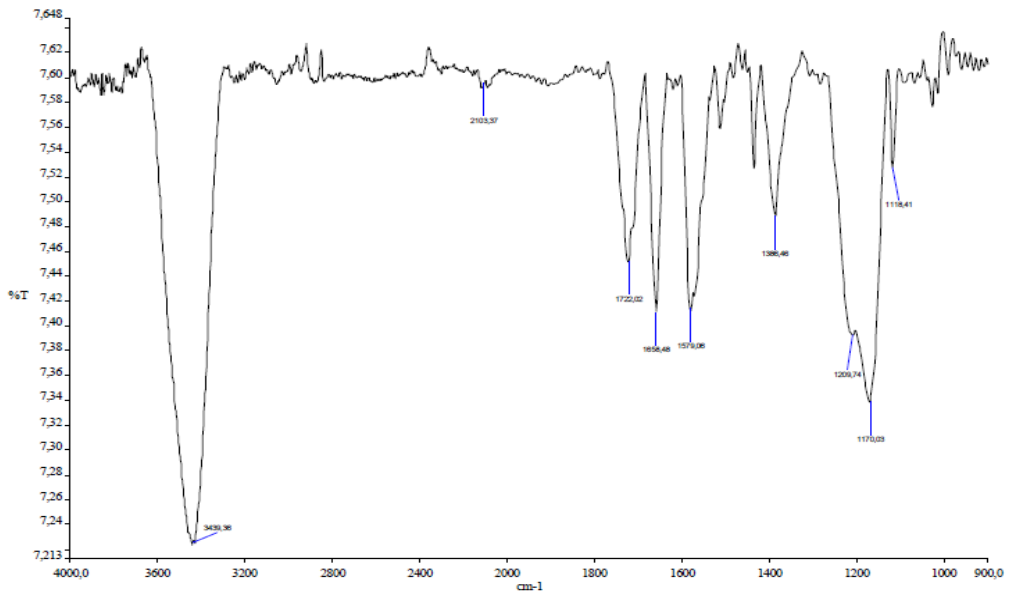
Figure 16. FT-IR spectrum OxMWCNTs-Click-PO (13).
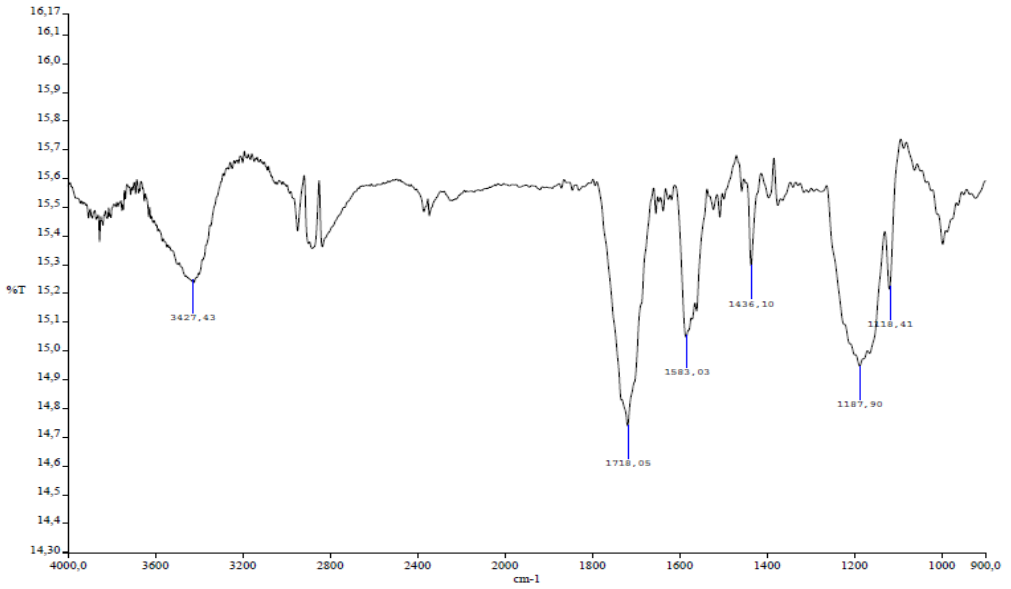
Figure 17. FT-IR spectrum OxMWCNTs-Tour-P (**6**-red).
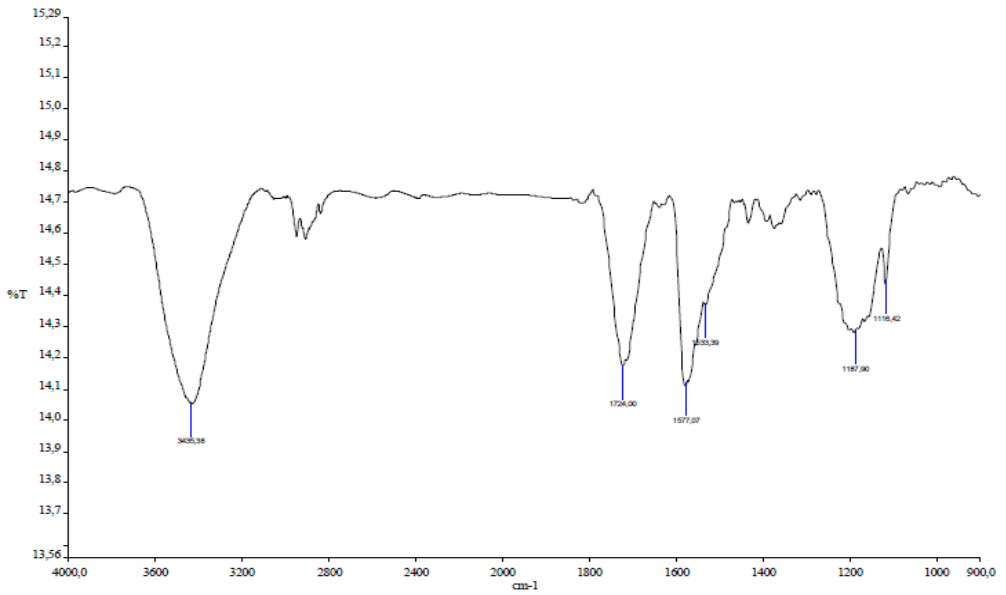
Figure 18. FT-IR spectrum OxMWCNTs-Nit-P (**8**-red).
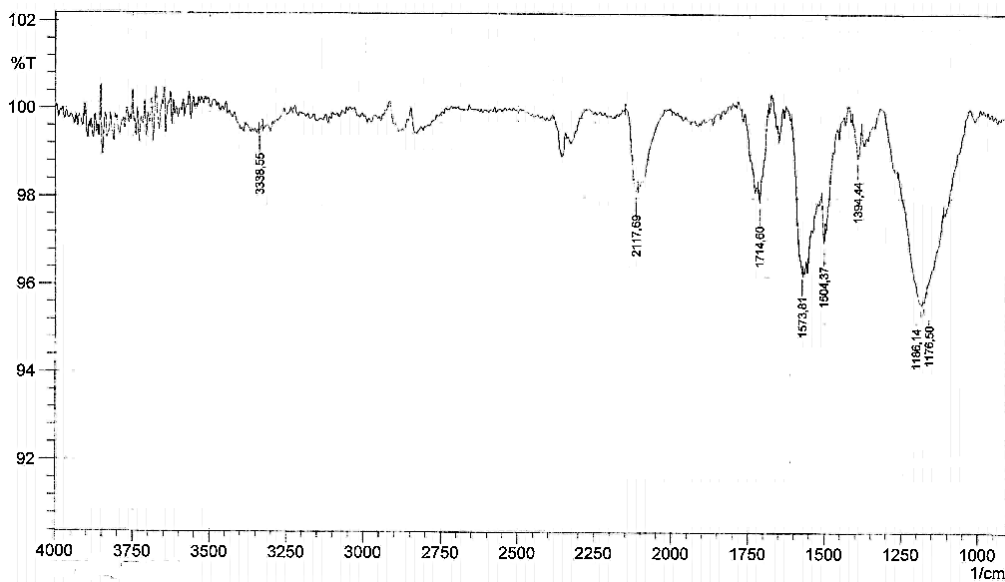
Figure 19. FT-IR spectrum OxMWCNTs-N$_3$ (11).
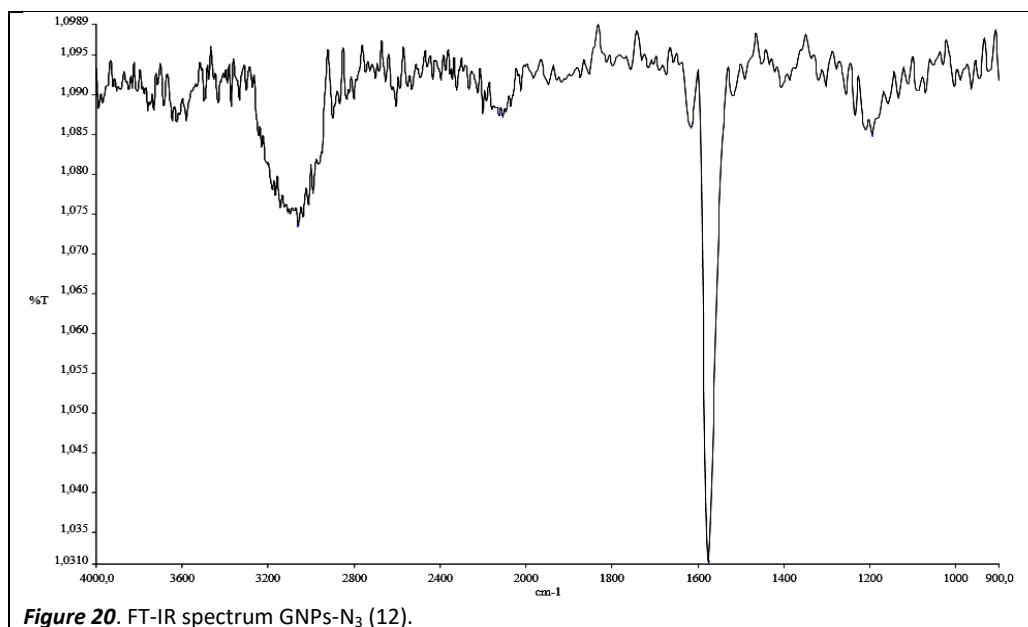
Figure 20. FT-IR spectrum GNPs-N$_3$ (12).

Raman Measurements

Raman spectra were measured by a Renishaw RM2000 instrument, equipped with a diode laser emitting at 785 nm. Sample irradiation was accomplished by using the 50x microscope objective of a Leica Microscope DMLM. The beam power was~3mW, and the laser spot size was adjusted between 1 and 3 micrometers. The backscattered Raman signal was fed into the monochromator through 40 micrometer slits and detected by an air-cooled CCD (2.5 cm-1 per pixel) filtered by a double holographic Notch filters system. Spectra were calibrated with respect to a silicon wafer at 520 cm-1.
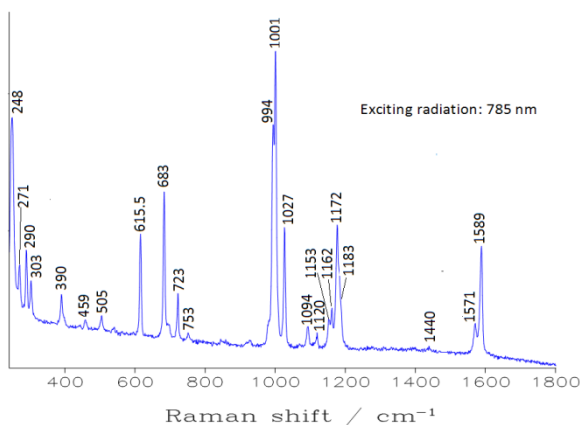
Raman Freq.	Assignment
615.5	ring bending in plane
683	ring bending in plane
994	Ring breathing mode
1001	Ring breathing mode
1027	Ring trigonal mode
1094	P-Ph stretching
1120	P-Ph stretching
1153	H ring bending in plane
1162	H ring bending in plane
1172	P=O stretching
1571	C=C ring stretching
1589	C=C ring stretching

Figure 21. On the left the raman spectrum of phosphine oxide 2, on the right the signal assignment.
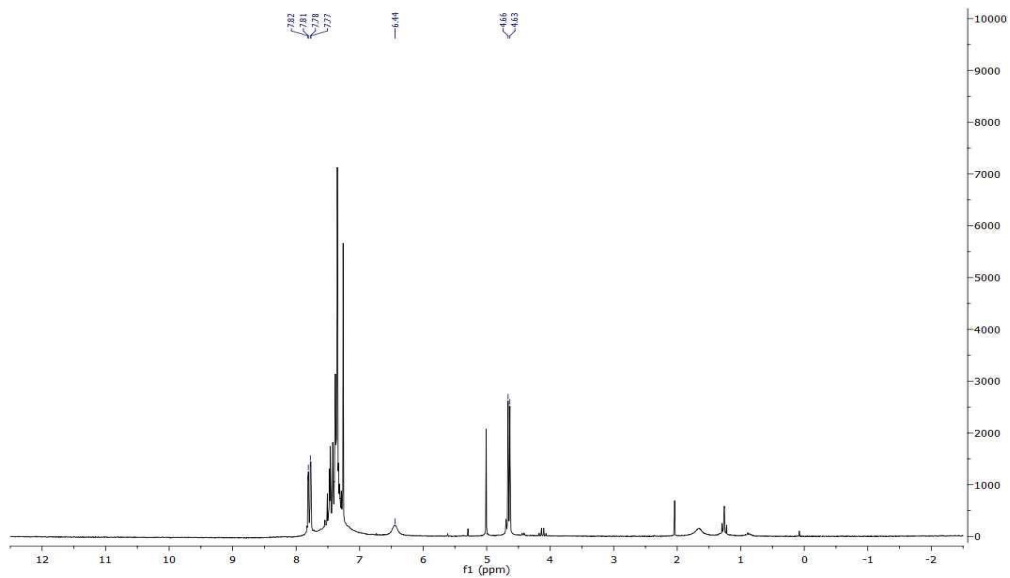
Figure 22. ^{1}H-NMR (200 MHz CDCl$_3$) of product **17**.
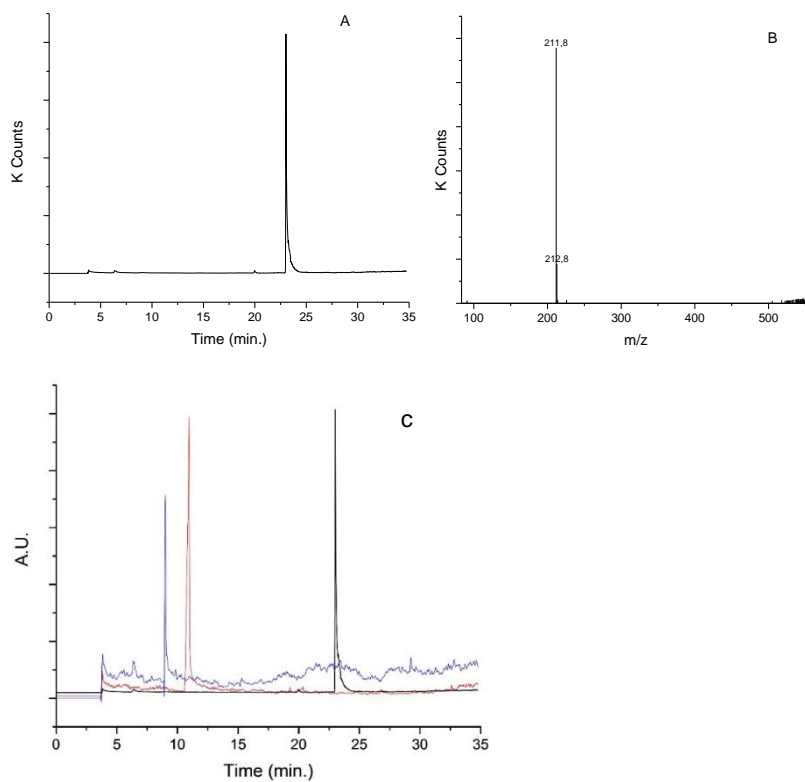
Figure 23. GC-MS Spectra of compound **17**: A) Chromatogram of the purified product; B) Mass spectrum with chemical ionization; C) Comparison three different chromatograms: black product 17, blue benzyl azide and benzoic acid red.

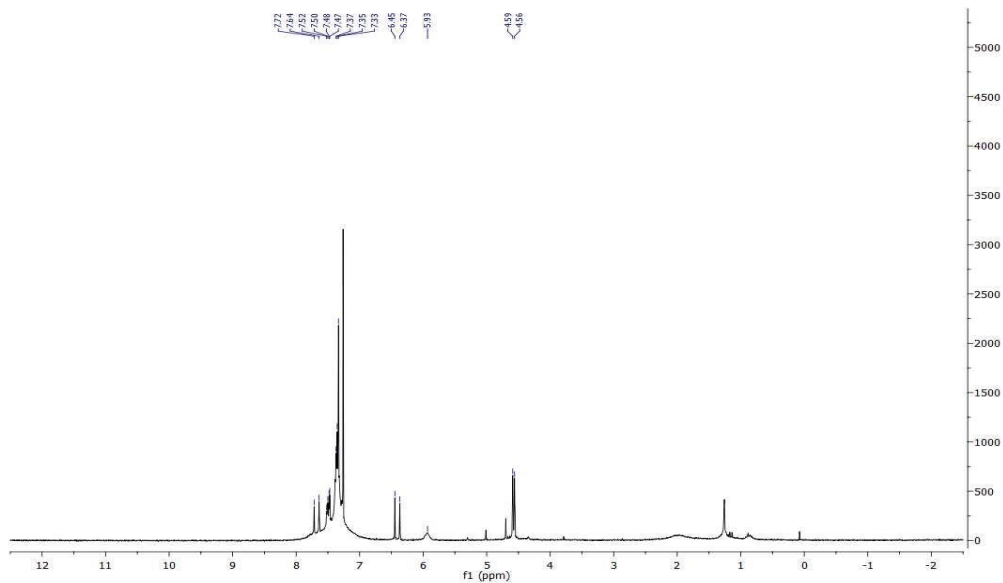*Figure 24.* ^{1}H-NMR (200 MHz CDCl$_3$) of Product **19**.
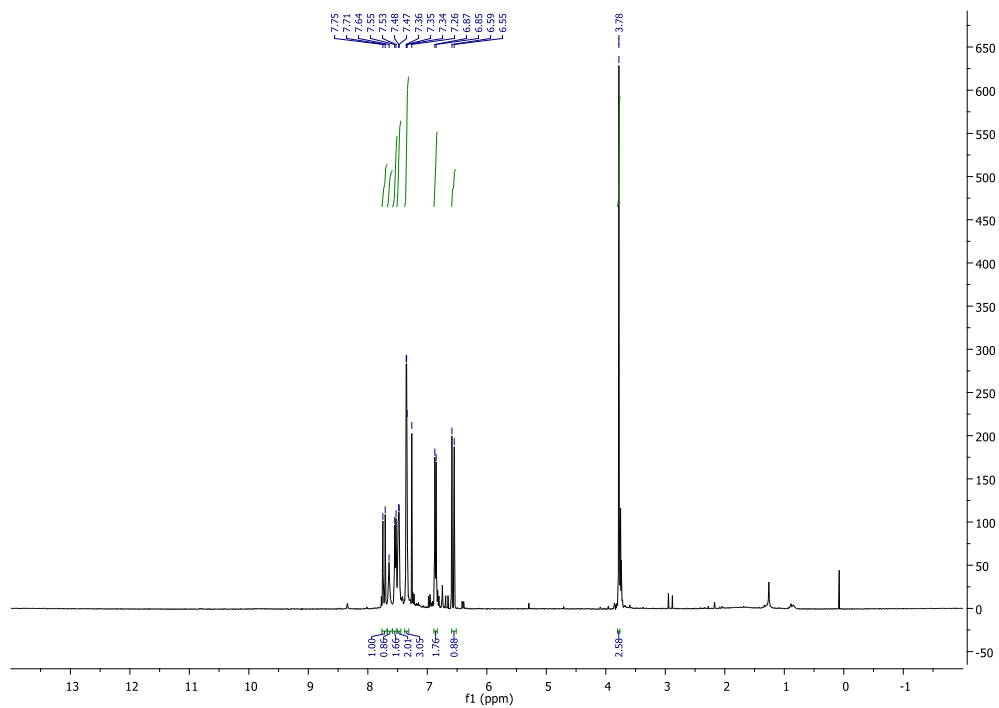
Figure 25. ^{1}H-NMR (400 MHz CDCl$_3$) of Product **21**.
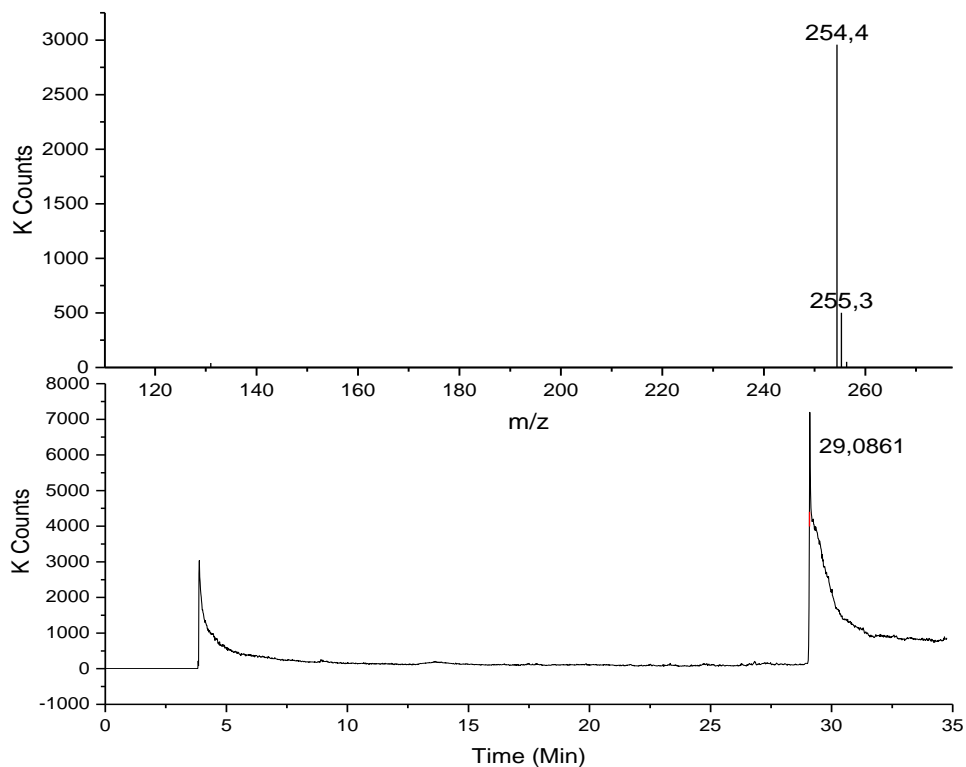
Figure 26. GC-MS Spectra of compound **21**: top Mass spectrum with chemical ionization; bottom chromatogram of the purified product.

References

(1)   Webster, T. J. *Int. J. Nanomedicine* **2006**, *1* (2), 115–116.

(2)   Iijima, S. *Nature* **1991**, *354* (6348), 56–58.

(3)   Tasis, D.; Tagmatarchis, N.; Bianco, A.; Prato, M. *Chem. Rev.* **2006**, *106* (3), 1105–1136.

(4)   Kumar, I.; Rana, S.; Cho, J. W. *Chem. - A Eur. J.* **2011**, *17* (40), 11092–11101.

(5)   Kumar, S.; Rani, R.; Dilbaghi, N.; Tankeshwar, K.; Kim, K.-H. *Chem. Soc. Rev.* **2017**, *46* (1), 158–196.

(6)   Corma, A.; Garcia, H.; Leyva, A. *J. Mol. Catal. A Chem.* **2005**, *230* (1–2), 97–105.

(7)   Hong, S. Y.; Tobias, G.; Al-Jamal, K. T.; Ballesteros, B.; Ali-Boucetta, H.; Lozano-

Perez, S.; Nellist, P. D.; Sim, R. B.; Finucane, C.; Mather, S. J.; et al. *Nat. Mater.* **2010**, *9* (6), 485–490.

(8) Fedeli, S.; Paoli, P.; Brandi, A.; Venturini, L.; Giambastiani, G.; Tuci, G.; Cicchi, S. *Chem. - A Eur. J.* **2015**, *21* (43), 15349–15353.

(9) Tasis, D.; Tagmatarchis, N.; Bianco, A.; Prato, M.; Tasis, D.; Tagmatarchis, N.; Bianco, A.; Prato, M. **2006**, *106* (February), 1105–1136.

(10) Wohlstadter, J. N.; Wilbur, J. L.; Sigal, G. B.; Biebuyck, H. A.; Billadeau, M. A.; Dong, L.; Fischer, A. B.; Gudibande, S. R.; Jameison, S. H.; Kenten, J. H.; et al. *Adv. Mater.* **2003**, *15* (14), 1184–1187.

(11) Xiong, J.; Zheng, Z.; Qin, X.; Li, M.; Li, H.; Wang, X. *Carbon N. Y.* **2006**, *44* (13), 2701–2707.

(12) Mooney, E.; Dockery, P.; Greiser, U.; Murphy, M.; Barron, V. *Nano Lett.* **2008**, *8* (8), 2137–2143.

(13) Kumar, S.; Rani, R.; Dilbaghi, N.; Tankeshwar, K.; Kim, K. H. *Chem. Soc. Rev.* **2017**, *46* (1), 158–196.

(14) Karousis, N.; Tagmatarchis, N.; Tasis, D. *Chem. Rev.* **2010**, *110* (9), 5366–5397.

(15) Tromp, R. M.; Afzali, A.; Freitag, M.; Mitzi, D. B.; Chen, Z. *Nano Lett.* **2008**, *8* (2), 469–472.

(16) Kim, U. J.; Furtado, C. A.; Liu, X.; Chen, G.; Eklund, P. C. *J. Am. Chem. Soc.* **2005**, *127* (44), 15437–15445.

(17) Dresselhaus, M. S.; Dresselhaus, G.; Saito, R.; Jorio, A. *Phys. Rep.* **2005**, *409* (2), 47–99.

(18) Kane, A. B.; Hurt, R. H.; Gao, H. *Toxicol. Appl. Pharmacol.* **2018**, No. June.

(19) Grosse, Y.; Loomis, D.; Guyton, K. Z.; Lauby-Secretan, B.; El Ghissassi, F.; Bouvard, V.; Benbrahim-Tallaa, L.; Guha, N.; Scoccianti, C.; Mattock, H.; et al. *Lancet Oncol.* **2014**, *15* (13), 1427–1428.

(20) Takagi, A.; Hirose, A.; Nishimura, T.; Fukumori, N.; Ogata, A.; Ohashi, N.; Kitajima, S.; Kanno, J. *J. Toxicol. Sci.* **2008**, *33* (1), 105–116.

(21) Nagai, H.; Okazaki, Y.; Chew, S. H.; Misawa, N.; Yamashita, Y.; Akatsuka, S.; Ishihara, T.; Yamashita, K.; Yoshikawa, Y.; Yasui, H.; et al. *Proc. Natl. Acad. Sci.* **2011**, *108* (49), E1330–E1338.

(22) Muller, J.; Delos, M.; Panin, N.; Rabolli, V.; Huaux, F.; Lison, D. *Toxicol. Sci.* **2009**, *110* (2), 442–448.

(23) Rittinghausen, S.; Hackbarth, A.; Creutzenberg, O.; Ernst, H.; Heinrich, U.; Leonhardt, A.; Schaudien, D. *Part. Fibre Toxicol.* **2014**, *11* (1), 1–18.

(24) Donaldson, K.; Poland, C. A.; Murphy, F. A.; MacFarlane, M.; Chernova, T.; Schinwald, A. *Adv. Drug Deliv. Rev.* **2013**, *65* (15), 2078–2086.

(25) Kagan, V. E.; Konduru, N. V.; Feng, W.; Allen, B. L.; Conroy, J.; Volkov, Y.; Vlasova, I. I.; Belikova, N. A.; Yanamala, N.; Kapralov, A.; et al. *Nat. Nanotechnol.* **2010**, *5* (5), 354–359.

(26) Sureshbabu, A. R.; Kurapati, R.; Russier, J.; Ménard-Moyon, C.; Bartolini, I.;

Meneghetti, M.; Kostarelos, K.; Bianco, A. *Biomaterials* **2015**, *72*, 20–28.

(27)   Mata, D.; Amaral, M.; Fernandes, A. J. S.; Colaço, B.; Gama, A.; Paiva, M. C.; Gomes, P. S.; Silva, R. F.; Fernandes, M. H. *Nanoscale* **2015**, *7* (20), 9238–9251.

(28)   Russier, J.; Oudjedi, L.; Piponnier, M.; Bussy, C.; Prato, M.; Kostarelos, K.; Lounis, B.; Bianco, A.; Cognet, L. *Nanoscale* **2017**, *9* (14), 4642–4645.

(29)   Pantarotto, D.; Briand, J.-P.; Prato, M.; Bianco, A. *Chem. Commun. (Camb).* **2004**, No. 1, 16–17.

(30)   Lee, Y.; Geckeler, K. E. *Adv. Mater.* **2010**, *22* (36), 4076–4083.

(31)   Kam, N. W. S.; Dai, H. *Phys. Status Solidi Basic Res.* **2006**, *243* (13), 3561–3566.

(32)   Zhou, F.; Xing, D.; Wu, B.; Wu, S.; Ou, Z.; Chen, W. R. *Nano Lett.* **2010**, *10* (5), 1677–1681.

(33)   Cherukuri, P.; Bachilo, S. M.; Litovsky, S. H.; Weisman, R. B. *J. Am. Chem. Soc.* **2004**, *126* (48), 15638–15639.

(34)   McDevitt, M. R.; Chattopadhyay, D.; Kappel, B. J.; Jaggi, J. S.; Schiffman, S. R.; Antczak, C.; Njardarson, J. T.; Brentjens, R.; Scheinberg, D. A. *J. Nucl. Med.* **2007**, *48* (7), 1180–1189.

(35)   Zhang Z. Zhang, and Y. Zhang, W. *Nanoscale Res. Lett.* **2011**, *6* (555), 1–22.

(36)   Li, J.; Pant, A.; Chin, C. F.; Ang, W. H.; Ménard-Moyon, C.; Nayak, T. R.; Gibson, D.; Ramaprabhu, S.; Panczyk, T.; Bianco, A.; et al. *Nanomedicine Nanotechnology, Biol. Med.* **2014**, *10* (7), 1465–1475.

(37)   Fedeli, S.; Brandi, A.; Venturini, L.; Chiarugi, P.; Giannoni, E.; Paoli, P.; Corti, D.; Giambastiani, G.; Tuci, G.; Cicchi, S. *J. Mater. Chem. B* **2016**, *4* (21), 3823–3831.

(38)   Biagiotti, G.; Fedeli, S.; Tuci, G.; Luconi, L.; Giambastiani, G.; Brandi, A.; Pisaneschi, F.; Cicchi, S.; Paoli, P. *J. Mater. Chem. B* **2018**, *6* (14).

(39)   Yang, S.; Guo, W.; Lin, Y.; Deng, X.; Wang, H.; Sun, H.; Liu, Y.; Wang, X.; Wang, W.; Chen, M.; et al. *J. Phys. Chem. C* **2007**, *111* (48), 17761–17764.

(40)   Cherukuri, P.; Gannon, C. J.; Leeuw, T. K.; Schmidt, H. K.; Smalley, R. E.; Curley, S. A.; Weisman, R. B. *Proc. Natl. Acad. Sci.* **2006**, *103* (50), 18882–18886.

(41)   OWENSIII, D.; PEPPAS, N. *Int. J. Pharm.* **2006**, *307* (1), 93–102.

(42)   Yang, S.; Fernando, K. A. S.; Liu, J.; Wang, J.; Sun, H.; Liu, Y.; Chen, M.; Huang, Y.; Wang, X.; Wang, H.; et al. *Small* **2008**, *4* (7), 940–944.

(43)   Liu, X.; Tao, H.; Yang, K.; Zhang, S.; Lee, S. T.; Liu, Z. *Biomaterials* **2011**, *32* (1), 144–151.

(44)   Lacerda, L.; Soundararajan, A.; Singh, R.; Pastorin, G.; Al-Jamal, K. T.; Turton, J.; Frederik, P.; Herrero, M. A.; Li, S.; Bao, A.; et al. *Adv. Mater.* **2008**, *20* (2), 225–230.

(45)   Wang, J. T. W.; Fabbro, C.; Venturelli, E.; Ménard-Moyon, C.; Chaloin, O.; Da Ros, T.; Methven, L.; Nunes, A.; Sosabowski, J. K.; Mather, S. J.; et al. *Biomaterials* **2014**, *35* (35), 9517–9528.

(46)   Singh, R.; Pantarotto, D.; Lacerda, L.; Pastorin, G.; Klumpp, C.; Prato, M.; Bianco, A.; Kostarelos, K. *Proc. Natl. Acad. Sci. U. S. A.* **2006**, *103* (9), 3357–

3362.

(47) Ruggiero, A.; Villa, C. H.; Bander, E.; Rey, D. A.; Bergkvist, M.; Batt, C. A.; Manova-Todorova, K.; Deen, W. M.; Scheinberg, D. A.; McDevitt, M. R. *Proc. Natl. Acad. Sci. U. S. A.* **2010**, *107* (27), 12369–12374.

(48) Yang, S. T.; Luo, J.; Zhou, Q.; Wang, H. *Theranostics* **2012**, *2* (3), 271–282.

(49) Chen, M.; Zeng, G.; Xu, P.; Zhang, Y.; Jiang, D.; Zhou, S. *Environ. Sci. Nano* **2017**, *4* (3), 720–727.

(50) Kouznetsov, V. V.; Merchan-Arenas, D. R.; Tangarife-Castaño, V.; Correa-Royero, J.; Betancur-Galvis, L. *Med. Chem. Res.* **2016**, *25* (3), 429–437.

(51) Thorn, Caroline; Oshiro, Connie; Marsh, Sharon; Hernandez-Boussard, Tina; McLeod, Howard; Klein, Teri; Altman, R. *Pharmacogenet Genomics* **2012**, *21* (7), 440–446.

(52) Gabizon, a; Shmeeda, H.; Barenholz, Y. *Clin.Pharmacokinet.* **2003**, *42* (5), 419–436.

(53) Fedeli, S.; Brandi, A.; Venturini, L.; Chiarugi, P.; Giannoni, E.; Paoli, P.; Corti, D.; Giambastiani, G.; Tuci, G.; Cicchi, S. *J. Mater. Chem. B* **2016**, *4* (21), 3823–3831.

(54) Li, R.; Wu, R.; Zhao, L.; Wu, M.; Yang, L.; Zou, H. *ACS Nano* **2010**, *4* (3), 1399–1408.

(55) Pistone, A.; Iannazzo, D.; Ansari, S.; Milone, C.; Salamò, M.; Galvagno, S.; Cirmi, S.; Navarra, M. *Int. J. Pharm.* **2016**, *515* (1–2), 30–36.

(56) Mayer, M. J.; Klotz, L. H.; Venkateswaran, V. *Prostate Cancer Prostatic Dis.* **2015**, *18* (4), 303–309.

(57) Dowling, R. J. O.; Niraula, S.; Stambolic, V.; Goodwin, P. J. *J. Mol. Endocrinol.* **2012**, *48* (3).

(58) Hirsch, H. A.; Iliopoulos, D.; Tsichlis, P. N.; Struhl, K. *Cancer Res.* **2009**, *69* (19), 7507–7511.

(59) Orecchioni, S.; Reggiani, F.; Talarico, G.; Mancuso, P.; Calleri, A.; Gregato, G.; Labanca, V.; Noonan, D. M.; Dallaglio, K.; Albini, A.; et al. *Int. J. Cancer* **2015**, *136* (6), E534–E544.

(60) Iliopoulos, D.; Hirsch, H. A.; Struhl, K. *Cancer Res.* **2011**, *71* (9), 3196–3201.

(61) Peng, M.; Darko, K. O.; Tao, T.; Huang, Y.; Su, Q.; He, C.; Yin, T.; Liu, Z.; Yang, X. *Cancer Treat. Rev.* **2017**, *54*, 24–33.

(62) Yoo, S.; Hou, J.; Yi, W.; Li, Y.; Chen, W.; Meng, L.; Si, J.; Hou, X. *Sci. Rep.* **2017**, *7* (1), 1–9.

(63) Russell-Jones, G.; McTavish, K.; McEwan, J.; Rice, J.; Nowotnik, D. *J. Inorg. Biochem.* **2004**, *98* (10 SPEC. ISS.), 1625–1633.

(64) Ojima, I. *Acc. Chem. Res.* **2008**, *41* (1), 108–119.

(65) Fedeli, S.; Paoli, P.; Brandi, A.; Venturini, L.; Giambastiani, G.; Tuci, G.; Cicchi, S. *Chem. - A Eur. J.* **2015**, *21* (43), 15349–15353.

(66) Tuci, G.; Vinattieri, C.; Luconi, L.; Ceppatelli, M.; Cicchi, S.; Brandi, A.; Filippi, J.; Melucci, M.; Giambastiani, G. *Chem. - A Eur. J.* **2012**, *18* (27), 8454–8463.

(67)   Scheibe, B.; Borowiak-Palen, E.; Kalenczuk, R. J. *Mater. Charact.* **2010**, *61* (2), 185–191.

(68)   Sciortino, N.; Fedeli, S.; Paoli, P.; Brandi, A.; Chiarugi, P.; Severi, M.; Cicchi, S. *Int. J. Pharm.* **2017**, *521* (1–2), 69–72.

(69)   Bahr, J. L.; Tour, J. M. *Chem. Mater.* **2001**, *13* (11), 3823–3824.

(70)   Price, B. K.; Tour, J. M. *J. Am. Chem. Soc.* **2006**, *128* (39), 12899–12904.

(71)   Schmidt, G.; Gallon, S.; Esnouf, S.; Bourgoin, J. P.; Chenevier, P. *Chem. - A Eur. J.* **2009**, *15* (9), 2101–2110.

(72)   Lomeda, J. R.; Doyle, C. D.; Kosynkin, D. V.; Hwang, W.-F.; Tour, J. M. *J. Am. Chem. Soc.* **2008**, *130* (48), 16201–16206.

(73)   M??nard-Moyon, C.; Fabbro, C.; Prato, M.; Bianco, A. *Chem. - A Eur. J.* **2011**, *17* (11), 3222–3227.

(74)   Salice, P.; Fabris, E.; Sartorio, C.; Fenaroli, D.; Figà, V.; Casaletto, M. P.; Cataldo, S.; Pignataro, B.; Menna, E. *Carbon N. Y.* **2014**, *74* (2), 73–82.

(75)   Biagiotti, G.; Langè, V.; Ligi, C.; Caporali, S.; Muniz-Miranda, M.; Flis, A.; Pietrusiewicz, K. M.; Ghini, G.; Brandi, A.; Cicchi, S. *Beilstein J. Nanotechnol.* **2017**, *8* (1), 485–493.

(76)   Simões, R. V.; Serganova, I. S.; Kruchevsky, N.; Leftin, A.; Shestov, A. A.; Thaler, H. T.; Sukenick, G.; Locasale, J. W.; Blasberg, R. G.; Koutcher, J. A.; et al. *Neoplasia* **2015**, *17* (8), 671–684.

(77)   Dennison, J. B.; Molina, J. R.; Mitra, S.; Gonzalez-Angulo, A. M.; Balko, J. M.; Kuba, M. G.; Sanders, M. E.; Pinto, J. A.; Gomez, H. L.; Arteaga, C. L.; et al. *Clin. Cancer Res.* **2013**, *19* (13), 3703–3713.

(78)   Vineberg, J. G.; Wang, T.; Zuniga, E. S.; Ojima, I. *J. Med. Chem.* **2015**, *58* (5), 2406–2416.

(79)   Smith, B. R.; Ghosn, E. E. B.; Rallapalli, H.; Prescher, J. A.; Larson, T.; Herzenberg, L. A.; Gambhir, S. S. *Nat. Nanotechnol.* **2014**, *9* (6), 481–487.

(80)   Andón, F. T.; Digifico, E.; Maeda, A.; Erreni, M.; Mantovani, A.; Alonso, M. J.; Allavena, P. *Semin. Immunol.* **2017**, *34* (September), 103–113.

(81)   Købler, C.; Poulsen, S. S.; Saber, A. T.; Jacobsen, N. R.; Wallin, H.; Yauk, C. L.; Halappanavar, S.; Vogel, U.; Qvortrup, K.; Mølhave, K. *PLoS One* **2015**, *10* (1), e0116481.

(82)   Jacobsen, N. R.; Møller, P.; Clausen, P. A.; Saber, A. T.; Micheletti, C.; Jensen, K. A.; Wallin, H.; Vogel, U. *Basic Clin. Pharmacol. Toxicol.* **2017**, *121*, 30–43.

(83)   Liu, Z.; Davis, C.; Cai, W.; He, L.; Chen, X.; Dai, H. *Proc. Natl. Acad. Sci.* **2008**, *105* (5), 1410–1415.

(84)   Ingle, T.; Dervishi, E.; Biris, A. R.; Mustafa, T.; Buchanan, R. A.; Biris, A. S. *J. Appl. Toxicol.* **2013**, *33* (10), 1044–1052.

(85)   Welsher, K.; Sherlock, S. P.; Dai, H. *Proc. Natl. Acad. Sci.* **2011**, *108* (22), 8943–8948.

(86)   Czarny, B.; Georgin, D.; Berthon, F.; Plastow, G.; Pinault, M.; Patriarche, G.;

Thuleau, A.; L'Hermite, M. M.; Taran, F.; Dive, V. *ACS Nano* **2014**, *8* (6), 5715–5724.

(87) Deng, X.; Yang, S.; Nie, H.; Wang, H.; Liu, Y. *Nanotechnology* **2008**, *19* (7), 075101.

(88) Lin, Z.; Zhang, H.; Huang, J.; Xi, Z.; Liu, L.; Lin, B. *Toxicol. Res.* **2013**, *3* (6), 497–502.

(89) Mulvey, J. J.; Villa, C. H.; McDevitt, M. R.; Escorcia, F. E.; Casey, E.; Scheinberg, D. A. *Nat. Nanotechnol.* **2013**, *8* (10), 763–771.

(90) Alidori, S.; Bowman, R. L.; Yarilin, D.; Romin, Y.; Barlas, A.; Mulvey, J. J.; Fujisawa, S.; Xu, K.; Ruggiero, A.; Riabov, V.; et al. *Nat. Commun.* **2016**, *7*, 12343.

(91) Liu, Z.; Cai, W.; He, L.; Nakayama, N.; Chen, K.; Sun, X.; Chen, X.; Dai, H. *Nat. Nanotechnol.* **2007**, *2* (1), 47–52.

(92) McDevitt, M. R.; Chattopadhyay, D.; Jaggi, J. S.; Finn, R. D.; Zanzonico, P. B.; Villa, C.; Rey, D.; Mendenhall, J.; Batt, C. A.; Njardarson, J. T.; et al. *PLoS One* **2007**, *2* (9), e907.

(93) Vaquero, J. J.; Kinahan, P. *Annu. Rev. Biomed. Eng.* **2015**, *17* (1), 385–414.

(94) Wadas, T. J.; Wong, E. H.; Weisman, G. R.; Anderson, C. J. *Chem. Rev.* **2010**, *110* (5), 2858–2902.

(95) Simon, G. M.; Niphakis, M. J.; Cravatt, B. F. *Nat. Chem. Biol.* **2013**, *9* (4), 200–205.

(96) Chang, E.; Liu, H.; Unterschemmann, K.; Ellinghaus, P.; Liu, S.; Gekeler, V.; Cheng, Z.; Berndorff, D.; Gambhir, S. S. *Clin. Cancer Res.* **2015**, *21* (2), 335–346.

(97) Seth T. Gammon1, Federica Pisaneschi, Madhavi L. Bandi, Melinda G. Smith, Yuting Sun, Yi Rao, Florian Muller, Franklin Wong, John De Groot, Jeffrey Ackroyd, Osama Mawlawi, Michael A. Davies, Y.N. Vashisht Gopal, M. Emilia Di Francesco, J. R. M. and D. P.-W. *Sci. Rep.* **2018**, *under revi*.

(98) Sancho, P.; Barneda, D.; Heeschen, C. *Br. J. Cancer* **2016**, *114* (12), 1305–1312.

(99) Sancho, P.; Burgos-Ramos, E.; Tavera, A.; Bou Kheir, T.; Jagust, P.; Schoenhals, M.; Barneda, D.; Sellers, K.; Campos-Olivas, R.; Graña, O.; et al. *Cell Metab.* **2015**, *22* (4), 590–605.

(100) Morandi, A.; Indraccolo, S. *Biochim. Biophys. Acta - Rev. Cancer* **2017**, *1868* (1), 1–6.

(101) Guideri, L.; De Sarlo, F.; Machetti, F. *Chem. - A Eur. J.* **2013**, *19* (2), 665–677.

(102) Biagiotti, G.; Cicchi, S.; De Sarlo, F.; Machetti, F. *European J. Org. Chem.* **2014**, *2014* (35), 7906–7915.

(103) Kaiser, E.; Colescott, R. L.; Bossinger, C. D.; Cook, P. I. *Anal. Biochem.* **1970**, *34* (2), 595–598.

(104) Morgat, C.; Hindié, E.; Mishra, A. K.; Allard, M.; Fernandez, P. *Cancer Biother. Radiopharm.* **2013**, *28* (2), 85–97.

(105) Wu, N.; Kang, C. S.; Sin, I.; Ren, S.; Liu, D.; Ruthengael, V. C.; Lewis, M. R.;

Chong, H. S. *J. Biol. Inorg. Chem.* **2016**, *21* (2), 177–184.

(106) Yang, S.-T.; Wang, Y.-W.; Liu, J.-H.; Wang, H. *J. Radioanal. Nucl. Chem.* **2013**, *295* (2), 1181–1186.

(107) Pellegrini, P. A.; Howell, N. R.; Shepherd, R. K.; Lengkeek, N. A.; Oehlke, E.; Katsifis, A. G.; Greguric, I. *Molecules* **2013**, *18* (6), 7160–7178.

(108) Mulvey, J. J.; Villa, C. H.; McDevitt, M. R.; Escorcia, F. E.; Casey, E.; Scheinberg, D. A. *Nat. Nanotechnol.* **2013**, *8* (10), 763–771.

(109) Al-Jamal, K. T.; Nunes, A.; Methven, L.; Ali-Boucetta, H.; Li, S.; Toma, F. M.; Herrero, M. A.; Al-Jamal, W. T.; Tena Eikelder, H. M. M.; Foster, J.; et al. *Angew. Chemie - Int. Ed.* **2012**, *51* (26), 6389–6393.

(110) Melsens, E.; De Vlieghere, E.; Descamps, B.; Vanhove, C.; Kersemans, K.; De Vos, F.; Goethals, I.; Brans, B.; De Wever, O.; Ceelen, W.; et al. *Radiat. Oncol.* **2018**, *13* (1), 1–8.

(111) Peeters, S. G.; Zegers, C. M.; Yaromina, A.; Van Elmpt, W.; Dubois, L.; Lambin, P. *Q. J. Nucl. Med. Mol. Imaging* **2015**, *59* (1), 39–57.

(112) Gopal B. Saha. **2004**, 208.

(113) Gong, L.; Goswami, S.; Giacomini, K. M.; Altman, R. B.; Klein, T. E. *Pharmacogenet. Genomics* **2012**, *22* (11), 820–827.

(114) Wilcock, C.; Bailey, C. J. *Xenobiotica* **1994**, *24* (1), 49–57.

(115) Andersen, J.; Madsen, U.; Björkling, F.; Liang, X. *Synlett* **2005**, No. 14, 2209–2213.

(116) Chittari, P.; Rajappa, S. *Helv. Chim. Acta* **1991**, *74* (5185).

(117) Li, C.; Winnard, P. T.; Takagi, T.; Artemov, D.; Bhujwalla, Z. M. *J. Am. Chem. Soc.* **2006**, *128* (47), 15072–15073.

(118) Kilian, K. *Reports Pract. Oncol. Radiother.* **2014**, *19*, S13–S21.

(119) Ren, J.; Shen, S.; Wang, D.; Xi, Z.; Guo, L.; Pang, Z.; Qian, Y.; Sun, X.; Jiang, X. *Biomaterials* **2012**, *33* (11), 3324–3333.

(120) Ji, Z.; Lin, G.; Lu, Q.; Meng, L.; Shen, X.; Dong, L.; Fu, C.; Zhang, X. *J. Colloid Interface Sci.* **2012**, *365* (1), 143–149.

(121) Huang, H.; Yuan, Q.; Shah, J. S.; Misra, R. D. K. *Adv. Drug Deliv. Rev.* **2011**, *63* (14–15), 1332–1339.

(122) Kroto, H. W.; Heath, J. R.; O'Brien, S. C.; Curl, R. F.; Smalley, R. E. *Nature* **1985**, *318* (6042), 162–163.

(123) Novoselov, K. S.; Raimond, J. M.; Brune, M.; Computation, Q.; Martini, F. De; Monroe, C.; Moehring, D. L.; Knight, P. L.; Plenio, M. B.; Vedral, V.; et al. *Science (80-.).* **2004**, *306* (5696), 666–669.

(124) Saeed, K.; Park, S. Y.; Lee, H. J.; Baek, J. B.; Huh, W. S. *Polymer (Guildf).* **2006**, *47* (23), 8019–8025.

(125) Dirian, K.; Herranz, M. Á.; Katsukis, G.; Malig, J.; Rodríguez-Pérez, L.; Romero-Nieto, C.; Strauss, V.; Martín, N.; Guldi, D. M. *Chem. Sci.* **2013**, *4* (12), 4335.

(126) Wong, B. S.; Yoong, S. L.; Jagusiak, A.; Panczyk, T.; Ho, H. K.; Ang, W. H.;

Pastorin, G. *Adv. Drug Deliv. Rev.* **2013**, *65* (15), 1964–2015.

(127) Campidelli, S.; Ballesteros, B.; Filoramo, A.; Díaz, D. D.; De La Torre, G.; Torres, T.; Rahman, G. M. A.; Ehli, C.; Kiessling, D.; Werner, F.; et al. *J. Am. Chem. Soc.* **2008**, *130* (34), 11503–11509.

(128) Strom, T. A.; Dillon, E. P.; Hamilton, C. E.; Barron, A. R. *Chem. Commun.* **2010**, *46* (23), 4097–4099.

(129) Lutz, J. F. *Angew. Chemie - Int. Ed.* **2007**, *46* (7), 1018–1025.

(130) Fedeli, S.; Brandi, A.; Venturini, L.; Chiarugi, P.; Giannoni, E.; Paoli, P.; Corti, D.; Giambastiani, G.; Tuci, G.; Cicchi, S. *J. Mater. Chem. B* **2016**, *4*, 3823–3831.

(131) Tuci, G.; Luconi, L.; Rossin, A.; Baldini, F.; Cicchi, S.; Tombelli, S.; Trono, C.; Giannetti, A.; Manet, I.; Fedeli, S.; et al. *Chempluschem* **2015**, *80* (4), 704–714.

(132) Choi, W.; Lahiri, I.; Seelaboyina, R.; Kang, Y. S. *Crit. Rev. Solid State Mater. Sci.* **2010**, *35* (1), 52–71.

(133) Muleja, a. a.; Mbianda, X. Y.; Krause, R. W.; Pillay, K. *Carbon N. Y.* **2012**, *50* (8), 2741–2751.

(134) Hamilton, C. E.; Ogrin, D.; McJilton, L.; Moore, V. C.; Anderson, R.; Smalley, R. E.; Barron, A. R. *Dalton Trans.* **2008**, No. 22, 2937–2944.

(135) Fareghi-Alamdari, R.; Haqiqi, M. G.; Zekri, N. *New J. Chem.* **2016**, *40* (2), 1287–1296.

(136) Methot, J. L.; Roush, W. R. *Adv. Synth. Catal.* **2004**, *346* (9–10), 1035–1050.

(137) Xu, S.; He, Z. *RSC Adv.* **2013**, *3* (38), 16885–16904.

(138) Xiao, Y.; Sun, Z.; Guo, H.; Kwon, O. *Beilstein J. Org. Chem.* **2014**, *10* (1), 2089–2121.

(139) Denton, R. M.; An, J.; Adeniran, B. *Chem Commun* **2010**, *46* (entry 7), 3025–3027.

(140) Denton, R. M.; Tang, X.; Przeslak, A. *Org. Lett.* **2010**, *12* (20), 4678–4681.

(141) Buonomo, J. A.; Aldrich, C. C. *Angew. Chemie - Int. Ed.* **2015**, *54* (44), 13041–13044.

(142) Kosal, A. D.; Wilson, E. E.; Ashfeld, B. L. *Angew. Chemie - Int. Ed.* **2012**, *51* (48), 12036–12040.

(143) Tang, X.; An, J.; Denton, R. M. *Tetrahedron Lett.* **2014**, *55* (4), 799–802.

(144) Wu, B.; Kuang, Y.; Zhang, X.; Chen, J. *Nano Today* **2011**, *6* (1), 75–90.

(145) Esumi, K.; Ishigami, M.; Nakajima, A.; Sawada, K.; Honda, H. *Carbon N. Y.* **1996**, *34* (2), 279–281.

(146) Shaffer, M. S. P.; Fan, X.; Windle, a. H. *Carbon N. Y.* **1998**, *36* (11), 1603–1612.

(147) Iannazzo, D.; Mazzaglia, A.; Scala, A.; Pistone, A.; Galvagno, S.; Lanza, M.; Riccucci, C.; Ingo, G. M.; Colao, I.; Sciortino, M. T.; et al. *Colloids Surfaces B Biointerfaces* **2014**, *123*, 264–270.

(148) Castelaín, M.; Martínez, G.; Merino, P.; Martín-Gago, J. Á.; Segura, J. L.; Ellis, G.; Salavagione, H. J. *Chem. - A Eur. J.* **2012**, *18* (16), 4965–4973.

(149) Georgakilas, V.; Otyepka, M.; Bourlinos, A. B.; Chandra, V.; Kim, N.; Kemp, K.

C.; Hobza, P.; Zboril, R.; Kim, K. S. *Chem. Rev.* **2012**, *112* (11), 6156–6214.

(150) Fedeli, S.; Paoli, P.; Brandi, A.; Venturini, L.; Giambastiani, G.; Tuci, G.; Cicchi, S. *Chem. - A Eur. J.* **2015**, *21* (43), 15349–15353.

(151) Sharma, R.; Baik, J. H.; Perera, C. J.; Strano, M. S. *Nano Lett.* **2010**, *10* (2), 398–405.

(152) Wu, H. C.; Yu, J. Q.; Spencer, J. B. *Org. Lett.* **2004**, *6* (25), 4675–4678.

(153) Swartz, W. E.; Ruff, J. K.; Hercules, D. M. *J. Am. Chem. Soc.* **1972**, *94* (15), 5227–5229.

(154) Zhang, X.; Liu, H.; Hu, X.; Tang, G.; Zhu, J.; Zhao, Y. *Org. Lett.* **2011**, *13* (13), 3478–3481.

(155) Ha-Thi, M.-H.; Souchon, V.; Hamdi, A.; Métivier, R.; Alain, V.; Nakatani, K.; Lacroix, P. G.; Genêt, J.-P.; Michelet, V.; Leray, I. *Chem. - A Eur. J.* **2006**, *12* (35), 9056–9065.

(156) Andersen, J.; Madsen, U.; Björkling, F.; Liang, X. *Synlett* **2005**, No. 14, 2209–2213.

(157) McConnell, I.; Li, G.; Brudvig, G. W. *Chem. Biol.* **2010**, *17* (5), 434–447.

(158) Leegwater, J. A. *J. Phys. Chem.* **1996**, *100* (34), 14403–14409.

(159) Chen, S.; Zhao, X.; Chen, J.; Chen, J.; Kuznetsova, L.; Wong, S. S.; Ojima, I. *Bioconjug. Chem.* **2010**, *21* (5), 979–987.

5.2 Synthesis of fluorescent dyes for the preparation of a donor-acceptor system

Light harvesting devices based on organic dyes are top trend topic in the field of optoelectronics. The possibility to fine tune the optic characteristics by modifying the structure of the organic dyes has greatly increased the interest of chemists and physics working in the field. However a deep understanding of the electron energy transfer process is often not trivial. The full comprehension of the overall mechanism involves the identification of the energy pathways in the molecular system. Ultrafast pump-probe techniques are a perfect tool to investigate excited state dynamics and energy transfer mechanisms with sub-picoseconds time-scale.[157,158] In this work, three different dimers bearing a bodipy donor and different acceptor moieties were synthesized and characterized (**figure 1**). The photo-physics behavior of these compounds was studied in different solvent by stationary Transient Absorption spectroscopy. In order to have a good understanding of the roles played by the different factors in the energy transfer rate, we synthesized molecular dyads with different donors and varying the nature of the linker between donor and acceptor.
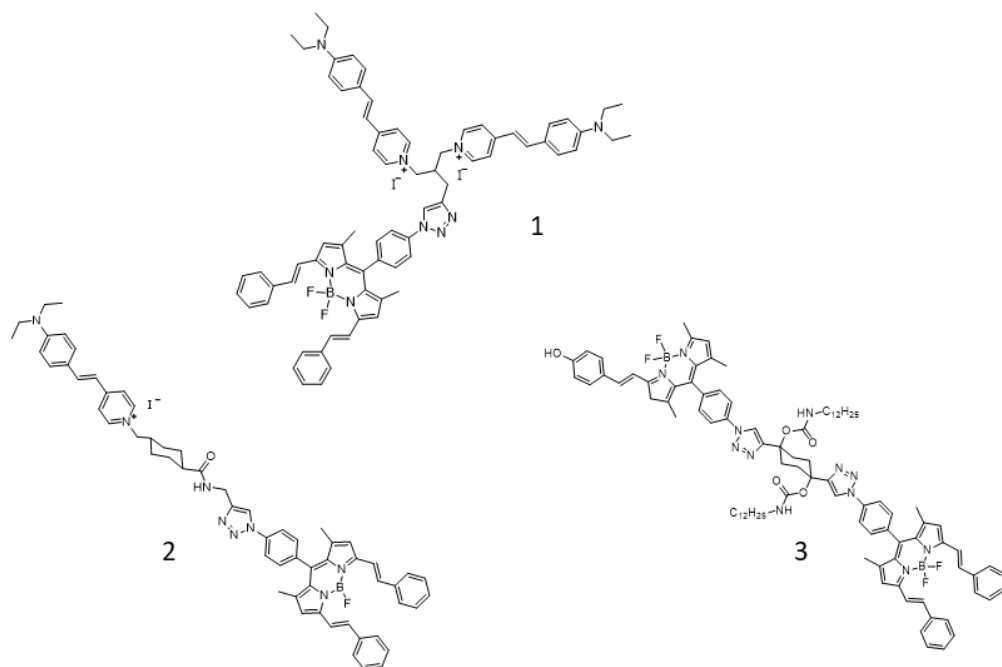
Figure 1. Structure of the three bichromophoric compounds synthesized

The complete synthetic approach for the preparation of compounds **1**, **2** and **3** is reported in **figures 2, 3** and **4.**
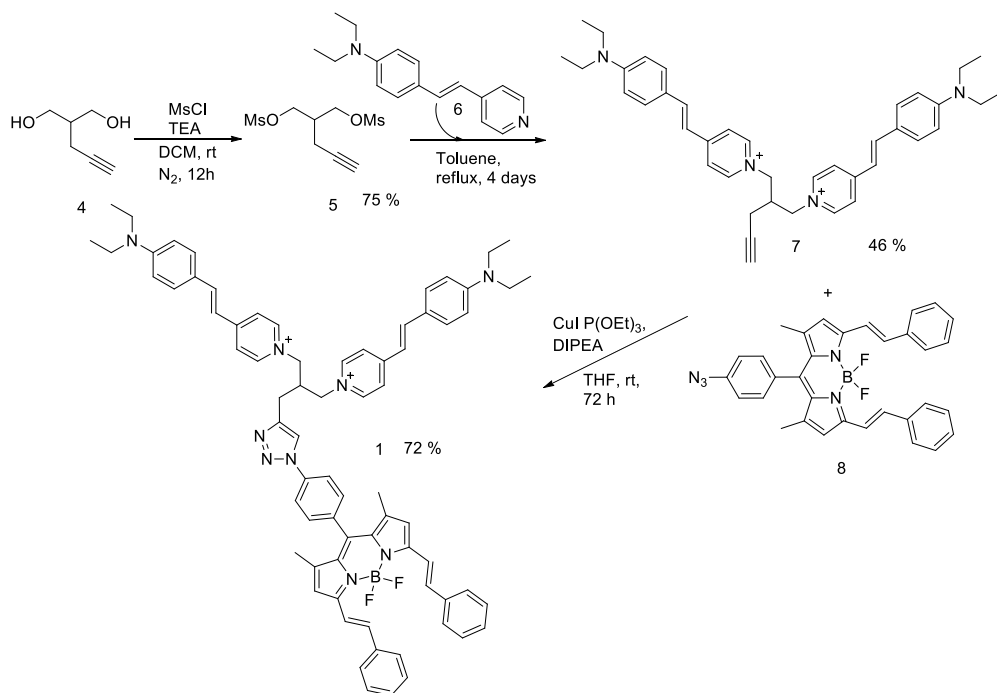
Figure 2. Synthesis of compound 1.
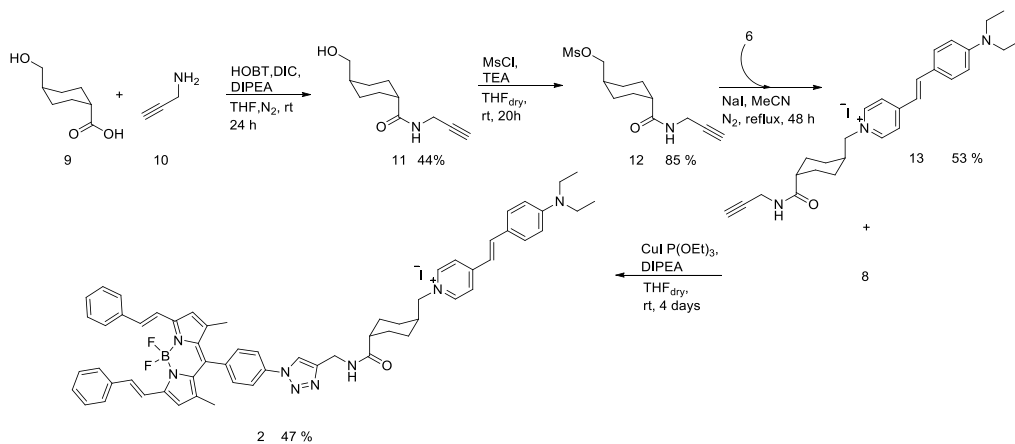
Figure 3. Synthesis of compound 2.
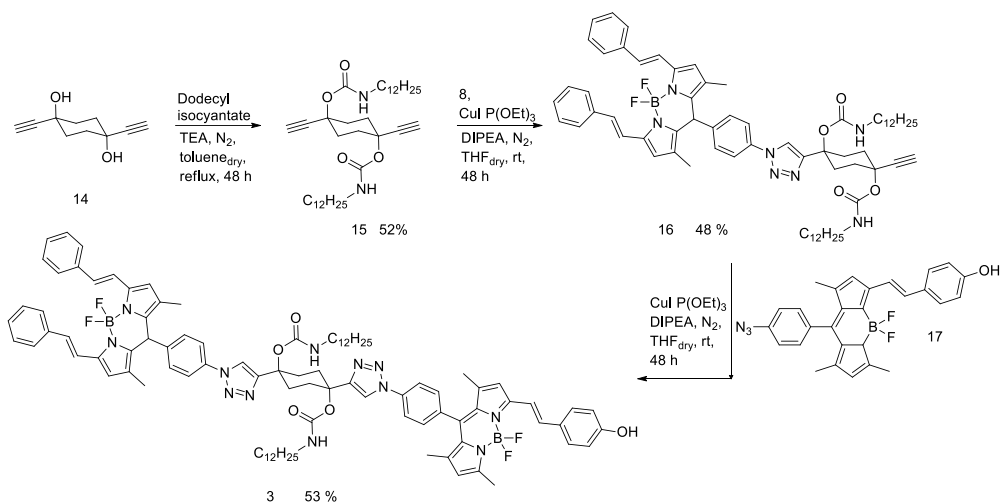
Figure 4. Synthesis of compound 3.

Synthesis of compound 5
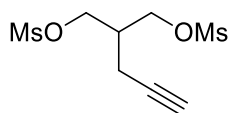
In a 10 mL round bottom flask 202 mg of 2-(prop-2-yn-1-yl)propane-1,3-diol (1.75 mmol, 1.5 eq) and 393 mg of TEA (3.9 mmol 2.2 eq) were dissolved in 7 mL of dry DCM under nitrogen atmosphere. Then 501 mg of mesyl chloride (4.4 mmol, 2.5 eq) were added dropwise and the reaction mixture stirred at room temperature overnight. Thr crude mixture was diluted to 10 mL with DCM and extracted three times with 5 mL of water and once with 5 mL of brine, the organic phase was recovered dried with sodium sulfate and the solvent removed under vacuum. The product was recovered after flash chromatographic column, rf 0.95 AcOEt/Chloroform 1:1. Yield 75%. MS-ESI m/z: 292.93 [M+Na]$^+$.

Synthesis of compound 7
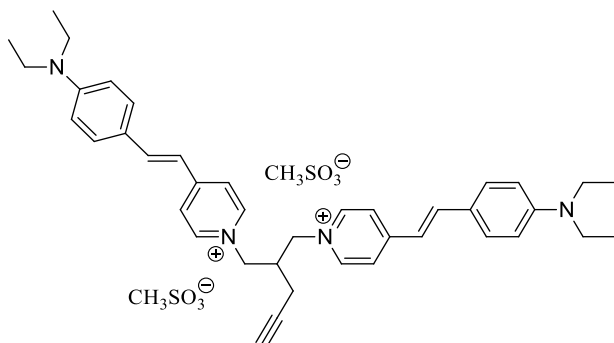
In a 25 mL round bottom flask 113 mg of alkyne **5** (1.14 mmol, 1 eq) were dissolved in toluene, then 287 mg of 4-[4-(Diethylamino)styryl]pyridine (1.14 mmol, 1.2 eq) were added and the reaction mixture refluxed for 72 h. Three different fractions were naturally formed at the end of the reaction, the product was isolated from the orange oily fraction after filtration and chromatographic column (eluent AcOEt/ methanol 5:1, 4:1, 3:1, 2:1, 1:1 and 1:2) rf 0.1 AcOEt/ methanol 1:1. Yield 35%. ^{1}H-NMR δ= 1.19 (t, ^{3}J 8 Hz, 12H), 2.32 (bs, 2H), 2.72 (pseudo t, 1H), 3.18 (bs, 1H), 3.45 (q, ^{3}J 8 Hz, 8H), 4.66 (m, 4H), 6.71 (d, ^{3}J 8 Hz, 4H), 7.02 (d, ^{3}J 16Hz, 2H), 7.93 (d,^{3}J = 8 Hz, 4H), 8.62 (d, ^{3}J = 8 Hz, 4H). ^{13}C NMR δ= 13.8, 19.7, 41.8, 46.4, 61.6, 76.12 e 79.9, 113.6,117.9, 124.3, 124.5, 133.2, 145.5, 146.4, 152.7, 158.0. ESI MS m/z 292.2 [M]$^{2+}$.

Synthesis of compound 1
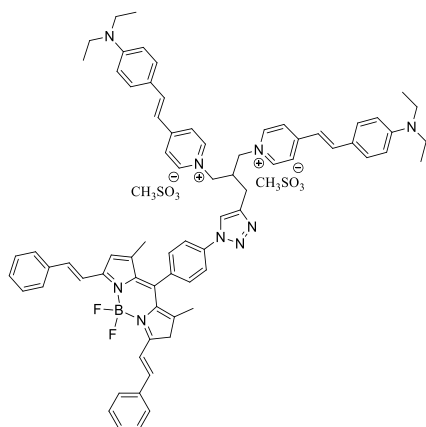
In a 5 mL round bottom flask 27.1 mg of azide bodipy **8** (0.05 mmol, 1 eq), 32.5 mg of compound **7** (0.06 mmol, 1.25 eq), 12.9 mg of DIPEA (0.1 mmol, 2 eq) and 5.34 mg of copper iodide triethyl sulfite (0.015 mmol, 0.3 eq) were dissolved in 3 mL of dry and degassed THF. The mixture was stirred at room temperature for 72 h, then the product was recovered after flash chromatographic column rf 0.35 DCM/methanol. Yield 72 %.

^{1}H NMR (400 MHz, CDCl$_3$) δ = 9.37 d (5H,^{3}J = 7.2 Hz), 9.03 s (1H), 8.05 d (2H, ^{3}J = 8.8), 7.61 d (4H, ^{3}J = 7.2 Hz), 7.75 d (2H, ^{3}J = 16.8 Hz), 7.62 d (4H, ^{3}J = 7.2), 7.57 d (2H, ^{3}J = 15.6 Hz), 7.40 m (11H), 7.31 d (2H, ^{3}J = 7.2 Hz), 7.24 d ("H, ^{3}J = 16.4 Hz), 6.74 d (2H, ^{3}J = 15.6 Hz), 6.59 m (5H), 5.24 pd (1H, ^{3}J = 8.0 Hz), 4.97 t (1H, ^{3}J = 9.6), 4.05 bs (1H), 3.36 q (8H, ^{3}J = 6.8), 3.15 d (1H, ^{3}J = 5.2 Hz), 1.41 s (6H), 1.19 m (3H) e 1.15 ppm t (12H, ^{3}J = 6.8 Hz). ^{13}C NMR (400 MHz, CDCl$_3$) δ = 12.61, 15.15, 29.69, 41.02, 44.65, 59.11, 111.51, 115.60, 118.06, 119.14, 121.04, 121.51, 122.28, 127.58, 128.79, 129.02, 130.08, 131.25, 136.46, 137.22, 141.98, 143.51, 143.74, 144.07, 150.36, 152.85, 152.85, 154.65 four isochron carbon. FT-IR λ : 3423 bb OH stretching, 2968 e 2921 w CH stretching, 1640 circa w H-C=C stretching, 1575 s, 1523 C=C s stretching,1168 e 1153 m C-N stretching. MS-ESI m/z: 562.71 [M]$^{2+}$.

Sintesi del (1*S*,4*S*)-4-(hydroxymethyl)-*N*-(prop-2-yn-1-yl)cyclohexanecarboxamide 11
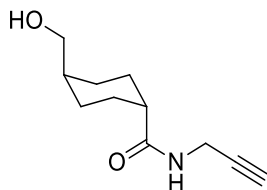
In a 25 mL two necked round bottom flask 100 mg of *trans*-4-(hydroxymethyl)-cyclohexyl carboxylic acid (0.63 mmol, 1 eq), 127.7 mg of *N*-hydroxy-benzotriazole (0.945 mmol, 1.5 eq), 79.5 mg of DIC (0.63 mmol 1 eq) and 81.4 mg of DIPEA (0.63 mmol, 1 eq) were dissolved in 3 mL of dry THF under nitrogen atmosphere. After 20 minutes 41.9 mg of propargyl amine (0.76 mmol, 1.2 eq) in 3 mL of dry THF were added and the mixture stirred for 24 h at room temperature. The solvent was removed under vacuum and the solid dissolved in 30 mL of ethyl acetate and washed with: 2 X 10 mL of water, 2 X 10 mL of saturated sodium carbonate solution, 2 X 10 mL of 0.5 M HCl solution and 2 X 10 mL of brine. The organic phase was dried over sodium sulfate and the solvent removed under vacuum. The pure product was recovered after flash chromatographic column, rf 0.24 ethyl acetate : DCM 1:1. Yield 44%. MS-ESI m/z 195.1[M$^-$]. ^{1}H-NMR 200 MHz CD$_3$OD δ = 1.01 m (2H cyclohexane), 1.46 m (3H cyclohexane), 1.85 bd (4H cyclohexane), 2.14 tt (1H in alfa at CO; ^{3}J$_{H-H}$ = 12.2 e 3.4 Hz), 2.56 t (1H alkyne, ^{4}J$_{H-H}$ 2.6 Hz), 3.4 d (2H CH$_2$OH, ^{3}J$_{H-H}$ 5.4 Hz) e 3.92 ppm d (2H CH$_2$NH, ^{4}J$_{H-H}$ 2.6 Hz). ^{13}C-NMR 50 MHz CD$_3$OD δ = 27.92 (1C), 28.48 (2C), 28.63 (2C), 39.66 (1C alfa CO), 44.88 (1C CH$_2$N), 67.12 (1C, CH$_2$OH), 70.47 (1C, CH alkyne) e 79.44 (1C, alkyne) e 177.25 ppm (1C CO). FT-IR λ = 3628 m OH stretching, 3454 m NH stretching, 3306 s CH stretching alkyne, 2928 e 2859 m CH stretching, 2246, 1667 s CO stretching, 1504 s , 1451 cm^{-1} d CH bending. Elemental analysis calculated C 67.66, H 8.78, N 7.17 % measured C 67.16, H 7.99 e N 6.88%.

Synthesis of ((1*R*,4*R*)-4-(prop-2-yn-1-ylcarbamoyl)cyclohexyl)methyl methanesulfonate 12
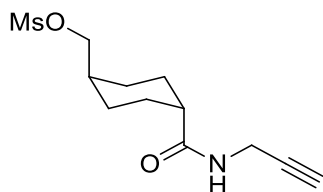
In a 5 mL round bottom flask 77.5 mg of compound **11** (0.4 mmol, 1 eq), 88.9 mg of dry TEA (0.88 mmol, 2.2 eq) were dissolved in a 1 mL of dry DCM, then 46.5 mg of mesyl chloride (0.6 mmol, 1.5 eq) in 1 mL of dry DCM were added dropwise and the mixture stirred for 12h. The TLC control evidenced the presence of starting material so 1.5 eq of mesyl chloride and 2.2 eq of dry TEA were added and the mixture stirred for 8 h. The crude mixture was diluted to 30 mL with DCM and washed with: 3 X 15 mL of water and 5 mL of brine; the organic phase was dried over sodium sulfate and the solvent removed under vacuum obtaining the clean product. Yield 85%. MS-ESI m/z 294.93 [M]$^+$. ^{1}H-NMR 200MHz CD$_3$OD δ =1.11 m (2H cyclohexane) 1.49 qd (2H cyclohexane; $^3J_{H-H}$ = 12.4 and 3 Hz), 1.87 m (5H cyclohexane), 2.16 tt (1H cyclohexane, $^3J_{H-H}$ = 12.2 e 3.4), 2.56 t (1H alkyne, $^4J_{H-H}$ = 2.6 Hz), 3.048 s (3H mesylate), 3.93 d (2H CH$_2$N, $^3J_{H-H}$ = 2.6 Hz) e 4.05 ppm d (2H CH$_2$O, $^3J_{H-H}$ = 6.2 Hz). ^{13}C-NMR 50 MHz CD$_3$OD δ =27.84 (3C cyclohexane), 28.23 (2C cyclohexane), 35.65 (1C cyclohexane alfa to CO), 36.78 (1C mesylate), 44.38 (1C CH$_2$N), 70.44 (1C CH alkyne), 74.53 (1C CH$_2$O), 79.38 (1C alkyne) e 186.85 ppm (1C CO). FT-IR λ = 3452 s NH stretching, 3307 s stretching CH alkyne, 2936 e 2859 m CH stretching, 2246, 1670 s CO stretching, 1507 s, 1452 m CH bending, 1358, 1338 m e 1176 cm^{-1} s SO stretching mesylate. Elemental analysis CHN: calculated C 52.73, H 7.01 e N 5.12 % , measured C 53.12, H 6.64 e N 5.08 %.

Syntesis of 4-((E)-4-(diethylamino)styryl)-1-(((1R,4R)-4-(prop-2-yn-1-ylcarbamoyl)cyclohexyl)methyl)pyridin-1-ium iodide 13
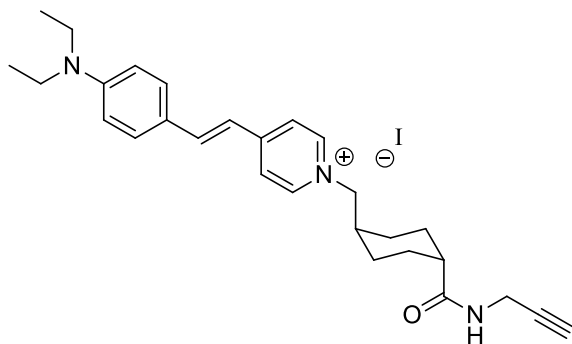
In a 25 mL two necked round bottom flask 132.4 mg of styryl pyridine (0.22 mmol, 2.4 eq), 98.9 mg of sodium iodide (0.66 mmol, 3 eq) and 60 mg of compound **12** (0.22, 1 eq) were dissolved in 9 mL of dry MeCN under nitrogen atmosphere. The mixture was refluxed under stirring for 48 h, the solvent was removed under vacuum and the product recovered after flash chromatographic column (Al$_2$O$_3$ Brockmann grade 3), gradient of polarity of eluent: DCM/AcOEt 1:1, AcOEt, AcOEt/methanol 3:1). Yield 53%.

^{1}H-NMR 400 MHz δ = 1.19 t (8H, CH$_3$ + 2H cyclohexane, $^3J_{H-H}$ 6.2 Hz), 1.47 m (2H, cyclohexane), 1.59 m (2H, cyclohexane), 1.78 m (3H cyclohexane), 2.21 m (1H cyclohexane alfa CO), 2.57 t (1H alkyne, $^4J_{H-H}$ = 2.6 Hz), 3.51 q (4H CH$_2$N, $^3J_{H-H}$ = 6.2 Hz), 3.92 d (2H, CH$_2$NH, $^4J_{H-H}$ 2.6 = Hz), 4.23 d (2H, CH$_2$N$^+$, $^3J_{H-H}$ = 7.2 Hz), 6.75 d (2H pyridine, $^3J_{H-H}$ = 9.2 Hz), 7.05 (1H alkene, $^3J_{H-H}$ = 16.2 Hz), 7.59 d (2H pyridine, $^3J_{H-H}$ = 9.2 Hz), 7.83 d (1H alkene, $^3J_{H-H}$ = 16.2 Hz), 7.95 d (2H phenyl, $^3J_{H-H}$ = 7 Hz), 8.52 ppm d (2H phenyl, $^3J_{H-H}$ = 7 Hz). ^{13}C NMR (101 MHz, CD$_3$OD) δ = 176.52(s), 155.08 (s), 150.20 (s), 143.23 (s), 143.03(d), 130.69 (d), 122.01 (d), 121.99 (d), 115.69 (d), 111.27 (d), 79.33 (s), 70.63 (d), 64.85 (t), 44.10(t), 44.03 (t), 38.52 (s), 28.53 (t), 28.11 (t), 27.91(d), 11.52 (q). MS-ESI m/z: 430.28 [M]$^+$.

Synthesis of compound 2
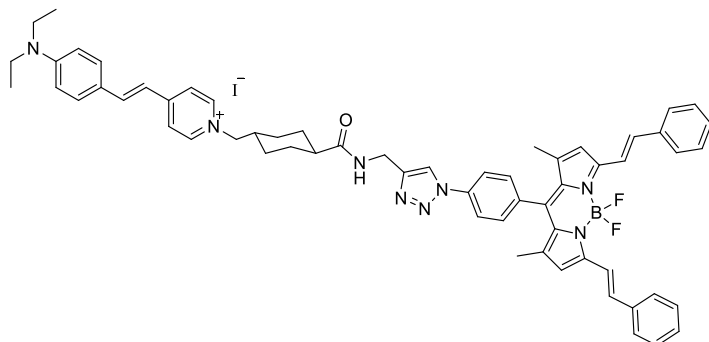
In a round bottom flask 16 mg of compound **13** (0.03 mmol, 1 eq), 20 mg of azide bodipy **8** (0.035 mmol, 1.1 eq) and 3.2 mg copper iodide triethyl sulfite (0.009 mmol, 0.3 eq) were dissolved in dry THF under nitrogen atmosphere, then 7.8 mg of DIPEA (0.06 mmol, 2 eq) were added and the mixture stirred at room temperature for 4 days. The solvent was removed under vacuum and the product recovered after flash chromatographic column (Al_2O_3 Brockmann grade 3) r*f* 0.4 DCM:Methanol 30:1. Yield 47%. ^{13}C NMR (101 MHz, $CDCl_3$) δ = 176.02, 154.34, 152.93, 150.26, 146.75, 143.29, 141.92, 137.53, 137.09, 136.70, 136.42, 135.18, 133.14, 131.16, 130.07, 129.05, 128.79, 127.59, 122.25, 121.61, 121.14, 120.80, 119.02, 118.20, 115.62, 111.51, 65.05, 44.59, 44.12, 38.82, 30.90, 28.77, 28.48, 15.05, 12.58 ppm. ^1H NMR (400 MHz, $CDCl_3$) δ = 8.77 pd (*J* = 6.3 Hz, 2H), 8.45 s (1H), 7.95 d (*J* = 8.4 Hz, 2H), 7.78 d (*J* = 5.9 Hz, 2H), 7.69 d(*J* = 16.4 Hz, 2H), 7.61 d (*J* = 7.4 Hz, 6H), 7.50 d (*J* = 8.8 Hz, 2H), 7.39 (*J* = 8.1 Hz, 5H), 7.36 − 7.24 (m, 4H), 6.85 d (*J* = 15.8 Hz, 1H), 6.64 (s, 2H), 6.62 d (*J* = 8.9 Hz, 2H), 4.62 pd (*J* = 4.9 Hz, 2H), 4.48 pd (, *J* = 8.3 Hz, 2H), 3.37 (q, 7.0 Hz, 4H), 2.38 m (1H), 1.96 bs (4H), 1.81 bs (4H), 1.66 bs (1H), 1.44 s (6H), 1.16 (t, *J* = 7.1 Hz, 6H). ESI-MS m/z 971.87 [M$^+$]. FT-IR: 3429 bb NH stretching, 2926 w CH stretching, 1641 e 1616 m CO stretching, 1575 e 1523 s NH bending, 1444, 1409, 1325, 1299, 1269, 1201, 1166, 1108 e 1043 cm^{-1}. HRMS-ESI [M$^+$] m/z calculated 970.51385, measured 970.51436 δ = 0.52 ppm.

Synthesis of (1*R*,4*R*)-1,4-diethynylcyclohexane-1,4-diyl bis(dodecylcarbamate) 15
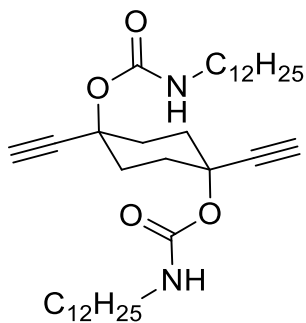
In a 25 mL two necked flask 100 mg of cyclohexane **14** (0.61 mmol, 1 eq) and 12.3 mf of TEA (0.122 mmol, 0.2 eq) were dissolved in 5 mL of dry toluene under nitrogen atmosphere, then 298 mg of dodecyl isocyanate (1.4 mmol, 2.3 eq) in 5 mL of dry toluene were added dropwise. The reaction mixture was refluxed under stirring for 48h, the product was recovered after flash chromatographic column *rf* 0.3 DCM:AcOEt 10:1.Yield 52 %. ^{13}C NMR (101 MHz, CDCl$_3$) δ 154.47, 83.50, 72.77, 40.83, 33.19, 31.89, 29.91, 29.62, 29.60, 29.55, 29.52, 29.32, 29.25, 26.76, 22.66, 14.09. ^{1}H NMR (400 MHz, CDCl$_3$) δ = 4.64 m (2H, NH), 3.17 m (4H, CH$_2$N), 2.61 s (2H, alkyne), 2.22 m (8H, cyclohexane), 1.49 m (4H CH$_2$ beta to NH), 1.25 m (36H), 0.88 t (6H CH$_3$). MS-ESI m/z : 609.44[M+Na]$^+$.
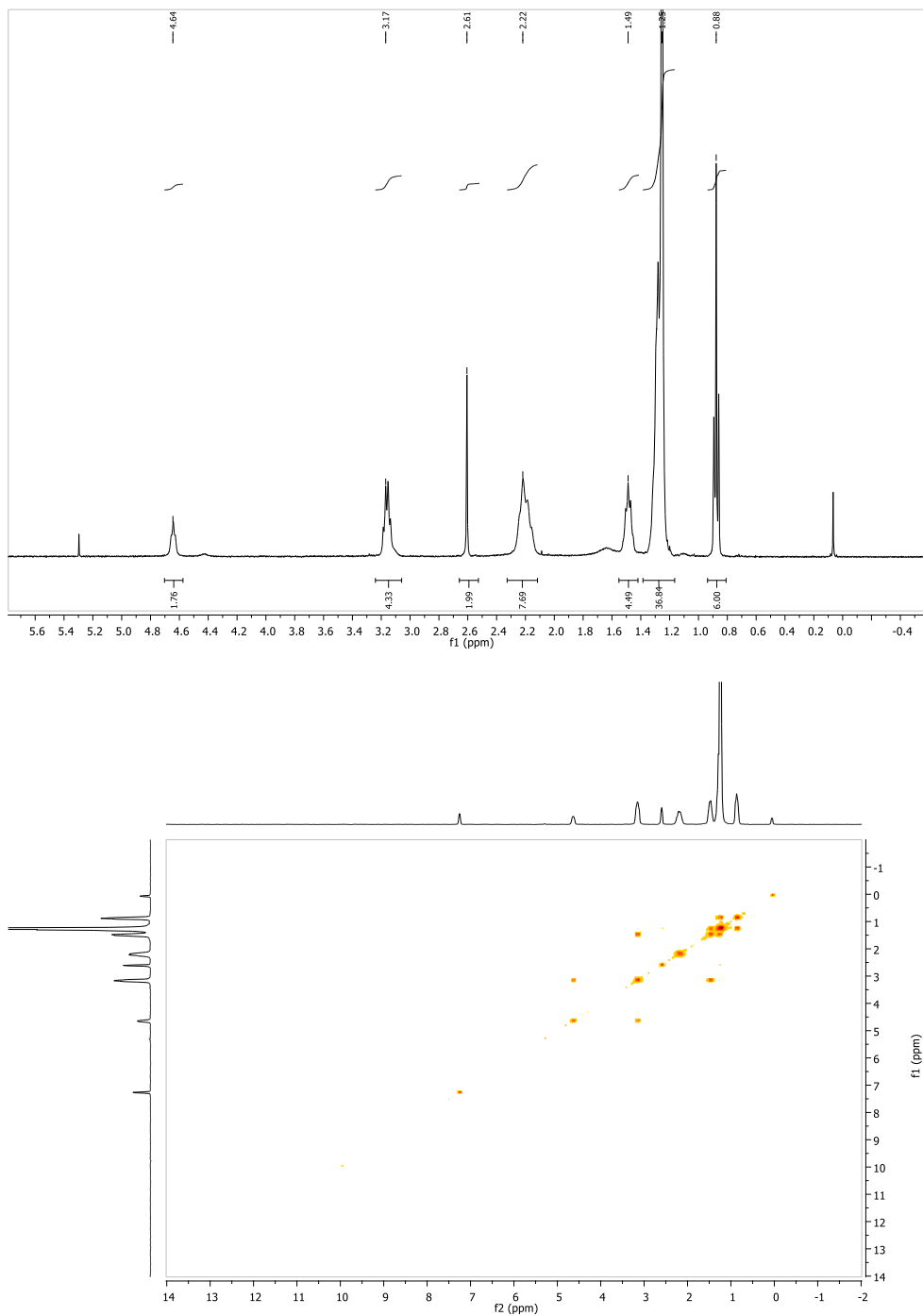
Figure 5. ¹H-NMR and H-H COSY NMR of compound **15**.
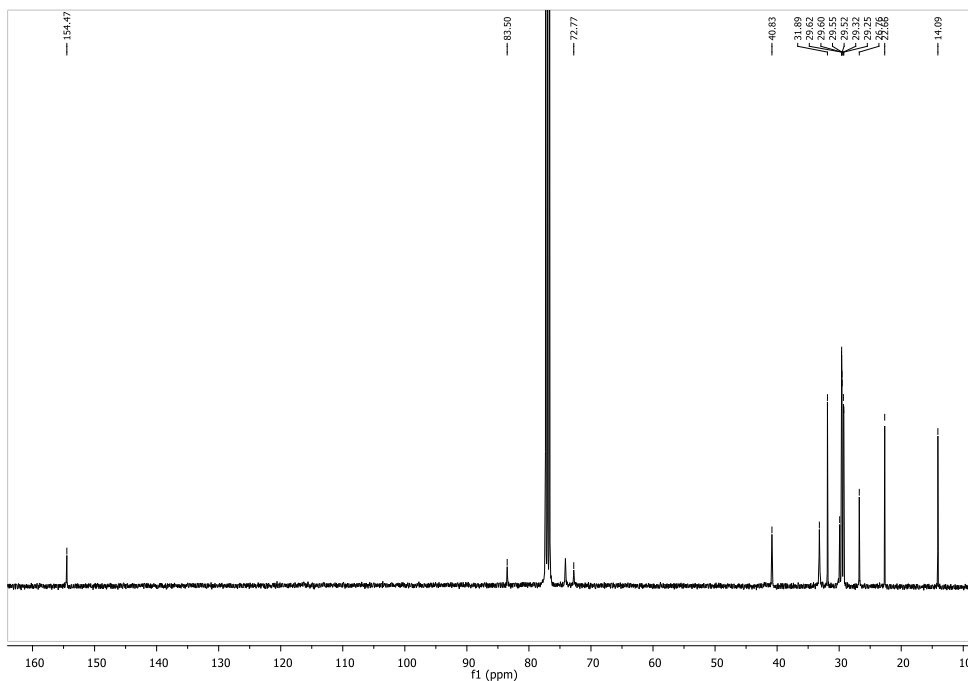
Figure 6. ^{13}C-NMR of compound **15**.

Synthesis of compound 16

In a 5 mL round bottom flask 40 mg of alkyne **15** (0.068 mmol, 1 eq), 18.5 mg of bodipy azide **8** (0.034 mmol, 0.5 eq), 14.6 mg copper iodide triethyl phosphite (0.041 mmol, 0.6 eq) were dissolved in 5 mL of dry THF under nitrogen. Then 3.5 mg of dry diisopropyl ethyl amine (0.027 mmol, 0.4 eq) was added and reaction mixture stirred at room temperature for 48 h. The product was recovered after flash chromatographic column *rf* 0.4 DCM/ethyl acetate 40:1. Yield 48%.^{1}H NMR (400 MHz, CDCl$_3$) δ = 8.14 s (1H, j), 7.95 d (2H, J^3$_{H-H}$ = 7.95 Hz; h and h'), 7.75 d (2H, J^3$_{H-H}$ = 7.75 Hz, e and e'), 7.63 d (4H, J^3$_{H-H}$ = 7.63 Hz; c, c, 'c'' and c'''), 7.51d (2H, J^3$_{H-H}$ = 7.51 Hz; i and i'), 7.41 t (4H, J^3$_{H-H}$ = 7.41 Hz; b, b', b'' and b'''), 7.32 m (4H; a, a', d and d'), 6.67 s (2H; f and f'), 4.80 bs (1H; m), 4.67 bs (1H; n), 3.15 bs (2H; o), 3.07 bs (2H; s), 2.64 s (1H; r), 2.37 bs (4H; k and k'), 2.21 bs (4h; l and l'), 1.51 s (6H; g and g'), 1.25 m (40H, p and p' 20 CH$_2$)and 0.87 ppm t (6H, J^3$_{H-H}$ = 8 Hz; q and q') . ^{13}C NMR (101 MHz, CDCl$_3$) δ = 155.04, 154.55, 153.06, 141.77,

137.50, 136.88, 136.70, 136.45, 135.55, 133.16, 130.14, 129.07, 128.79, 127.60, 120.72, 120.05, 119.12, 118.12, 84.37, 75.32, 73.28, 72.06, 40.82, 32.61, 31.89, 30.84, 29.88, 29.62, 29.55, 29.53, 29.32, 29.25, 26.79, 22.66, 15.05, 14.10. MS-ESI negative ionization: m/z 1126 [M]$^-$.
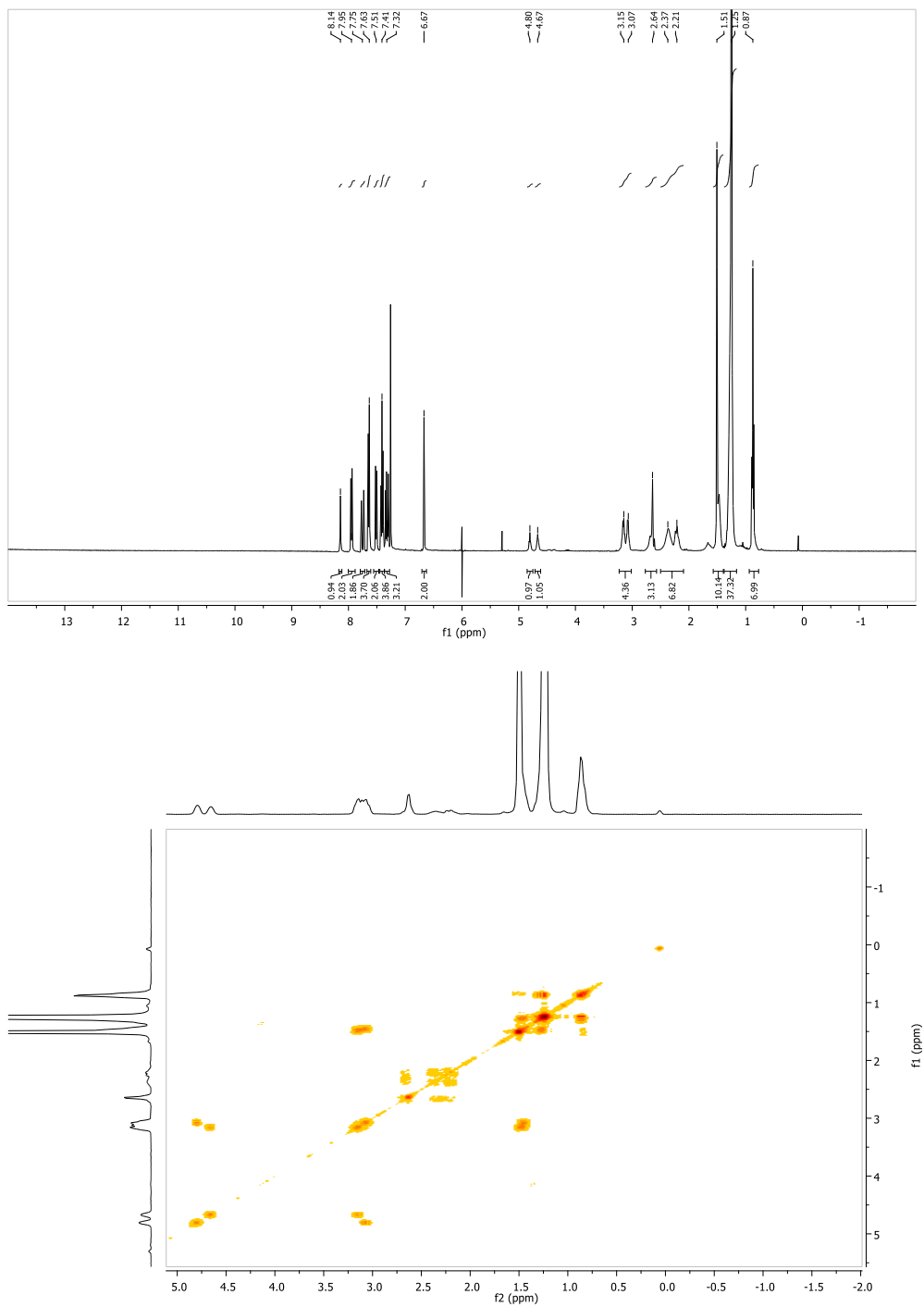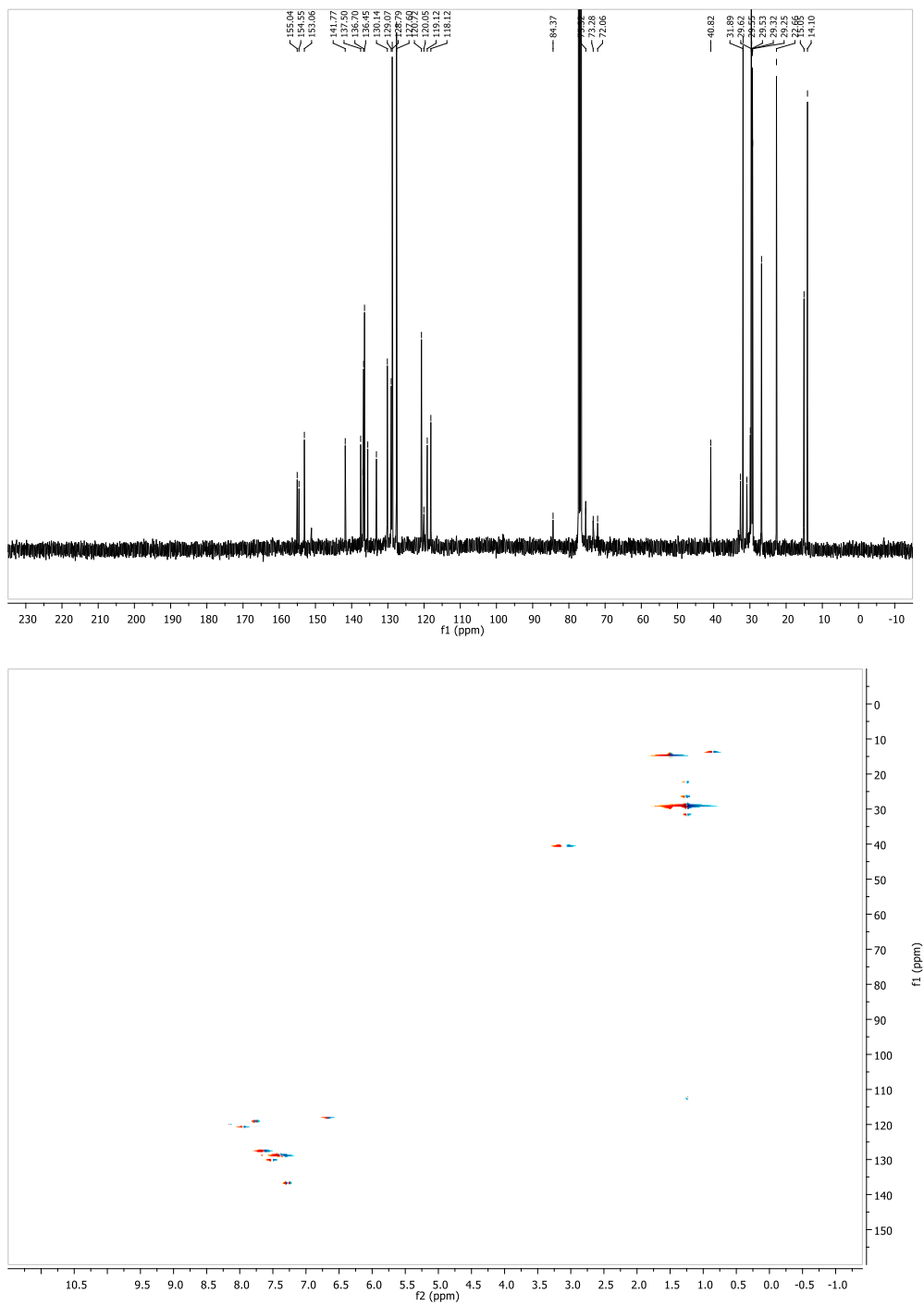
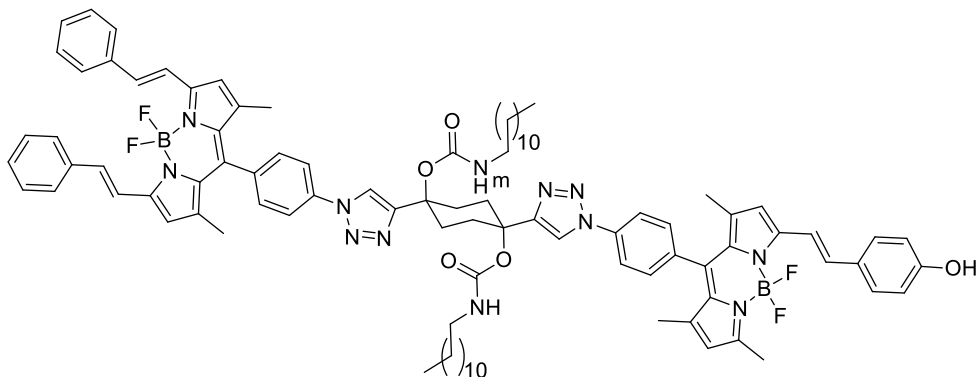***Figure 7.*** ^{1}H-NMR and H-H COSY of compound **16**.

Figure 8. ^{13}C-NMR and HSQC of compound **16**.

Synthesis of compound 3

Compound **3** was prepared following the same procedure for cycloaddition reported for compound **16**. The product was recovered after flash chromatography column with eluent: DCM/AcOEt (50:1, 40:1, 30:1, 20:1, 15:1, 10:1, 5:1, 2:1 and 1:1). Yield 53%. MS-ESI: m/z 1596.76 [M]$^-$. ^{13}C NMR CRYO (176 MHz, CDCl$_3$) δ = 161.44, 159.68, 155.28, 154.25, 154.06, 152.77, 150.83, 142.90, 142.39, 141.62, 138.81, 138.48, 138.34, 137.73, 136.50, 134.65, 133.16, 132.61, 131.12, 130.69, 130.53, 130.11, 129.95, 129.67, 129.61, 1127.72, 127.59, 121.66, 120.52, 119.19, 118.80, 118.53, 116.62, 115.20, 74.50, 64.14, 31.76, 30.99, 29.83, 29.48, 29.29, 29.19, 26.66, 22.56, 15.09, 14.74 and 14.40 ppm. ^{1}H NMR (400 MHz, dmso-D$_6$) δ = 9.98, 8.99, 8.20, 7.71, 7.24, 7.15, 7.04, 6.94, 6.84, 6.20, 4.08, 3.98, 3.16, 2.84, 2.26, 1.47, 1.20, 0.80 ppm.
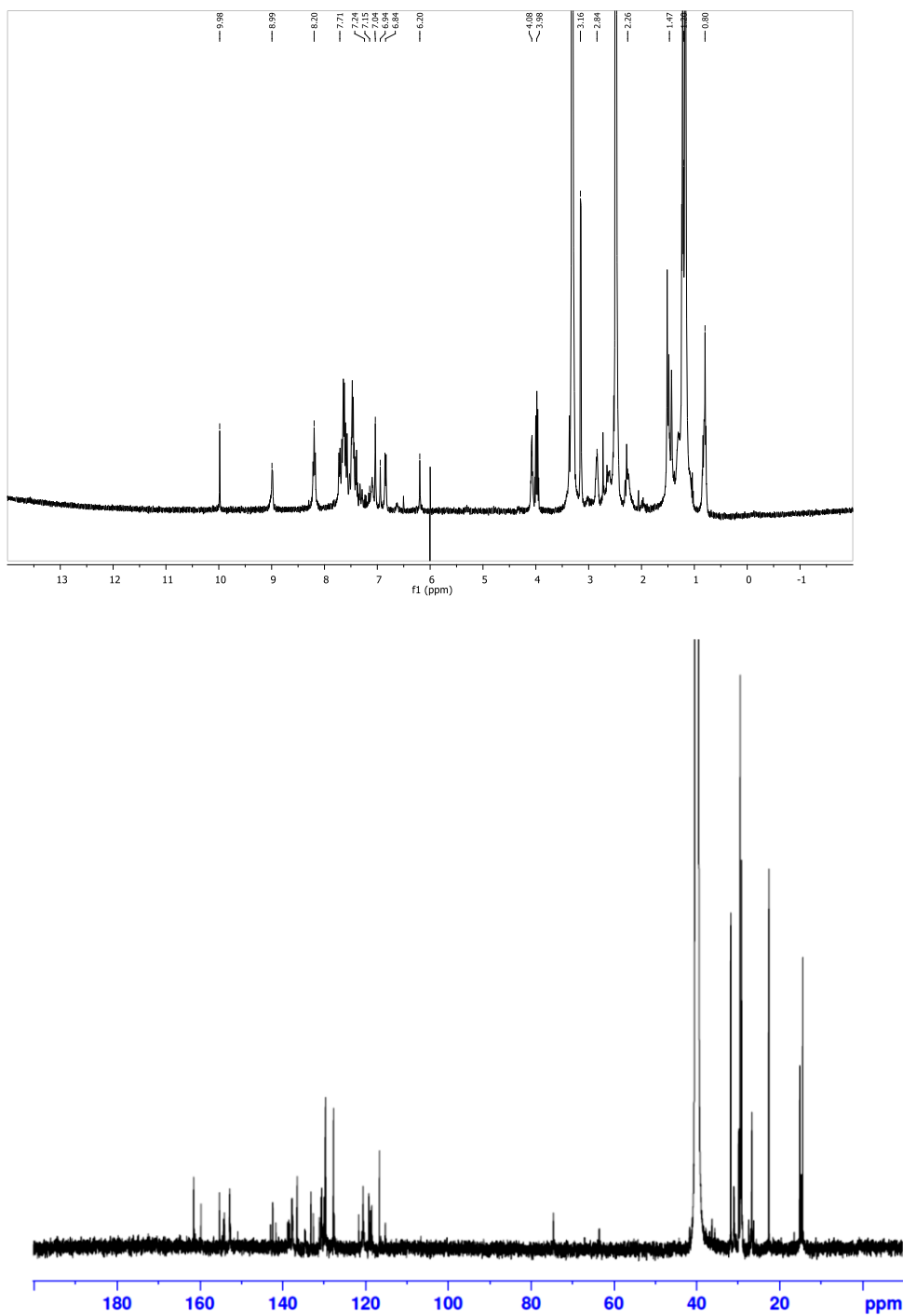
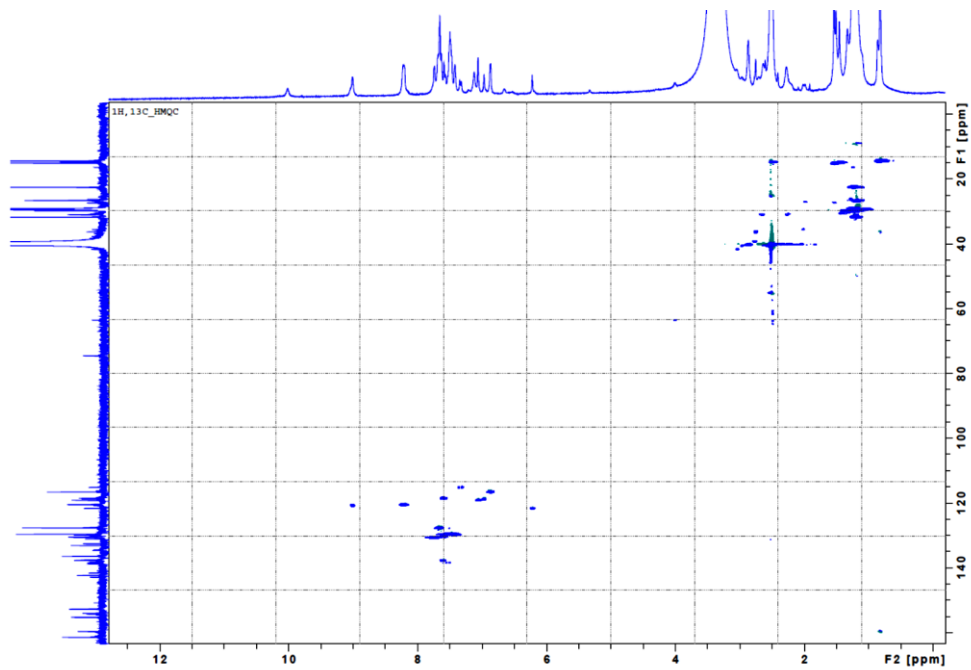*Figure 9.* ^{1}H-NMR on top and ^{13}C-NMR on bottom of compound **3**.
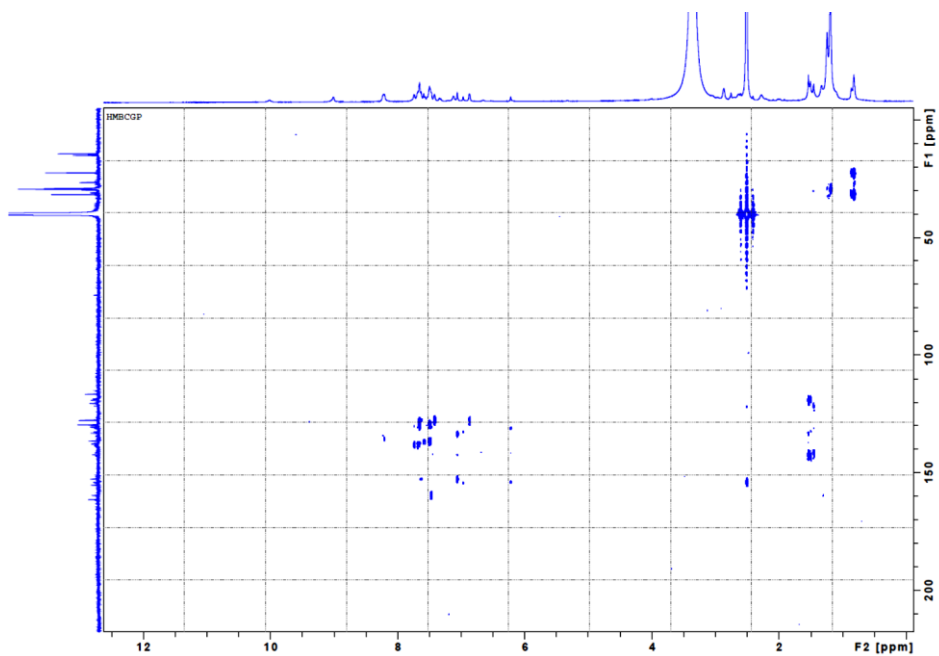
Figure 10. ¹H, ¹³C HMQC of compound **3**.

Figure 11. ¹H, ¹³C HMBC of compound **3**.

5.3 Synthesis of a Drug Delivery System based on multiwalled carbon nanotubes for the disposal of TACAs mimetic.

Cancer cells can be distinguished from normal cells by displaying aberrant levels and types of carbohydrate on their surface. These sugar moieties are known as Tumor-associated carbohydrates antigens (TACAS) and they are considered as promising candidate for the development of tumor vaccine. However, carbohydrates alone can evoke only poor immune responses. The problem can be solved by conjugation with helper-molecules which can allow the recognition by T cells and the activation of a strong immune response. Among all the possible candidate for the conjugation nanotubes represents a very promising platform. Indeed, opportunely functionalized CNTs not only can allow the recognition by immune cells, but also can increase the blood circulation time and give the possibility for the introduction of label compound to follow the recognition process. The DDS reported in **figure 1** was synthesized and characterized. The scope was to evaluate if CNTs were able to allow the recognition of a small molecule by the immune system. The DDS was designed as follows: oxidized multi-walled CNTs (by now CNTs) as carrier, a glycosyl derivative as antigen mimetic, and a substituted bodipy dye as fluorescent probe to visualize nanotubes by fluorescence in vitro. A flexible linker was included as spacer between CNTs and the antigen mimetic to facilitate the recognition of the active molecule.
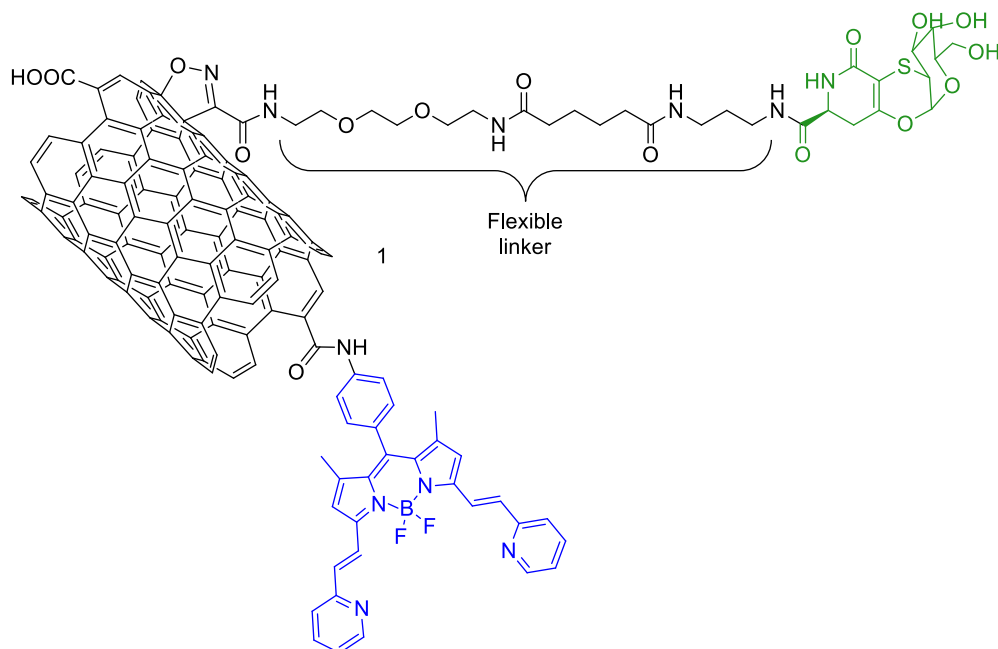
Figure 1. Structure of the complete DDS: the antigen mimetic is drawn in green, in blue the fluorescent probe.

After preparation of the amine modified CNTs we investigated the coupling reaction using two model compounds: glycoside X and galactoside X derivatives. The kinetics of the reaction were followed observing the formation of *p*-nitrophenolate by UV-Vis absorbance measurements. Indeed, *p*-nitrophenolate has a strong absorption band in the UV region which allows to evaluate the degree of consumption of the activated sugar moiety.
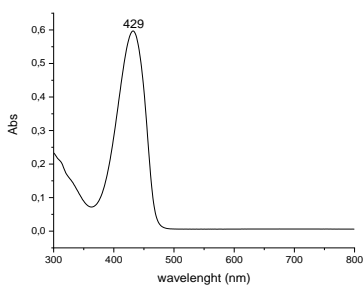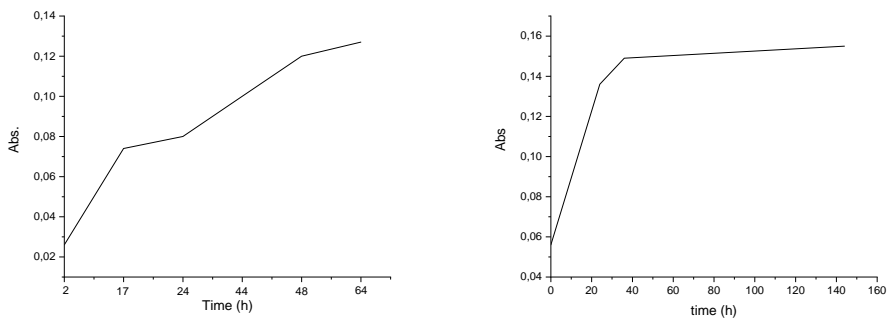

Figure 2. UV-Vis absorbance spectrum of compound **5.**

Measuring the absorbance of the supernatant in the reaction mixture and plotting the absorbance as function of time was possible to obtain the kinetic profile for the coupling reaction.
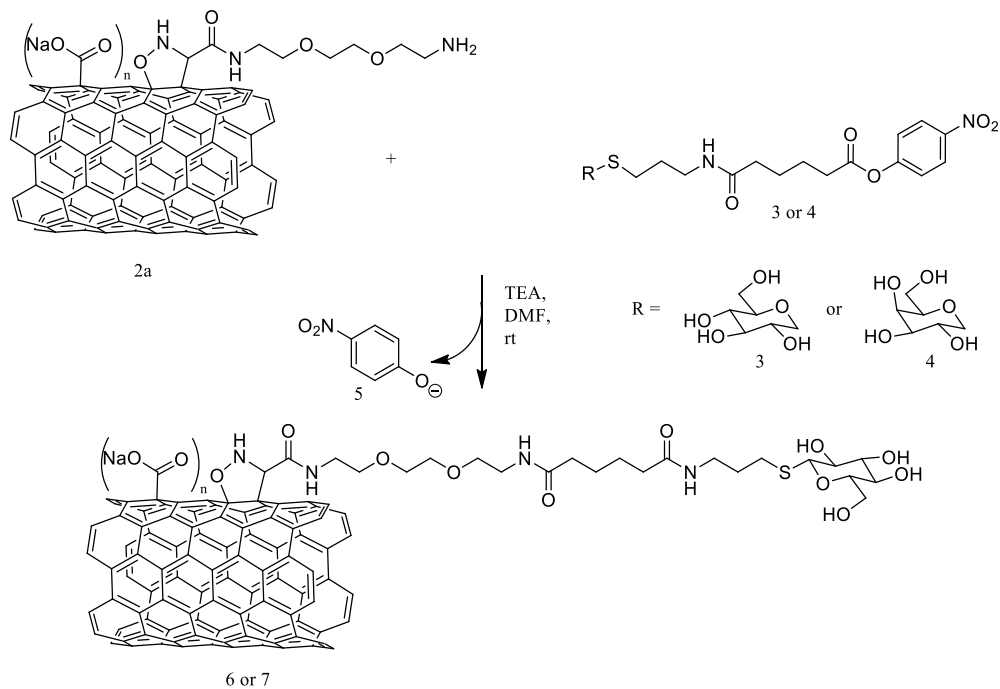
Figure 3. Schematic representation of the coupling reaction with glycoside.

Figure 4. Kinetic of the coupling reaction based on absorbance at 429 nm: on the left profile o reaction of compound **3** and on the right with compound **4**.

The kinetic of coupling reaction with compounds **3** and **4** is showed in figure **4**: the study demonstrates that most of the reaction is completed after 48 hours for both the model compounds; the higher conversion rate is obtained in the 20 hours, then the reaction rate slows down and leads to a plateau after 50 hours for compound **4**. The adducts were characterized by elemental analysis, ICP-AES and FT-IR spectroscopy (see experimental section). After the tuning of the coupling reaction the work was focused to find a synthetic strategy for the labeling with the fluorescent probe. The efforts were directed in the search of a convenient chemistry that avoids the use of metal catalysts. For this reason, the chemistry of carboxylic group was exploited: the use of a two steps reaction allowed to covalently bind with an amide bond the amine decorated bodipy **9**. The loading was confirmed by the UV-Vis absorption spectrum and the fluorescence emission excluded the supramolecular decoration, which would led to the quench of fluorescence emission.
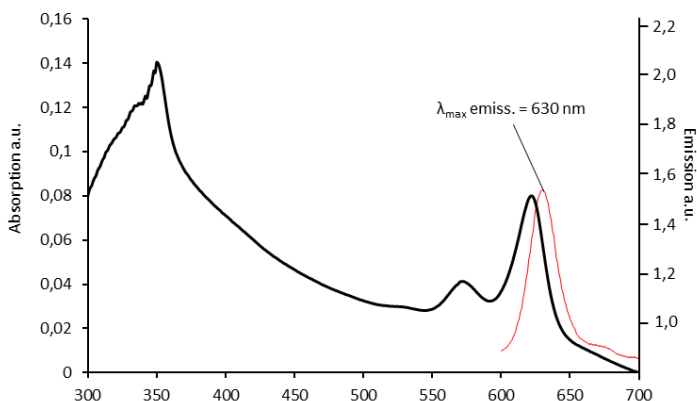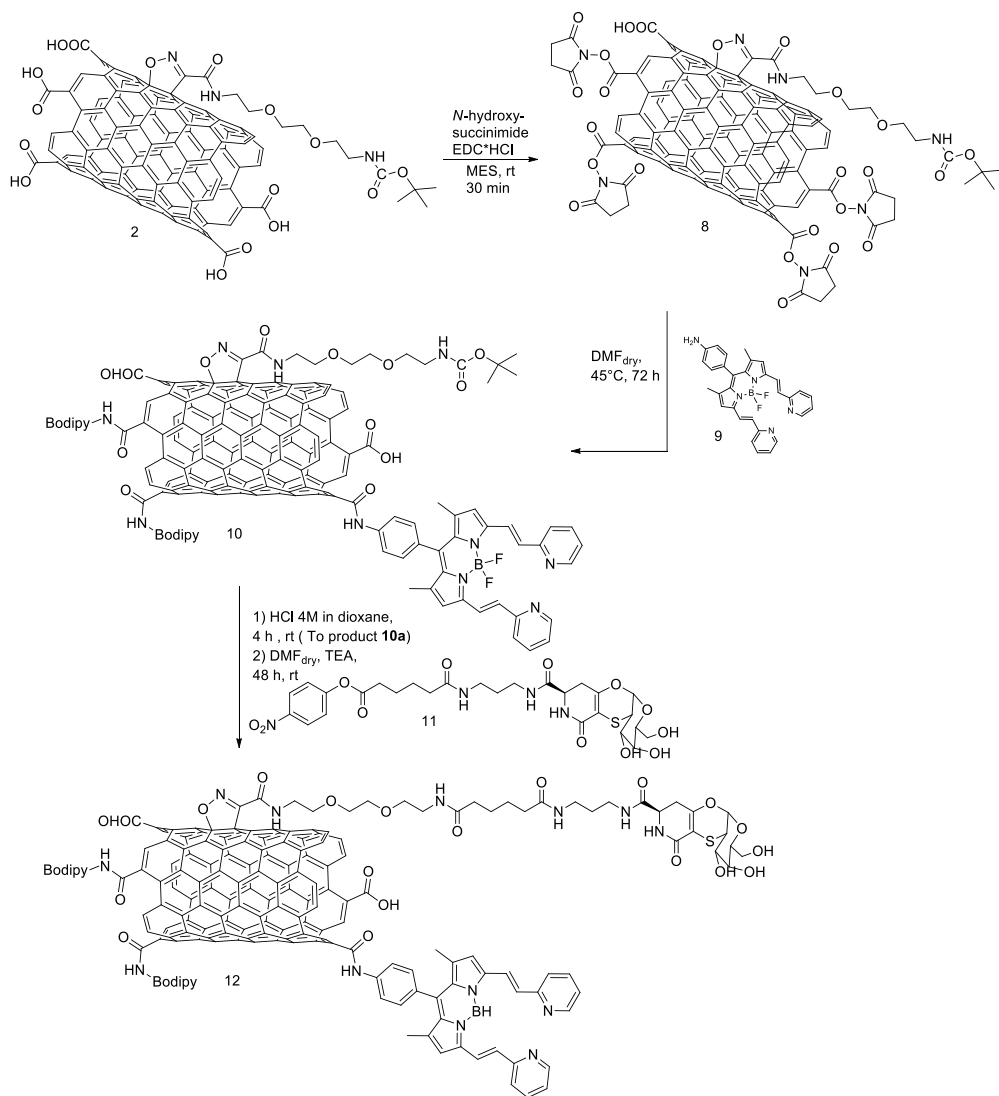
figure 5.

Figure 5. UV-Vis absorption and fluorescence emission spectra of compound **10**.

Then the DDS was completed by deprotection of amide group on material **2b** and coupling with the antigen mimetic **11**.

Figure 6. Synthesis of the complete DDS.

— Chapter 5 —

Experimental section

Synthesis of materials 2

Materials 2 was synthesized accordingly to the previously discussed procedure above in this work (**pg 69**). The material was characterized using TGA-MS showing a loss of weight around 30 to 40 % at 206°C with a peak in the mass spectrum at m/z 56.06, which can pe attribute to the isobutene due to the decomposition of *t*-butyl group. FT-IR : 3753 bb e 3453 bb NH, OH stretching, 2916 e 2852 CH stretching, 1717 CO stretching of carboxylic group, 1577 s CO stretching amide, 1402, 1348, 1223 and 1085 cm^{-1}.

Synthesis of material 2a

Materials 2a was synthesized accordingly to the previously discussed procedure above in this work (**pg 70**). FT-IR: 3412 NH stretching, 1716 stretching CO, 1570 stretching CONH, 1395, 1085 cm^{-1} stretching C-NH.

General procedure for the coupling with model compounds 3 and 4

In a sealed Pyrex tube were placed 5 mg of material **2b**, 3.5 mg of model compound **3** or **4**, 3.5 mg of TEA (34 μmol) and 300 μL of dry DMF, the mixture was sonicated for 10 min and then stirred at room temperature, aliquots of 10 μL were collected at different time point and used for the spectrophotometric analysis. After 72 h the reaction was stopped and the purified material recovered after different centrifugation cycles washing with: methanol:*i*-propanol 1:1, *i*-propanol: *di-i*-propyl ether 1:1, and *di-i*-propyl ether. FT-IR: 3406 OH and NH stretching, 2918 and 2856 CH stretching, 1730 CO stretching carboxylic group, 1583 , 1396 , 1215 , 1089 e 1031 cm^{-1}. ICP-AES analysis S % =0.32, 0.1 mmol of model/g of CNTs.

Synthesis material 8

In a 250 mL round bottom flask 35 mg of material **2** were dispersed in 84 mL of MES buffer, then 875 mg of *N*-hydroxysuccinimide and 210 mg of EDC-HCl were added. The mixture was stirred for 30 minutes at room temperature and the material recovered after filtration over 0.2 µm pore polycarbonate membrane washing with MES and water and dried under vacuum.

Synthesis of material 10

In a 5 mL round bottom flask 10 mg of material **8** and 40 mg of bodipy **9** were dispersed in 2.5 mL of dry DMF under nitrogen atmosphere using an ultrasound bath. Then the mixture was stirred at 45°C for 72 h . The decorated material **10** was recovered after filtration over a ptfe membrane (0.2 µm pores) washing with DMF and methanol until colorless solution obtained. Boron amount was quantified by ICP-AES in 0.4 mg/g. UV-Vis absorbance 0.477 at 622 nm and 0.537 at 350 nm (conc. 0.05 mg/mL).

Synthesis of material 10a

The deprotection protocol used is the same described above (pg 70).

Synthesis of material 12

In a pirex tube under nitrogen atmosphere were added CNTs-NH$_2$ (4.7 mg), the activated mimetic (4.5 mg), dry DMF (300 µL) and distilled triethyl amine (1.34 mg), the mixture was dispersed using an ultrasound bath and stirred under nitrogen at 45 °C for 72 h. Then the reaction mixture was diluted with methanol and centrifuged for 10 minutes at 1400 rcf, the precipitate was recovered with methanol and filtered over a 0.2 µm pores polycarbonate membrane washing with methanol, *i*-propanol and diisopropyl ether. The amount of mimetic was quantified analyzing the sulfur content with ICP-AES and found to be 0.1 mmol/g.

5.4 Synthesis of a self-immolate disulfide linker

Based on the results obtained in the main body of the project, and especially in the lack of target engagement observed in the FAZA experiment, we consider the possibility to use a self-cleavable linker for the release of the drug payload. Several suitable linkers are reported in literature with different cleavage mechanisms, amides, esters, hydrazones and disulfides. Among these, amides require the intervention of a protease enzyme and such mechanism requires to fit perfectly in the enzyme pocket which is not always trivial with CNTs. Esters are often too labile and can be cleaved also in the blood circulation. The choice was therefore reduced to hydrazones and disulfides, and firstly we decide to investigate the disulfide linkers efficiency. For this purpose the linker showed in **Figure 1** was synthesized modifying a reported procedure.[64,78,131,159]


R= bioactive molecule
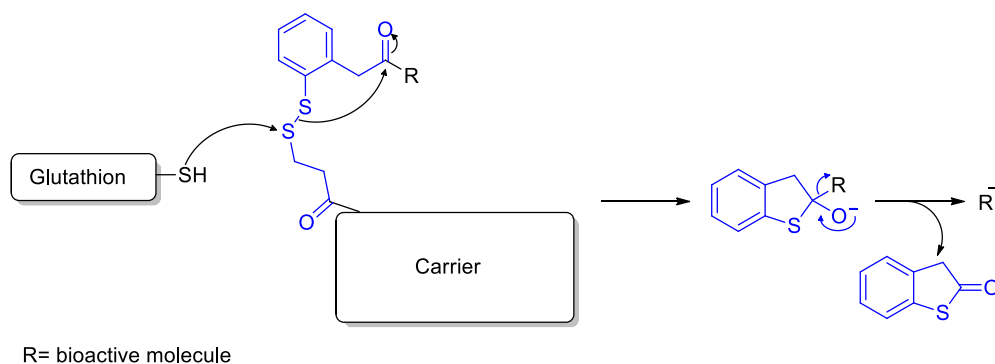
Figure 1. Drug release mechanism with disulfide linker. [159]

The optimized synthetic approach for compound **7** is reported in **Figure 2**. The disulfide linker was prepared starting from the commercially available compounds **1** and **4** through a 5 steps synthesis with a decent overall yield (53%). The key step is the disulfide coupling between compound **3** and **6** where the solvent plays an important role. The use of a non-polar solvent, such diethyl ether, strongly reduces the reactivity

of the pyridyl byproduct that otherwise can react with compound **7** strongly reducing the yield.
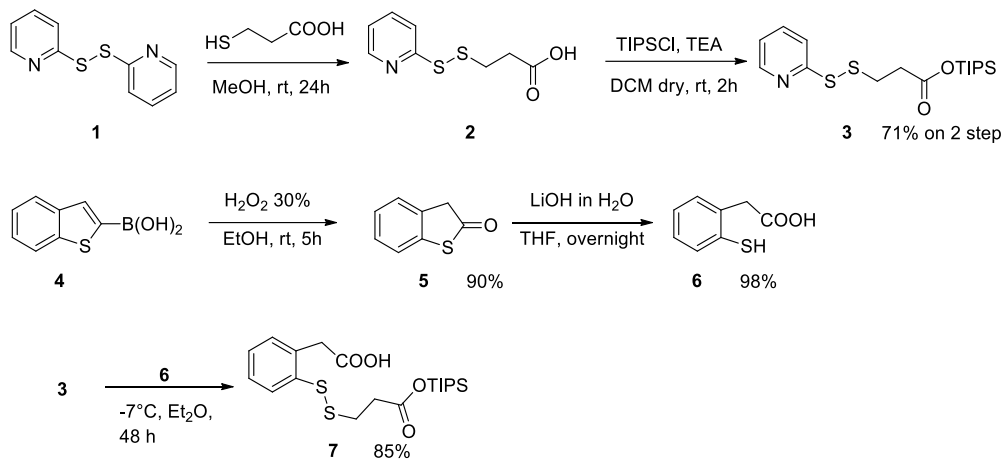
Figure 2. Scheme of disulfide linker **7** synthesis.

Experimental section

Synthesis of compound 2

In a 5 mL round bottom flask 160.3 mg of 3-sulfidryl propionic acid (1.51 mmol, 1 eq) were dissolved in 1.3 mL of methanol, then 500 mg of compound **1** (2.7 mmol, 1.5 eq) were added and the reaction mixture stirred for 2 h at room temperature. The complete conversion of the acid was confirmed by TLC analysis (hexane / Ethyl acetate 1:1). The solvent was removed under vacuum and the crude mixture used directly for the further reaction. ^{1}H NMR (300 MHz, CDCl3) δ = 10.4 (br, 1 H, -COOH), 8.48 (dd, J = 3.3, 1.2 Hz, 1 H, H$_{ar}$- 6), 7.66 (m, 2 H, H$_{ar}$ 3 e H$_{ar}$ 4), 7.14 (m, 1 H, H$_{ar}$ 5), 3.06 (t, J = 6.9 Hz, 2 H, S-CH2), 2.79 (t, J = 6.9 Hz, 2 H, CH2-COOH) ppm

13C ^{13}C NMR (75 MHz, CDCl3) δ = 176.1 (-COOH), 159.2 (C$_{ar}$-2), 149.4 (C$_{ar}$-6), 137.4 (C$_{ar}$-4), 121.2 (C$_{ar}$-5), 120.5 (C$_{ar}$-3), 34.1 (CH$_2$-COOH), 33.8 (S-CH$_2$) ppm.

-COOH), 33.8 (S-CH2) ppm.

Synthesis of compound 3

In a 25 mL two necked round bottom flask 325.1 mg of crude compound **2** (1.51 mmol, 1 eq) were dissolved in dry DCM under nitrogen atmosphere and 305.6 mg of dry TEA (3.02 mmol, 2 eq) were added dropwise, then the solution was cooled at 0°C and 349.4 mg of TIPSCl (1.81 mmol, 1.2 eq) were added dropwise. The reaction mixture was then stirred for 2 h at room temperature, then 5.44 mL of NH_4Cl saturated aqueous solution were added and the organic and the aqueous phases were collected and the second one extracted three times with 5.4 mL of DCM. The organic phases were collected and dried over sodium sulfate, the solvent was removed under vacuum yielding the crude product. The product was purified through flash chromatography column (4 cm d, h 15 cm) eluent petroleum ether : ethyl acetate 20:1. Yield 61%. ^1H NMR (200 MHz, $CDCl_3$) δ = 8.47 m (1H), 7.66 m (2H), 7.10 (1H), 3.03 t (2H), 2.80 t (2H), 1.25 m (3H) and 1.06 ppm d (18H, J^3_{H-H} = 8 Hz). ^{13}C NMR (100 MHz, CDCl3) δ = 171.61 (-COOSi-), 160.13 (C_{ar}-2), 149.84 (C_{ar}-6), 137.26 (C_{ar} -4), 120.92(C_{ar} -5), 119.94 (C_{ar}-3), 35.51 (CH2-COOSi-), 34.04 (SH-CH2), 17.93 (CH- CH3 x 3), 12.07 (CH-CH3 x 3) ppm. HRMS (ESI) m/z calculated for $C_{17}H_{30}NO_2S_2Si+$ (M + H+): 372.1487 measured: 372.1485 (Δ = 0.5 ppm).

Synthesis of compound 5

In a 10 mL round bottom flask 500 mg of compound **4** (2.8 mmol) were dissolved in 5 mL of ethanol, then under magnetic stirring 930 µL of hydrogen peroxide 30% in water were added dropwise and the mixture stirred at room temperature for 5 h. The reaction was quenched adding 17 mL of water, then the mixture was extracted three times with 12.5 mL of DCM, the organic phases were collected and dried over sodium sulfate, the solvent was removed under vacuum giving the purified product (pink oil). Yield 90%. ^1H-NMR (200 MHz, $CDCl_3$) δ = 7.34 m (4H) and 4.04 ppm s (2H). ^{13}C NMR (75 MHz, CDCl3) δ = 202.6 (CO), 136.7 (C_{ar}-2), 132.0 (C_{ar} -1), 128.1 (C_{ar} -3), 125.9 (C_{ar} -6), 124.5 (C_{ar}

-5), 122.7 (C_{ar} -4), 46.9 (CH2) ppm. HRMS-ESI m/z calculated for $C_8H_7OS^+$ (M + H$^+$): 150.0139, measured: 150.0138 (Δ = -0.7 ppm).

Synthesis of compound 6

In a 50 mL round bottom flask 378.1 mg of compound **5** (2.52 mmol, 1 eq) were dissolved in 12.6 mL of THF, then 361.7 mg of lithium hydroxide (15.1 mmol, 6 eq) dissolved in water were added at room temperature. After addition was completed the reaction mixture was heated at 60°C and stirred overnight. Then 2.7 mL of water and 13.3 mL of diethyl ether were added, and the reaction quenched with HCl 2 M till pH2. The organic and the aqueous phases were separated, and the aqueous phase was extracted three times with 23 mL of diethyl ether. The organic phases were collected and dried over sodium sulfate, the solvent was removed under vacuum giving the pure product. Yield 98%. ^{1}H NMR (400 MHz, CDCl3) δ = 10.10 (br, 1 H, -COOH), 7.41 (m, 1 H, H_{ar}-6), 7.18-7.29 (m, 3 H, H_{ar}-3, H_{ar}-4 e H_{ar} -5), 3.83 (s, 2 H, -CH2), 3.49 (s, 1 H, S-H) ppm. ^{13}C NMR (100 MHz, CDCl3) δ = 176.16 (-CO), 133.33 (C_{ar}-2), 132.41 (C_{ar} -1), 131.00 (C_{ar} -3), 130.74 (C_{ar} -6), 128.25 (C_{ar} -5), 126.94 (C_{ar} -4), 39.85 (-CH2) ppm. HRMS-ESI m/z calculated for $C_8H_8O_2S^+$ (M + H$^+$): 168.02450, measured: 168.02445 (Δ = 0.3 ppm).

Synthesis of compound 7

In a 5 mL round bottom flask 340 mg of compound **3** (0.917 mmol, 1 eq) were dissolved in dry diethyl ether under nitrogen atmosphere, the mixture was cooled at -7°C and 231.4 mg of compound **6** were added and the mixture stirred at -7°C for 48 h. The product was recovered after flash chromatographic column (15 cm h, 4 cm d) eluent diethyl ether *rf* 0.9. Yield 51 %. ^{1}H NMR (300 MHz, CDCl3) δ = 7.77 (d, J = 8.4 Hz, 1 H, H_{ar}-6), 7.28 (m, 3 H, H_{ar} -3, H_{ar} -4 e H_{ar} -5), 3.90 (s, 2 H, -CH2-COOH), 2.92 (t, J = 6.9 Hz, 2 H, -CH2-S-), 2.76 (t, J = 6.9 Hz, 2 H, -CH2-COOSi-), 1.31 (m, 3 H, CH-CH3 x 3), 1.22 (d, J = 7.2 Hz, 18 H, CH-CH3 x 3) ppm. ^{13}C NMR (75 MHz, CDCl3) δ = 176.55 (-COOH), 171.85 (-COO-Si), 137.00 (C_{ar} -2), 134.00 (C_{ar} -1), 131.18 (C_{ar} -3), 131.06 (C_{ar} -

6), 128.62 (C_{ar} -5), 128.23 (C_{ar} -4), 39.09 (- CH2-COOH), 35.53 (CH2-COOSi-), 33.78 (CH2-S-), 17.93 (CH-CH3 x 3), 12.05 (CH-CH3 x 3) ppm. HRMS-ESI m/z calculated for $C_{20}H_{33}O_4S_2Si^+$: 429.1590, measured: 429.1601 (Δ = 2.6 ppm).

List of Published works:

(1) Iagatti, A.; Cupellini, L.; Biagiotti, G.; Caprasecca, S.; Fedeli, S.; Lapini, A.; Ussano, E.; Cicchi, S.; Foggi, P.; Marcaccio, M.; et al. *J. Phys. Chem. C* **2016**, *120* (30), 16526–16536.

(2) Biagiotti, G.; Langè, V.; Ligi, C.; Caporali, S.; Muniz-Miranda, M.; Flis, A.; Pietrusiewicz, K. M.; Ghini, G.; Brandi, A.; Cicchi, S. *Beilstein J. Nanotechnol.* **2017**, *8* (1), 485–493.

(3) Biagiotti, G.; Fedeli, S.; Tuci, G.; Luconi, L.; Giambastiani, G.; Brandi, A.; Pisaneschi, F.; Cicchi, S.; Paoli, P. *J. Mater. Chem. B* **2018**, *6* (14).

(4) Biagiotti, G.; Ligi, M. C.; Fedeli, S.; Pranzini, E.; Gamberi, T.; Cicchi, S.; Paoli, P. *J. Drug Deliv. Sci. Technol.* **2018**, *47* (April), 254–258.

Acknowledgement

From now on we will speak Italian…
Tutti si aspetteranno citazioni epiche, frasi strappalacrime, commozione a fiumi etc. etc..
Beh se questo è quello che cercate tanto vale fermarvi qui, perché questi ringraziamenti saranno impregnati di pragmatismo schietto e forse un velo di polemica, in quanto queste sono le due caratteristiche che più rappresentano l'autore.
Si chiamano ringraziamenti quindi ringraziamo:
 – In primis il Prof. Brandi che mi ha dato la possibilità di svolgere il mio PhD nel suo gruppo.
 – Il Prof. Cicchi, di fatto il mio mentore nella chimica dei materiali, nonché baluardo di ottimismo nei periodi più bui, quando tutto sembra impossibile e vorresti solo farla finita (col Dottorato si intende).
 – Il Prof. Machetti che è stato il mio "padre scientifico" essendo stato colui che mi ha introdotto al mondo della ricerca, e che in questi anni è sempre stato prodigo di consigli utili.
 – Il Prof. Paoli per tutto il supporto fornito a questo lavoro.
 – Federica, che non è Prof. (per ora), che ha reso possibile la collaborazione che mi ha portato a Houston, ma non solo, è anche stata un mentore brillante per tutto ciò che riguarda la radiochimica e una costante fonte di ispirazione.
 – Dave che mi ha accettato nel suo gruppo e ha contribuito insieme a Seth in modo fondamentale al lavoro.
 – Tutti i ragazzi del DPW's group in particolare Yi, Sarah e Tracy che mi hanno fatto sentire a casa anche a 8952 km da Firenze.
 – Tutti i compagni di viaggio, che hanno reso meno pesante il fardello della ricerca con momenti di svago necessari a ritemprare corpo e mente.
 – Cristian e Ilaria che di fatto mi hanno aiutato tantissimo quando ero a Houston.
 – Il grande Ernesto che mi ha fatto fare un ripasso di tutta la chimica e mi ha scarrozzato per 7 mesi.

Carolina che mi ha sopportato e supportato con encomiabile pazienza, che ormai da tempo immemore è la mia ancora. Sempre pronta ad ascoltarmi anche quando c'erano 7 h di fuso e io la chiamavo nel bel mezzo della notte.
Infine, i miei genitori che hanno sempre creduto in me e mi hanno sostenuto per tutto questo periodo, a loro va il grazie più grande.